2003

Diffusion of a rodlike virus in complex solutions

Randall Charles Cush
Louisiana State University and Agricultural and Mechanical College

DIFFUSION OF A RODLIKE VIRUS IN COMPLEX SOLUTIONS

A Dissertation

Submitted to the Graduate Faculty of the
Louisiana State University and
Agricultural and Mechanical College
in partial fulfillment of the
requirements for the degree of
Doctor of Philosophy

in

The Department of Chemistry

by
Randall Charles Cush
B.S., Louisiana State University, 1997
May, 2003

ACKNOWLEDGMENTS

First, I wish to thank Prof. Ernest Blakeney at Centenary College of Louisiana, who encouraged me to participate in a NSF Research Experience for Undergraduates program at LSU. It was this experience that eventually led me to the decision to attend graduate school in chemistry. I also must thank a great teacher and friend, Prof. Rosemary Seidler, also at Centenary, for reminding me not to let school interfere with my education.

I thank Prof. Paul Russo of Louisiana State University in Baton Rouge for the excellent training I received in graduate school. His zeal for problems scientific was utterly contagious. He helped foster in me a child-like curiosity for science. I also thank him for supporting my decision to move to North Carolina in the midpoint of my graduate career; an endeavor to prove quite challenging for both of us. Finally, I thank him for helping me to relax and realize that nothing in life really matters very much and few things matter at all

After my decision to move to North Carolina, I was in need of a lab in which to complete my research. After meeting with several faculty members at the University of North Carolina at Chapel Hill, Prof. Nancy Thompson was the only one to make an effort to contact me about my decision. I thank her for her profound generosity in allowing me to finish my work in her lab. Without her help, I most likely would have bailed from the Ph.D. program to pursue a Master's degree. It has been a great pleasure working under her co-advisory and I thank her for many stimulating discussions, both scientific and non.

I thank my graduate committee for many insightful comments during my general exam and data defense. It wasn't until the latter part of my training that I fully appreciated the significance of the graduate committee in helping a student to realize his/her potential. It's something I think many students take for granted.

Of course, none of this would have been possible without the ceaseless support of my wife Sarah. Many a night she ate dinner alone while I was in the lab. She was also forced to spend many (most) weekends without my company. To describe all that she has done and sacrificed the past five years would require a document of this length all in itself.

The waking hours not spent with Sarah were of course spent with a multitude of lab mates. Fully aware of the challenge it was to tolerate my (usually annoying) presence in the lab, I thank Brian Fong, Garrett Doucet, Sibel Turksen, Elena Temyanko, Nadia Edwin, Alena Lieto, Tammy Starr, Jennifer Mitchell and Noah Allen for being great lab partners and friends.

Finally, I thank my family. Despite my moving nine hundred miles away from them, they were always close to me and always there for me. I owe *everything* to Raymond, Joanie, Ryan, and Dino, and dedicate this work to them.

TABLE OF CONTENTS

LIST OF TABLES

LIST OF FIGURES

LIST OF SYMBOLS

A_i	amplitude of species I
c	concentration
D_r	rotational diffusion coefficient
D_{r20w}	rotational diffusion coefficient temperature corrected for 20°C
D_t	translational diffusion coefficient
D_{t20w}	translational diffusion coefficient temperature corrected for 20°C
$E(t)$	electric field
f	coefficient of friction
G'	storage modulus
G''	loss modulus
g	acceleration due to gravity
$G^{(2)}(t)$	intensity autocorrelation function
$g^{(1)}(t)$	normalized electric field correlation function
Hv	geometry for depolarized dynamic light scattering
I	intensity
k	Boltzmann constant
M	molarity
M_c	critical molecular weight for entanglements
MW	molecular weight
M_w	weight average molecular weight
M_n	number average molecular weight

m	mass
n	refractive index
ρ	solvent density
q	scattering vector magnitude
R_h	hydrodynamic radius
R_g	radius of gyration
s	sedimentation coefficient
s_{20w}	sedimentation coefficient corrected for 20°C
T	absolute temperature
Uv	geometry for polarized dynamic light scattering
ν	partial specific volume
Γ	decay rate
λ_o	*in vacuo* wavelength
η	solution or melt viscosity
η_s	solvent viscosity
θ	scattering angle
τ	lag time
ξ	mesh size, average distance between entanglement points
ξ_{cm}	mesh size, average distance between chain centers of mass

LIST OF ABBREVIATIONS

CLF	contour length fluctuations
CR	constraint release
CONTIN	Laplace inversion algorithm
DDLS	depolarized dynamic light scattering
DLS	dynamic light scattering
5-DTAF	5-isomer of fluorescein dichlorotriazine
FITC	fluorescein isothiocyanate
FPR	fluorescence photobleaching recovery
GPC	gel permeation chromatography
GPCLS	gel permeation chromatography with light scattering detection
HPLC	high performance liquid chromatography
PAD	pulse amplifier/discriminator
PBLG	poly(γ-benzyl-α,L-glutamate)
SLS	static light scattering
TMV	tobacco mosaic virus

ABSTRACT

Entanglement phenomena in concentrated polymer solutions remain an interesting and challenging problem. It is still unclear how entanglement onset affects polymer chain motion at small distance scales. One way to study such motion is to follow the diffusion of a probe particle while increasing the concentration of the polymer. Many such studies have been done using probes ranging from linear and star polymers to various colloidal particles; however, relatively few studies have used rodlike probes. Rodlike probes are potentially more interesting due to the added information that may be gained by following rotational as well as translational diffusion. The anisotropic diffusion may allow the probe to sense something different as chains begin to entangle.

The situation is unclear even for the simpler polymeric structures such as rigid rods. Due to lack of experimental data, the nature of interactions of rigid rods in concentrated solutions remains uncertain. Given the vast theoretical descriptions available, the current challenge is to find suitable rigid model particles. To date, self diffusion data for truly rigid rods is limited to only one system, colloidal boehmite, which was quite polydisperse. [1;2]

Described here is the use of depolarized dynamic light scattering to measure the rotational and translational diffusion of the rodlike virus, Tobacco Mosaic Virus (TMV), through solutions of random coil and globular polysaccharides, taken separately. The polymers are effectively invisible in the depolarized scattering experiment allowing only the TMV probe to be seen. Also described is the use of fluorescence photobleaching recovery to measure the self-diffusion of TMV as a function of concentration in the isotropic regime.

CHAPTER 1

INTRODUCTION

1.1 SEMI-DILUTE POLYMER SOLUTIONS

The dynamics of random coil polymers in dilute solution has been studied for many decades and are well understood. In the semi-dilute regime, where interchain interactions begin to become important, the nature of polymer motion remains somewhat obscure. It is widely accepted that chain "entanglements" occur above a certain concentration, but this phenomenon is not well understood. Despite several decades of work to understand polymer behavior in this regime, many uncertainties still exist. At sufficiently high concentrations, behavior is again fairly well understood, though recent works have emphasized some discrepancies. [3-7]

The concept of polymer chain entanglement is often associated with the theoretical work of Nobel laureate Pierre-Gilles DeGennes who developed the well-known reptation model. [5] This model is based on the assumption that, as polymer concentration increases, a point is reached where polymer domains must overlap, forming a "transient" network involving topological constraints. Beyond this entanglement concentration, polymers must diffuse along their length (or reptate) through a "tube" created by neighboring chains, which hinder sideways motion.[6] A consequence of this model is that one can define a mesh size, ξ, that corresponds to the average distance between entanglement points. Beyond the entanglement concentration, this mesh size is molecular weight independent but becomes smaller with increasing polymer concentration according to $\xi \sim c^{-0.75}$ for polymers in a good solvent. In his reptation plus scaling model, deGennes predicts that entangled polymers will diffuse as $D \sim M^{-2}c^{-\nu}$ where ν is 1.75 and 3 in good and theta solvents respectively.[8] The reptation model [5-6;9] has also been used to predict that viscosity should scale as $\eta \sim M^{3}$.

In general, the reptation model seems to provide a good framework for describing dynamics of entangled systems, but significant discrepancies remain as recently reviewed. [3;4]

The most consistent one is the experimentally observed [10] scaling of viscosity as $\eta \sim M^{-3.4\pm 0.2}$, significantly higher than the predicted exponent of 3. This suggests that reptative modes alone may not be sufficient at describing entangled systems, but this seems to conflict with the observed scaling of diffusion as $D \sim M^{-2}$, as predicted, for various polymer melts.[6;7] Such discrepancies could be reconciled using modifications to the reptation model including constraint release (CR) [7;11]and contour length fluctuations (CLF).[6;12] Constraint release considers the mobility of neighboring chains which can free up regions of space around the test chain, while CLF allows for a chain end to withdraw inside the tube and explore other regions of space, without full reptation of the entire chain through the tube. These processes would both serve to decrease the time an entangled chain spends in a particular tube. [3] Further complicating the matter are diffusion measurements in highly concentrated *solutions* that reveal higher molecular weight exponents than 2, at around 2.4, [13-16]while the viscosity scales as $\eta \sim M^{-3.4}$ as in melts.[10;17] This suggests that there is some difference in entanglement dynamics between melts and highly-concentrated solutions that is not taken into account by reptation models.[3] Recent work by Lodge[3;4] has found that $D \sim M^{-2.3}$ for concentrated *solutions and melts* of hydrogenated polybutadiene (hPB) and that literature data reveal a universally stronger exponent of about 2.3 for melts of other polymer systems.

There exist opposing views to the reptation theory. A notable one is that of George Phillies who claims that reptation is not an important mechanism for semi-dilute polymer diffusion. His argument, originally based on a phenomenological approach after surveying the literature, is that polymer motion is governed primarily by hydrodynamic interactions, not topological constraints.[18] He later supported this approach with theoretical work, finding that polymer diffusion follows not a power law but a "universal" stretched exponential equation. [19;20]

He points out that this equation is backed by many experiments. [20] Given the inherent flexibility of stretched exponentials, the relevance of such approaches could be called into question.[21;22]

This issue of whether topological constraints or hydrodynamic interactions govern polymer chain motion in semi-dilute solution remains controversial. [23] The challenge to uncover the true behavior of polymers in this regime is being met by techniques known as probe diffusion experiments. The results of such studies reveal uncertainty as to the behavior of entangled chains at short distance scales and to the limits of describing a polymer solution as a continuum medium.

If one turns to more simple polymeric architectures such as rigid rods, the situation is not much better. The term entanglement has been applied to systems of rodlike polymers, though the physical picture of such a phenomenon is less clear. For this reason, the term "enmeshment" seems more appropriate.[24] The situation is similar to that for random coil polymers in that sideways motion is hindered by neighboring rods, forcing an enmeshed rod to escape by longitudinal motion. The diffusion of the rodlike polypeptide poly(γ-benzyl-α,L-glutamate), PBLG, in the semidilute regime depends on molecular weight as $D \propto M^{-1.8}$, quite similar to the expectation for random coil polymers in the melt as described earlier ($D \propto M^{-2}$). As rods cannot reptate in the conventional sense, this demonstrates the dangers of "signature" exponents; seeing $D \propto M^{-2}$ does not confirm a reptative process.

The challenge to understand rodlike dynamics in concentrated solution has been met by several theories [25-33] but experimental data are scarce, [1;2;24;34-38] especially for rods in the very rigid limit. [1,2] Theoretical treatments began with the work of Doi and Edwards[11,12] which supposes the onset of rod entanglement to occur at a number density $\nu = 1/L^3$, where L is the rod length. Without affecting longitudinal translation, topological constraints prevent lateral motion,

causing D_{self} to fall to half its value in dilute solution. In this elegantly simple theory, the transition to this condition is not described, nor are effects due to finite diameter and hydrodynamic interactions. Previous studies on PBLG show that interactions begin at much higher concentrations with more severe effects on the reduction of D_{self}. The only studies to date using very rigid rodlike particles [1;2] also reveal more dramatic decreases in $D_{self,}$ yet without a concentration independent region at low concentrations as seen in the PBLG study. It was postulated that flexibility of PBLG underlies this discrepancy. Clearly, more data for diffusion in concentrated solutions of very rigid systems is needed.

1.2 PROBE DIFFUSION EXPERIMENTS

One of the popular approaches to study the motion of polymers in solution is probe diffusion. One adds a dilute concentration of probe particles to a solution of polymers to be studied. By following the diffusion of the probe, one hopes to gain insight into the dynamics of the surrounding polymers. An assumption in such an experiment is that the probe itself does not alter the behavior of surrounding polymers; it will be seen later that this may not be always be valid. [39;40] Understanding the motion of probe particles in concentrated polymer solutions has other scientific implications related to such problems as biopolymer transport in cells, DNA separation, the drying of paints, and the development of solution-processed composite materials.

Probe diffusion in polymer solutions was first studied experimentally by Turner and Hallett[41] who used dynamic light scattering to follow the diffusion of polystyrene spheres in aqueous solutions of dextran. Since then, a wealth of probe diffusion data using probes of various shapes and sizes has appeared in the literature along with many theoretical works. Due to the extent of this literature, a complete review would be too lengthy for treatment here and a summary of various probes used will be provided. More comprehensive reviews[39;42] exist.

Theoretical considerations were introduced by Langevin and Rondelez[43] for spherical probes in a solution of random coils. In this early work it was suggested that spherical particles much larger than the aforementioned mesh size, ξ, should become "trapped" and sense (nearly) the viscosity of the "entangled solution" while probes much smaller than ξ should diffuse almost as easily as they would in pure solvent. Usually, the diffusion of spheres in a small molecule solvent of viscosity η is described by the Stokes-Einstein (SE) equation:

$$D = \frac{kT}{6\pi\eta R_h} \qquad (1.1)$$

where R_h is the sphere radius. The question still remains as to whether (or when) this equation should hold for spheres diffusing through a polymer solution. If probes much larger than ξ sense the macroscopic solution viscosity, then one may expect SE diffusion. A scan of the literature reveals both adherence [44 22;45-47] to and deviation [48,49 50-56] from SE behavior for large probes. If such SE deviation is due to failure of the continuum assumption, then it is important to understand when a continuum viewpoint should be replaced by a more molecular picture.

Many experiments have used spherical probes to study polymer solutions but interpretations can be misleading. To understand the nature of a transient network one would compare the diffusion of probes smaller than and larger than the mesh size, ξ, as described by de Gennes. [5] Using spheres smaller than the mesh size (roughly 50 – 100 Å by ref. 5) is quite difficult by the more common light scattering methods. As a result, many studies fail to use probes that are really small enough, with one notable exception. [57] Easier experiments using large probes may be plagued by a different problem. A study by Gold et al. suggests the importance of polymer depletion zones in probe diffusion studies. [39] Areas of polymer depletion develop as the result of polymer chain repulsion near the probe surface. This is due to a decrease

in the number of configurations available to chains that approach too closely. Consequently, the diffusing spheres may alter the local polymer (or "network") structure they are probing. This could result in positive deviations from SE behavior as the probe senses a local viscosity that is lower than the bulk value.

A more realistic approach is to use chains as probes. Such experiments have yielded results that generally agree with deGennes' predictions, with some exceptions [3;4] as noted in the previous section. A review of these experiments [42] has recently been published. Star polymers with chain-like arms have also been used but with mixed results.[58;59]

A more recent and novel method has been to use anisotropic probes which allows one to follow *rotational diffusion* of the particles, something ignored by all but a few studies. [56;60-62] This lack of such studies is unfortunate as new information may be gained by following this anisotropic diffusion. A study by Hill and Soane used electric birefringence techniques to follow rotation of rodlike collagen molecules in aqueous poly(ethyleneoxide) solutions.[60] The same group also derived a theory for the diffusion of rods in semi-dilute polymer solutions.[60] A study by our lab used the rodlike tobacco mosaic virus to probe solutions of the random-coil polysaccharide, dextran.[56] We observed a transition that could be explained as the onset of dextran entanglement, but as will be seen, some of the results revealed a need for more testing. The intent of the current study was to further explore the diffusion of tobacco mosaic virus particles in solutions of the random coil polysaccharide, dextran, and to extend the study to solutions of a compact, globular polysaccharide known as ficoll, which should not entangle.

CHAPTER 2

PURIFICATION AND CHARACTERIZATION OF TOBACCO MOSAIC VIRUS

2.1 INTRODUCTION

First crystallized in 1935 by the American scientist Wendell Stanley, Tobacco Mosaic Virus (TMV) was the first infectious agent identified as a virus.[63] Since then, it has been extensively characterized and its structure is well known. Less certain are its physical properties in solution. The rod-like plant virus consists of single-stranded RNA of about 6400 nucleotides protected by a protein sheath of 2130 protein subunits that spiral around the RNA in a helix. The overall structure is that of a hollow tube of length 300 nm and diameter 18 nm.[64;65] An electron micrograph of TMV appears in Figure 1. The proteins are bound to the RNA noncovalently. This has important consequences as it allows for fragmentation of the virus particles during preparation. A study by Steere et al. has shown that the smaller TMV fragments can be separated from intact virus by agar-gel chromatography.[66] In addition, it is known that the virus particles can form end-to-end aggregates under certain conditions.[66] Due to these two potential causes of polydispersity, much work has been done to try to improve the quality and reproducibility of TMV preparations.

TMV has been isolated by a variety of methods such as salt or solvent precipitation,[67;68] differential centrifugation,[65;66] electro-extraction [69]and thin layer centrifugation.[70] The techniques vary greatly in the quality and quantity of TMV produced. The most common and reproducible method seems to be differential centrifugation. While most agree on the general procedure, there is some uncertainty as to what salts should or should not be present in solution to prevent aggregation. [71] The differential centrifugation method was chosen for TMV isolation in this study.

Much work has been done to characterize TMV behavior in solution, including measurements of various solution properties such as sedimentation, rotational and translational

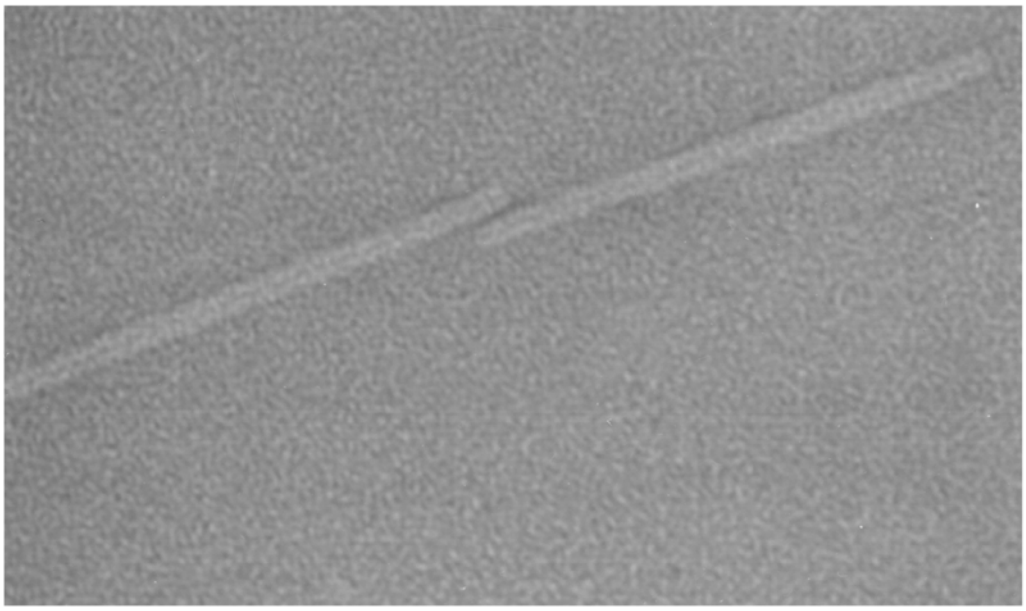

Figure 1. Electron micrograph of Tobacco Mosaic Virus (TMV) taken at about 80,000 × magnification.

diffusion coefficients. Sedimentation measurements are typically made using an analytical ultracentrifuge, and most studies of TMV report similar values for the sedimentation coefficient. Translational and rotational diffusion coefficients of TMV have been extensively measured by dynamic light scattering. [56;71-86] With this large effort, discrepancies in measured diffusion coefficients remain. This is likely due in part to the aforementioned "problems" with the virus including fragmentation and aggregation. Described next is the characterization of the TMV used in this study, including experimental and theoretical data from previous studies.

2.2 PURIFICATION OF TOBACCO MOSAIC VIRUS

The TMV used in this study was isolated from the infected leaves of plants grown for these experiments. Young *Nicotiana tobacum* plants were infected by rubbing small areas of the leaves with cheesecloth soaked in a dilute solution of the U1 strain of TMV containing a small amount of corborundum powder. The site of application was covered with ordinary adhesive bandages (Curad) to protect it from unwanted secondary infections. After a few weeks, the infected leaves were harvested and frozen.

The procedure used to isolate the TMV, which is a hybrid of two techniques used previously, [65;66] is described in the supplemental information of Ref 56. The frozen tobacco leaves were first thawed at room temperature for several hours and the stems were removed via razor blade. The leaves were then weighed and re-frozen. The rest of the procedure was performed in a cold room at 4°C. The leaves were dipped in 0.05 M EDTA, pH= 9.5, cut into roughly 1 cm^2 pieces and then pulverized in a large mortar & pestle. After a few minutes of maceration, 1 gram of Na_2HPO_4 was sprinkled on the mash for every 120 grams of leaves used. The leaves were re-pulverized several minutes more and the entire wad of plant mash was placed into a piece of cheesecloth and squeezed over a funnel into an iced flask. A few mL of 0.05 M

EDTA was added to the mash which was placed back into the pestle, re-pulverized and the juice extraction repeated. The juice collected was dark green in color. The juice was quickly adjusted to pH 7.2 by addition of NaOH as 1.0 M solution. After the pH was adjusted, five grams of diatomaceous earth and five grams of activated charcoal were added for every 100 mL of juice collected. The solution was then swirled for several minutes.

The next step involves removing the large plant material, diatomaceous earth and charcoal from the juice. The juice was filtered through Whatman Filter paper #54, covered with about 1/4 inch of diatomaceous earth, using a Büchner funnel and water aspirator. Holes had previously been punched in the paper using a needle to increase flow rate. The usually clear filtrate was collected in the attached vacuum flask sitting in ice.

The final purification steps involve repeated cycles of low and high-speed centrifugation. In the first step (low speed) the solution was spun at 8,200 RPM in a Sorvall centrifuge using an SS-34 angled rotor for about 20 minutes. The supernatant was removed and the pellet discarded. In the second centrifugation step (high speed), the solution was spun at 21,750 RPM in the TI-70 or TI-65 rotor of a Beckman ultracentrifuge. Three to four cycles were needed to produce clear TMV pellets, which occasionally had a very slight green tinge. The nature of solutes present in the solution used to recover the pellet has an effect on the quality of TMV isolated. [66] The pellet was recovered in the first cycle using a solution of 0.1 M phosphate buffer and 0.01M EDTA, pH =7.2. The pellet from subsequent cycles was recovered using water from a Barnstead Nanopure water purification system, switching to 0.01 M phosphate buffer with 0.003 M sodium azide, pH =7.5 in the last cycle. Buffer used to recover the pellets was filtered through a 0.1 μm Millipore Millex VV syringe filter directly into the centrifuge tube to reduce the amount of dust in the final TMV solution. All glassware, the mortar, pestle, and all centrifuge tubes were cleaned

thoroughly using RNase Zap (Sigma) to inactivate RNases which can be a troublesome contaminant in TMV preparations.[67] Centrifuge tubes were rinsed thoroughly with dust free water prior to use.

2.3 CHARACTERIZATION BACKGROUND

2.3.1 DYNAMIC LIGHT SCATTERING

2.3.1.1 PRINCIPLES

Dynamic light scattering (DLS) is one of the most powerful techniques for studying molecular diffusion. Complete theoretical treatment of DLS principles can be found in other sources. [87-89] Described here will be a brief summary of DLS as applicable to this study.

When light impinges on a molecule, the electrons in the molecule are induced to oscillate. If the polarizability of the molecule is different from that of its surroundings, the acceleration of the electrons results in radiation of light in all directions or scattering. The scattered intensity is much less than that of the incident light. If two particles are present, the scattered light arriving at some point will be the sum of that scattered from each of the particles. The relative position of the two particles determines the phase relationship of the two waves arriving at a point. Scattered waves arriving in phase interfere constructively (higher intensity) and those out of phase interfere destructively (lower intensity). The total intensity of light scattered from a collection of scatters will vary in time, fluctuating around some average intensity as the scatterers move relative to each other. The rate at which these fluctuations take place is related to the speed at which the scatterers are moving. On a long time scale these fluctuations appear random or uncorrelated; but, the intensity at two closely spaced times will be similar or correlated. The nature of this correlation can be described using a mathematical construct known as a correlation function.

The autocorrelation function measured in DLS is of scattered light *intensity*:

$$G^{(2)}(\tau) = \langle I(0)I(t)\rangle = \left\langle |E(0)|^2 |E(t)|^2 \right\rangle = \lim_{T\to\infty}\left(\frac{1}{2T}\right)\int_{-T}^{T} I(t)I(t+\tau)dt \qquad (2.1)$$

In DLS notation, the capital "G" indicates data that are not normalized and the superscript "2" indicates a second-order autocorrelation function, since the detectors used in light scattering detect intensity, the square of the electric field, *E*, as seen above. The correlation function is calculated for a wide range of values for τ (the lag time) by the correlator, which will be described in more detail below. Assuming the scattering is a random Gaussian process and is homodyne (self-beat method), the correlator estimates the autocorrelation function:

$$G^{(2)}(\tau) = \left(1 + f\left|g^{(1)}(\tau)\right|^2\right) \qquad (2.2)$$

where *f* is an instrument parameter related mostly to the spatial coherence, and $g^{(1)}(\tau)$ is the normalized (note the lower-case "*g*") electric-field autocorrelation function. For a monodisperse solution,

$$g^{(1)}(\tau) = \exp(-\Gamma t) \qquad (2.3)$$

where Γ is the decay rate, while a polydisperse sample yields a $g^{(1)}(\tau)$ that is a weighted sum of discrete exponentials that can be approximated by a continuous distribution:

$$g^{(1)}(\tau) = \sum_i A_i \exp(-\Gamma_i \tau) \approx \int_0^\infty A(\Gamma)\exp(-\Gamma\tau)d\Gamma \qquad (2.4)$$

For an optically isotropic scatterer in a Uv geometry (detection of all scattered light from vertically polarized incident light),

$$\Gamma_{Uv} = q^2 D_t \qquad (2.5)$$

where D_t is the translational diffusion coefficient and q is the magnitude of the scattering vector,

$$q = \frac{4\pi n \sin(\theta/2)}{\lambda_o} \tag{2.6}$$

where n is the solution refractive index, θ is the scattering angle, and λ_o is the *in vacuo* incident light wavelength. Optically anisotropic particles contribute a rotational component, which, at high q, adds additional exponential terms. If such particles are cylindrically symmetrical and rigid like TMV, then in the Hv geometry (detection of horizontal light from vertical incident light),

$$\Gamma_{Hv} = q^2 D_t + 6D_r \tag{2.7}$$

where D_r is the rotational diffusion coefficient. A plot of Γ vs. q^2 yields D_t (slope) and D_r (intercept) simultaneously. This equation holds if the rod rotates many times while diffusing a distance of roughly q^{-1}, meaning absence of translation-rotation coupling. DLS in the Hv geometry is also known as depolarized dynamic light scattering (DDLS).

2.3.1.2 EXPERIMENTAL METHOD

Instruments for DLS can now be purchased commercially but many scientists use home-built systems. Most designs have some basic components in common, including a coherent light source such as a laser (though not strictly necessary), lenses, sample holder and scattering cell, detector, signal analyzer (interferometer or correlator) and some form of temperature regulator. The home-built apparatus used for DDLS in this study is depicted in Figure 2. For the Uv experiment, the horizontal analyzer was removed. The lasers used were a Spectra Physics Millennia, frequency-doubled, Nd-YAG laser at 532 nm and a Coherent Innova 90 argon ion laser at 514.5 nm. The Coherent laser was used for experiments performed during an extended stay at the University of North Carolina at Chapel Hill. About 2.0 W of vertically polarized light

was available from both lasers but 200 mW was typically used. The sample holder consists of an index matching vat containing toluene which is nearly isorefractive with the glass DLS cells which are ordinary 13 mm culture tubes with PTFE-lined caps. The vat toluene was de-dusted by recirculation through a 0.2 μm PTFE Nalgene filter via pump and the vat temperature was maintained by a Neslab RTE-110 water bath with external Pt-100 Omega temperature probe. The index-matching vat was not always used and a Lauda RM6 water bath was then used to regulate the temperature of a copper cell holder. The electronics consisted of a Pacific Precision model 126 pulse amplifier/discriminator (PAD), a Hamamatsu R928p photomultiplier tube, and an ALV-5000 multi-tau correlator card installed in a personal computer. The setup also has a viewing port with 100× magnification, which allowed for viewing of the beam to be measured. The angle was varied manually by moving the detector arm to each angle as needed.

Five angles were usually measured, ranging from 30 to 90 degrees. The beam was viewed at each angle to verify that it was in focus, to check for optical anomalies such as bubbles/stray light in the vat, and to check for dust. The collection duration used for each sample varied, but usually data were collected as one long run with a duration several orders of magnitude longer than the apparent decay time of $g^{(2)}(t)$.

For the Hv geometry, the polarizers were aligned as follows. The horizontal analyzer was set in place (no vertical polarizer) and the arm rotated to 90 degrees. The analyzer was rotated to minimize the scattering signal from a dilute solution of TMV. Alternatively, a sample of latex spheres could be used, yielding the same minimization point. Once minimized, the vertical polarizer was put into position, the sample removed and the arm rotated to zero degrees. The vertical polarizer was then tweaked to minimize the light coming through the viewing port. The data were analyzed by a regularization method, based on Provencher's CONTIN, that is

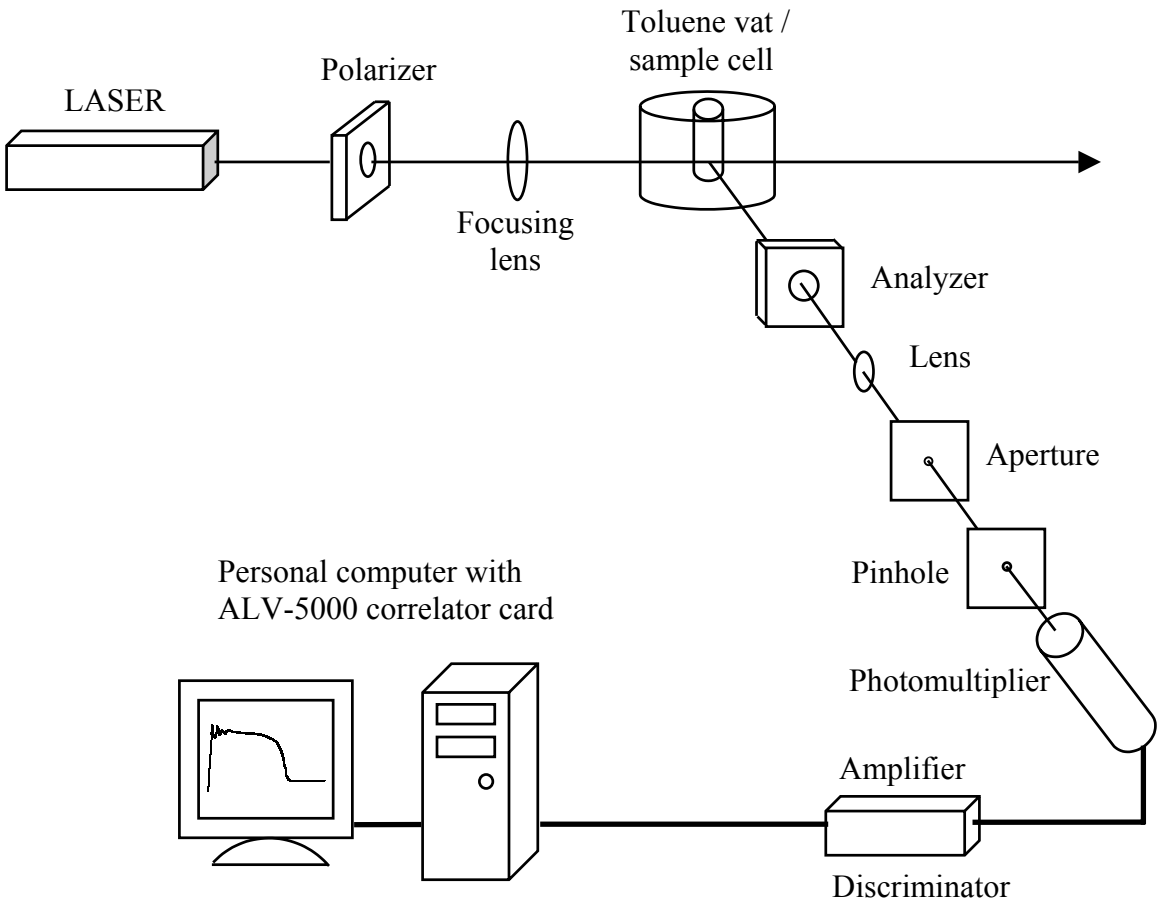

Figure 2. Diagram of the dynamic light scattering setup.

included in the ALV5000 software. [90;91] This method was chosen over cumulants analysis due to bimodal spectra that contained a fast mode possibly corresponding to fragmented TMV in some preparations. This fast mode was sufficient to affect the average decay rate that would be determined via cumulants analysis. It is felt that failure to remove it, or differences in how it is treated, may underlie the discrepancies in TMV D_t and D_r values determined by DLS. [56]

2.3.2 ANALYTICAL ULTRACENTRIFUGATION

2.3.2.1 PRINCIPLES

Analytical ultracentrifugation is a technique that involves spinning a solution in an ultracentrifuge and following the movement or redistribution of dissolved particles. There are two different sedimentation experiments: sedimentation equilibrium, used to measure solute molecular weight, and sedimentation velocity, used to measure sedimentation and diffusion coefficients. Only sedimentation velocity will be treated here, and the interested reader should consult other sources for principles of sedimentation equilibrium. [92;93]

To begin a discussion of sedimentation one must first consider a particle sinking through a fluid in a gravitational field. Three forces act on the particle: a gravitational force, a buoyant force and a frictional force. If the particle is sinking, the gravitational force is greater than the buoyant force or

$$mg > m\nu\rho g \qquad (2.8)$$

where ν is the particle partial specific volume, g is the acceleration due to gravity, ρ is the solvent density and m is the mass of the particle. As the particle moves, it experiences friction with the solvent with a frictional force that is proportional to its velocity, V, and a frictional coefficient, f. At some point a terminal velocity, V_t, is reached where the sum of the three forces is zero.

$$mg - m\nu\rho g - fV_t = 0 \tag{2.9}$$

Solving for V_t gives:

$$V_t = \frac{m(1-\nu\rho)\omega^2 r}{f} \tag{2.10}$$

In a sedimentation velocity experiment the gravitational acceleration is replaced by the negative of the centripetal acceleration (or centrifugal acceleration in some texts), $\omega^2 r$ where ω is the angular velocity of the rotor and r is the distance from the center of the rotor. The ratio of the terminal velocity to this "centrifugal acceleration" is defined as the sedimentation coefficient, s.

$$s = \frac{V_t}{\omega^2 r} \tag{2.11}$$

or

$$s = \frac{m(1-\nu\rho)}{f} \tag{2.12}$$

using equation 2.10.

An optical system follows the position of the particles over time. To obtain a sedimentation coefficient it is convenient to rewrite equation 2.11 as the differential equation:

$$s = \left(\frac{dr}{dt}\right)\left(\frac{1}{\omega^2 r}\right) \tag{2.13}$$

Integrating this equation gives:

$$\ln\left(\frac{r}{r_o}\right) = \omega^2 st \tag{2.14}$$

A plot of $ln\ (r/r_o)$ versus $\omega^2 t$ should yield a straight line with slope s. The sedimentation coefficient has units of seconds but is most commonly expressed in units of Svedbergs, S, where $1\ S = 10^{-13}$ seconds

In a typical experiment, a solution containing a large number of particles is used. In this case, the particles will sediment as a boundary that moves down the cell. Because of the generated concentration gradient, diffusional forces contribute to particle transport by opposing the sedimentation. The rotor angular velocity is selected as to allow sedimentation to overwhelm diffusion, which tends to broaden the otherwise sharp boundary. Usually the particle position used in the calculation of s is taken as the midpoint (inflection point) of this boundary.

2.3.2.2 EXPERIMENTAL METHOD

The analytical ultracentrifuge used in this study is a Beckman XL-A. The instrument uses absorption optics to measure the concentration of sedimenting particles. The instrument is essentially a preparative ultracentrifuge equipped with a Xenon lamp coupled to a stepper motor and a monochromator. The lamp flashes through the windows of a cell and desired wavelengths are selected via a monochromator and detected by a photomultiplier tube. A detector slit sweeps the length of the cell, which consists of a double-sector centerpiece, sandwiched by two quartz windows. The sectors are wedge-shaped to allow the particles to freely sediment radially without hitting the sides of the sector. Usually one of the sectors contains solvent only and the other contains solvent plus solute. The instrument subtracts the solvent absorbance from that of the solution at each point in the solution column.

Typically, a rotor speed is chosen to produce a sharp, sedimenting boundary while still allowing several scans to be taken before the material pellets out of solution. Rotor speeds of 7,000 to 8000 revolutions per minute were typically used. The wavelength is usually chosen as

to give an initial plateau absorbance of about 0.5-1.0. The Beckman XL-A is capable of scanning at wavelengths from 190 to 800 nm.

The simplest method of extracting the sedimentation coefficient from sedimentation velocity data is by taking the slope of the $ln(r/r_o)$ versus $\omega^2 t$ plot as mentioned earlier. The value of r is taken as the midpoint of the boundary. Not described here are other analysis methods which involve curve fitting the sedimenting boundary. This can theoretically yield both sedimentation and diffusion coefficients from one data set. The data analysis package used in this study came with the instrument. To allow for more standard comparison, the s value is often reported as the value for 20°C in water and so is corrected accordingly by taking into account the temperature dependence of the viscosity and density of water:

$$s_{20,w} = \frac{s\left(\frac{\eta}{\eta_{20,w}}\right)\left(1-\nu\rho_{20,w}\right)}{\left(1-\nu\rho\right)} \qquad (2.15)$$

2.4 PREPARATION OF SAMPLES

2.4.1 DYNAMIC LIGHT SCATTERING SAMPLES

One of the biggest obstacles to preparing useful light scattering samples is the elimination of the large particulate matter commonly referred to as dust. Unfortunately, intact TMV particles are relatively large and fragile, rendering sample filtration difficult, though some studies have described TMV filtration through syringe filters .[82;86] For this study, only the buffer was filtered and the TMV used as prepared from the purification procedure. The low concentrations of TMV used ensure that dust from preparations is small.

The glass culture tubes used for DLS were rinsed well with water from a Barnstead Nanopure water purification system, which produces dust-free, de-ionized water. Cells were

checked for dust by viewing a rinsed cell full of this ultrafiltered water at an angle of 30 degrees in the DLS instrument using the 100x magnification viewing port. If no dust was seen for about 15 seconds the cell was considered clean, dried in a vacuum oven and weighed. As the viewing volume is many times larger than that during measurement, 15 seconds is an adequate indicator of cleanliness. Buffer, consisting of 0.01 M phosphate, 0.003 M sodium azide at pH = 7.5, was filtered directly into the cell through a 0.1 μm Millipore Millex VV syringe filter. The cell was checked again for dust at 30 degrees in the DLS apparatus. An appropriate amount of stock TMV was added via a Pipetman pipettor, the tip of which was well rinsed with Nanopure water. The TMV concentration was chosen to be 0.5 mg/mL as used in the experiment in Ref 44. The concentration of the stock was determined using an absorbance of 3000 cm^2g^{-1} at 260 nm.[65] The TMV solution was mixed by rotation (about 10 rpm) at a 30-degree angle from the horizontal using a home-designed rotator made from a standard hobby servo. Samples were mixed for several hours each day for 3-4 days. This slow mixing method was chosen to prevent shear degradation of the particles that might occur with more violent mixing action. When light scattering runs produced intensity traces with no large-scale "waves", the solution was deemed mixed. The TMV solution was stored at 4°C when not in use.

2.4.2 ANALYTICAL ULTRACENTRIFUGATION SAMPLES

The samples for analytical ultracentrifugation characterization were prepared exactly as for DLS except that the solution was prepared in a clean machine vial, not a DLS cell. Sedimentation runs were made at a dilute TMV concentration of 0.5 mg/mL. The solutions were added to the centrifuge cell via a Pipetman fitted with a gel-loading tip. All TMV solutions were stored at 4°C when not in use.

2.5 RESULTS AND DISCUSSION

The Hv DLS correlation functions were analyzed by a regularization method (based on CONTIN, a Laplace inversion program) included in the ALV-5000 software. A bimodal distribution of decay rates was usually present for TMV at 0.5 mg/mL (dilute regime) with a very weak fast mode (most likely TMV fragments, which are a known contaminant in TMV preparations) and a larger, slower mode which varied linearly with q^2 as seen in the example in Figure 3. The intercept leads to $D_r = 343 \pm 6\ s^{-1}$ at 24.8 °C. Correcting to 20 °C gives $D_{r20w} = 299 \pm 6\ s^{-1}$ which is well within the range of literature values[77] which have a mean of about 315 s^{-1}. Agreement with theoretical predictions is quite good with $D_r = 294\ s^{-1}$ expected for L= 300 nm and d = 18 nm from Broersma's equations for diffusion of rods. [94-96] The predicted value from another theoretical description gives $D_r = 316\ s^{-1}$. [97;98] The slope of Figure 3 gives $D_t = (5.1 \pm 0.1) \times 10^{-8}\ cm^2\ s^{-1}$ at 24.8 ºC. Correcting to 20 ºC gives $D_{t20w} = (4.5 \pm 0.1) \times 10^{-8}\ cm^2\ s^{-1}$. This value is higher than many literature values which average about $3.4 \times 10^{-8}\ cm^2\ s^{-1}$; however, a study by Wilcoxon and Schurr revealed a value of $D_{t20w} = 4.19 \pm 0.10 \times 10^{-8}\ cm^2\ s^{-1}$ and the authors discussed some of the problems with earlier studies. [86] The value measured here is about 10% higher than the Wilcoxon and Schurr value and very close to the theoretical prediction of $4.52 \times 10^{-8}\ cm^2\ s^{-1}$ by Tirado.[97] Within experimental error, our value is about 10% higher than that of Broersma's prediction of of $4.02 \times 10^{-8}\ cm^2\ s^{-1}$.[94-96]

Raw sedimentation data for TMV at 0.3 mg/mL (dilute regime) is found in Figure 4, which is an overlay plot of several scans taken 15 minutes apart at a rotor speed of 9,000 RPM. The large negative peak is the meniscus in the reference cell and the large positive peak is the sample meniscus which represents the initial radial position, r_o, to which the radial position of the moving boundary, r, is referenced. The boundary is fairly sharp with some diffusional

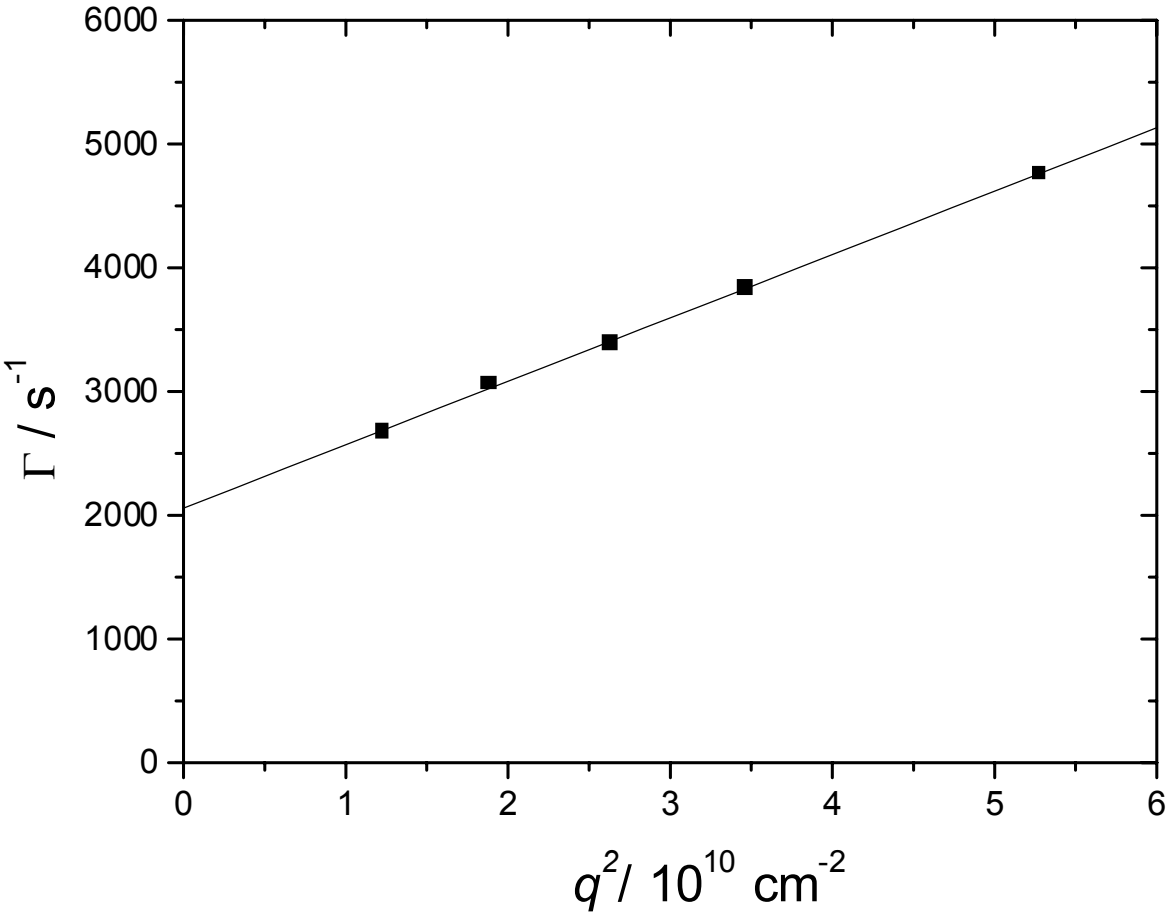

Figure 3. Dependence of Γ_{Hv} on squared scattering vector magnitude for TMV in buffer (c= 0.5 mg/mL) at 24.8 ºC.

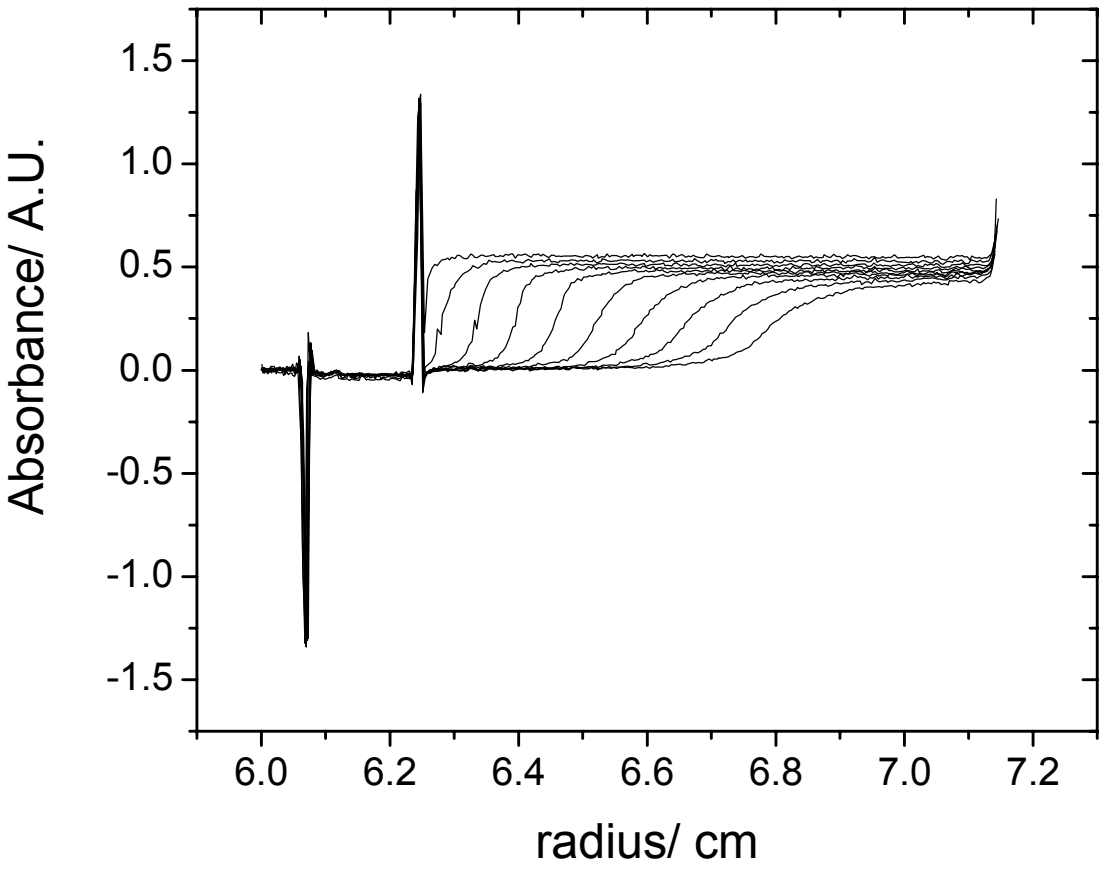

Figure 4. Overlay plot of radial scans with a 15 minute interval at a rotor speed of 9,000 RPM for TMV at 0.3 mg/mL.

broadening in the later scans. The decreasing absorbance at the plateau as the run progresses is normal and is the result of radial dilution.[92;93] A plot of $ln\ (r/r_o)$ versus $\omega^2 t$ appears in Figure 5. The slope of a linear fit yields $s_{20w} = 190 \pm 5$ S, which agrees well with 188 S at infinite dilution obtained by Boedtker and Simmons. [65] The TMV molecular weight can be obtained using

$$M = \frac{sRT}{D_t(1-\nu\rho)} \tag{2.16}$$

where R is the gas constant, ρ is the solvent density and ν is the partial specific volume. Using ν= 0.73 mL/g and the measured s and D_t values gives M= 38.0×10^6 which is a normal value. [65]

2.6 SUMMARY

Tobacco mosaic virus, a rod-like plant virus, was isolated from infected leaves via differential centrifugation. The virus particles obtained were characterized by analytical ultracentrifugation, which measures the sedimentation coefficient, and depolarized dynamic light scattering which measures translational and rotational diffusion coefficients. All the solution constants measured agree well with published literature values and theoretical predictions yielding $s_{20w} = 191 \pm 5$ S, $D_{t20w} = (4.5 \pm 0.1) \times 10^{-8}$ cm^2 s^{-1}, and $D_{r20w} = 299 \pm 6$ s^{-1}. The TMV was found to be intact and behaving normally.

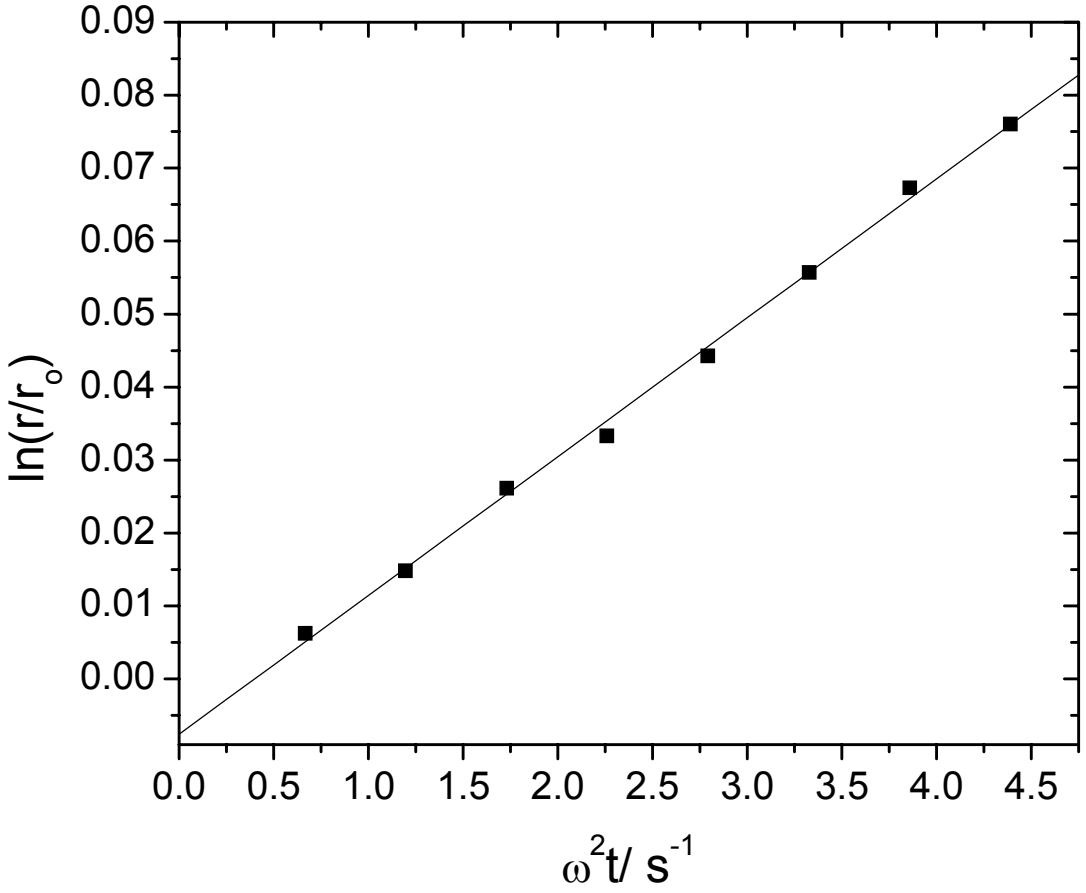

Figure 5. Dependence of the log of the ratio of the position of the moving sedimenting boundary to the meniscus position as a function of the product of $\omega^2 t$. The slope gives the sedimentation coefficient, *s*.

CHAPTER 3

CHARACTERIZATION OF FICOLL AND DEXTRAN

3.1 INTRODUCTION

The goal in selecting the matrix polymers was to find one system resembling a random coil that should entangle at high concentration and one system resembling a spherical globule that should not entangle, and to compare them. The polymers selected for this probe diffusion study were two polysaccharides, dextran (coil-like) and ficoll 400 (globular). Dextran is a natural, linear polysaccharide found in bacteria and yeasts and consists of α-1-6 linked glucose residues with occasional α-1,2, α-1,3, or α-1-4 linked branches; the type and degree of branching depends on the organism species from which it is derived. [99] [100;101] The dextrans used in this study were derived from the bacteria Leuconostoc mesenteroides B-512 which produces a dextran with 95% α-1,6 linkages and 5% α-1,3 branch linkages.[101] About 85% of the branches consist of only one or two glucose units, [102] but the nature of longer branches remains uncertain. Above a molecular weight of 2000, dextran behaves nearly as a random-coil polymer, [103-105] despite the small amount of branching that detracts from the ideality of the system as a model random coil. Ficoll is a highly internally-crosslinked copolymer of sucrose and epichlorhydrin and behaves as a compact, globular particle in solution. [106;107] The structures of both polysaccharides are shown in Figure 6. [108;109]

In studies involving polymers, it is important to know the average polymer size and size distribution. In probe diffusion studies, knowing the radius of gyration of the matrix polymers allows for estimation of the chain overlap concentration, which can be blurred by high polydispersity. One of the most powerful methods for obtaining the size and size distribution of polymers is Gel Permeation Chromatography with Light Scattering detection (GPCLS).

Another often-used polymer characterization method is rheology, which deals with the way a system responds to an imposed mechanical force. Its most simple form, viscometry, is

a.

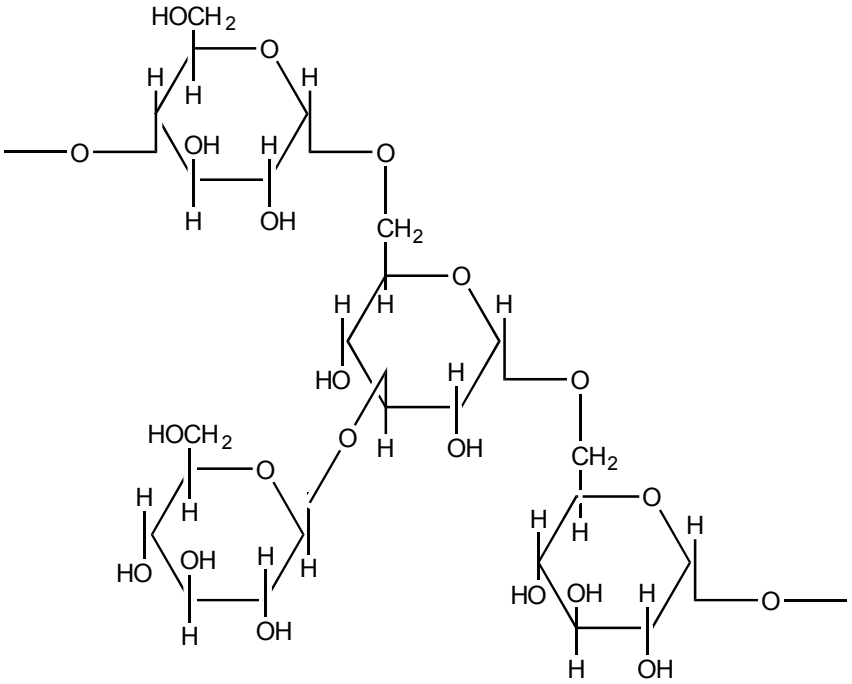

b.

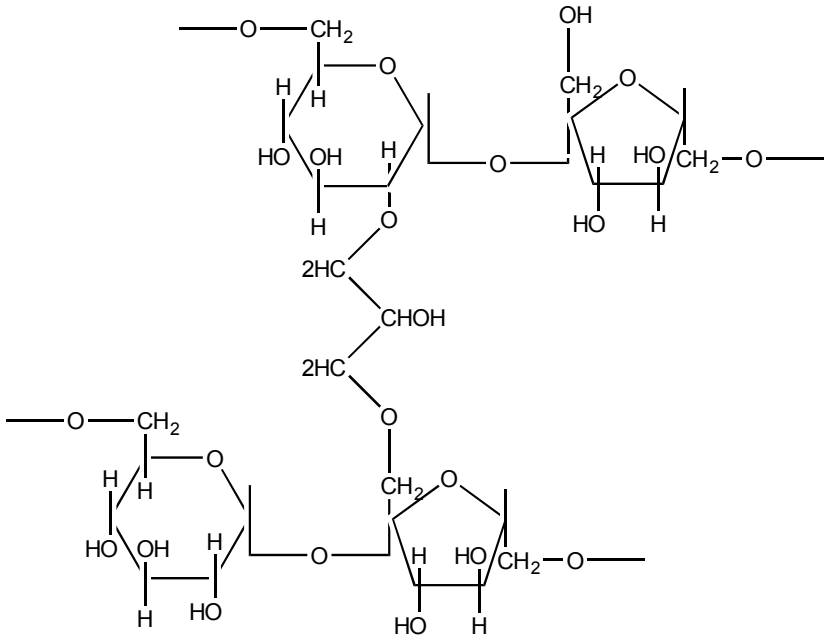

Figure 6. Structures of dextran (a) including a branch linkage (α1,3) and ficoll (b).

used to measure the viscosity of polymer solutions. The concentration dependence of the viscosity can be used to obtain such information as polymer molecular weight, shape, degree of branching and the concentration at which coils begin to overlap. Viscometry was used in this study simply for measuring the macroscopic viscosity of ficoll and dextran solutions at various concentrations and for obtaining an estimate of the coil overlap concentration from the intrinsic viscosity.

3.2 BACKGROUND

3.2.1 GEL PERMEATION CHROMATOGRAPHY

3.2.1.1 PRINCIPLES

Gel Permeation Chromatography (GPC) is a form of High Performance Liquid Chromatography (HPLC) that involves the separation of molecules according to their hydrodynamic size. It is one of the most powerful and widely used polymer characterization techniques. Combined with light scattering detection it can be used to determine the molecular weight, radius of gyration and molecular weight distribution of most polymers.

The separation is accomplished by means of columns packed with spherical, porous particles. A polymer solution is injected onto the column and polymers that are small enough diffuse or permeate the column particle pores, becoming temporarily trapped. Hydrodynamically smaller polymers spend more time in pores (less time in the mobile phase) and so elute later than larger polymers. In plain GPC, the time required for sample elution is compared to a standard curve generated using polymers of similar structure to the sample and of known size. In GPCLS (Gel Permeation Chromatography with Light Scattering detection), no calibration is needed as the size of eluting particles is determined absolutely by static light scattering (SLS) using an inline detector that follows the separation column. Briefly, static light

scattering involves measuring the time-averaged scattering intensity of a macromolecule solution as a function of scattering angle. Combined with a concentration detector, one can measure (absolutely) the molecular weight and radius of gyration by

$$\frac{Kc}{R} = \frac{1}{M}\left(1 + \frac{q^2 R_g^{\ 2}}{3}\right) \qquad (3.1)$$

in the limit of low concentration and low qR_g where K is an optical constant, c is concentration, R is the Rayleigh ratio (proportional to the excess scattering of the solution), and q is the scattering vector magnitude. The value of R_g can only be measured for macromolecules that have a R_g greater than about $\lambda_o/50n$ where n is the refractive index. The instruments measure the intensity at many angles simultaneously using several fixed photodetectors arranged around a fixed scattering flow cell. Concentration, which is measured online, is usually very low by the time the macromolecules reach the light scattering detector due to the small loading volume and subsequent separation process. Since the concentration and molecular weight of each separated species is known, the weight average molecular weight (M_w) and number average molecular weight (M_n) can be determined. The ratio M_w/M_n characterizes the polydispersity of the sample.

3.2.1.2. EXPERIMENTAL METHOD

A schematic of the GPCLS setup used in this study is given in Figure 7. The mobile phase, which was filtered and degassed by simultaneous sonication and vacuum filtration through a 0.1 μm Gelman filter, was delivered via Waters 5000M dual piston pump. A 0.2 μm Whatman inline filter/degasser was placed before the pump and a 0.5 μm inline filter was placed after the pump. Samples were filtered through 0.2 or 0.45 μm Nalgene syringe filters upon injection to remove dust. The column was a Polymer Labs PL-Aquagel mixed bed column with a molecular weight exclusion range of about 500 to 5,000,000 for compact structures. The light

scattering detector was a Wyatt Dawn DSP-F that was followed in line by a Waters 501 differential refractive index detector which provides concentration information The Wyatt calibration constant was measured using 0.1 μm filtered toluene and the DRI detector constant using potassium chloride solutions. The Wyatt detectors were normalized using bovine serum albumin.

The samples characterized by GPCLS include ficoll 400 (Pharmacia) and dextrans of molecular weights ranging from 40k to 2,750k. Dextrans were obtained from several sources including Polysciences for dextrans of MW ≈ 40k to 600k (cat# 19412, 19413, 19414, 19415), Polymer Standards Services for dextran of MW ≈ 670k to 2,750,000 (cat# dxt670k, dxt2370k, dxt2750k), and Sigma for dextran of MW ≈ 413k (cat# D-1037). Samples were run at concentrations ranging from about 2mg/mL for the largest dextrans to 8mg/mL for the smallest ones using an injector loop holding 50μL. A flow rate of 0.8ml/min was usually used.

3.2.2 VISCOMETRY

3.2.2.1 PRINCIPLES

Rheology is the study of flow and deformation of matter. Its simplest form, viscometry, is used to measure the macroscopic viscosity of a solution. A brief introduction to viscometric principles will be given here; details can be found in other sources.[110;111]

The simplest "rheometer," the viscometer, imposes a shearing flow on a liquid sample and measures the resulting stresses. The samples can be sheared in various ways, depending on the geometrical arrangement of the instrument. The simplest such design is the plate-plate geometry where a solution is sandwiched between two closely spaced parallel disks, one of which rotates. The most commonly used design is the cone-plate method where the rotating disk is replaced by a low angle cone-shaped spindle that rotates at a precise speed very close to a

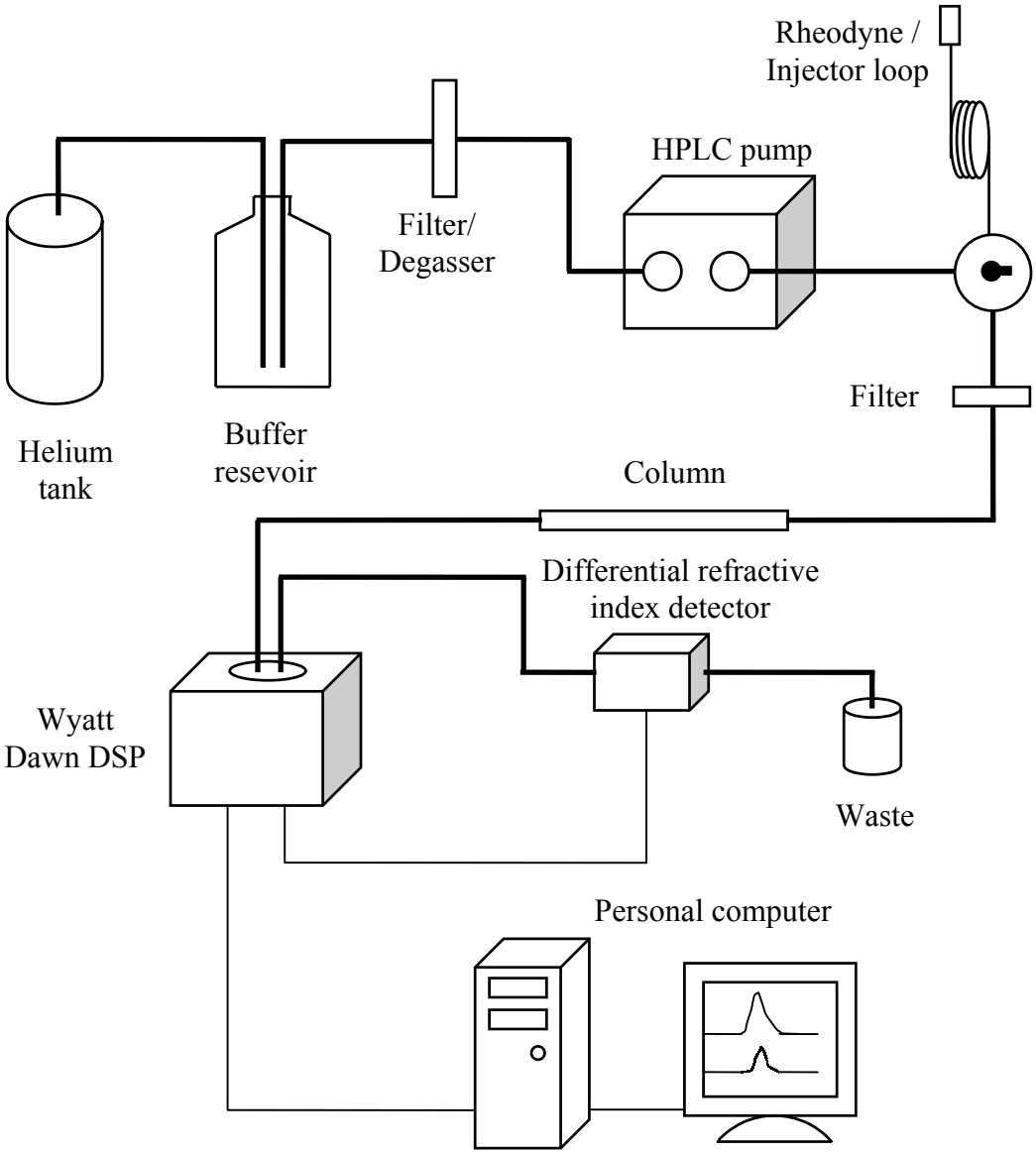

Figure 7. Diagram of the gel permeation chromatography with light scattering detection setup. Thick lines represent solvent flow and thin lines represent data flow.

stationary flat plate. Again, the sample is sandwiched in between the cone and plate. The device measures the torque necessary to overcome the viscous drag caused by the presence of the solution and this torque is proportional to the solution viscosity, η. By varying the speed of rotation, the shear rate can be varied. The cone-shaped spindle provides constant shear rate at all points along the radius, an advantage over the simpler plate-plate design.

The viscosity of a solution of polymer chains usually increases slowly (almost linearly) at low concentrations and then builds more rapidly at higher concentrations as polymer chains begin to overlap. This overlap concentration, c^*, can be related to a quantity known as the intrinsic viscosity, [η], which is defined as:

$$[\eta] = \lim_{c \to 0} \frac{\eta_{sp}}{c} \equiv \lim_{c \to 0} \frac{\ln \eta_{rel}}{c} \qquad 3.2$$

where η_s is the solvent viscosity, the specific viscosity $\eta_{sp} = (\eta - \eta_s)/\eta_s$ and the relative viscosity $\eta_{rel} = \eta/\eta_s$. The intrinsic viscosity can be determined from a plot of η_{sp}/c versus c or from a plot of $\ln \eta_{rel}/c$ for a series of low concentrations by extrapolating to zero concentration. Essentially, the intrinsic viscosity represents the volume occupied by a polymer per unit mass, as suggested by the inverse concentration units. The value of $1/[\eta]$ represents the concentration within a polymer and is often used as an approximation for c^*.

One of the signatures of an entangled solution or melt is the $\eta \sim M^{3.4}$ observed scaling for viscosity. [7;10] Due to lack of material, viscosities of the dextrans of varying molecular weights used in this study were not measured. Previous studies of dextran have found a scaling exponent of only 0.8 for 25 wt% dextran solutions. [112] Other rheological evidence for onset of entanglement is a plateau in the measured storage modulus, G', the value of which is often called the entanglement plateau modulus, G^0_N. [110] The storage modulus measured by dynamic viscosity

measurements in which oscillatory shearing is taking place. The applied strain oscillates sinusoidally, and the resulting sinusoidally varying stress can be represented as

$$\sigma(t) = \gamma_0 \left[G'(\omega)\sin(\omega t) + G''(\omega)\cos(\omega t) \right]. \qquad 3.3$$

The term proportional to $G'(\omega)$ is the storage modulus and is in phase with the strain. The $G''(\omega)$ term is in phase with the rate of strain and is called the loss modulus. The storage modulus G' represents the storage of elastic energy and would be a level function of the shear rate for a solid, and increasing function for a liquid. At shear rates high enough to overcome losses due to reptation, it is expected that G' will increase with shear rate and level off in entangled solutions and melts. In melts the minimum molecular weight at which such a plateau is observed is often called the M_c or critical molecular weight. Attempts to measure G' of the various dextrans used in this study failed due to equipment problems. Work by others suggests that there is not a plateau modulus for dextran, even at very high concentrations. [112;112;113]

3.2.2.2 EXPERIMENTAL METHOD

The cone-plate viscometer used in this study is a Wells-Brookfield LVTDCP. The instrument reports the torque data digitally which is then converted to a viscosity using a factor appropriate for a given spindle model and shear rate. The sample cup temperature was controlled to ± 0.1 °C using a Lauda recirculating bath. Sample size for the spindle used in this setup was 0.5 mL. The system calibration was verified with pure water before measurement.

Ficoll and dextran samples used in this experiment were made by dissolving an appropriate amount of polymer in 0.01 M phosphate buffer, pH = 7.5. Sodium azide, a bactericide, was not added due to possible chemical reaction with the stainless steel sample cup and spindle. All samples were measured within three days of preparation and stored at 4°C when not in use. Due to instrumental limitations, viscosities at only one or two shear rates were

possible and values were averaged. When two or more points were available, there was no significant dependence of viscosity on shear rate. Other studies confirm the Newtonian behavior of dextran and ficoll. [107;112;114]

3.3 RESULTS AND DISCUSSION

The GPCLS results for the dextrans appear in Table 1. The measured molecular weights and polydispersity values agree with the advertised values for many of the dextrans. The higher molecular weight dextrans (>2 million advertised MW) were consistently found to have lower molecular weights than advertised. Data sheets accompanying these samples suggest that the advertised values were derived from measurements by straight GPC without light scattering data, which is not an absolute method. Runs using very sharp fractions of well-characterized pullulan standards consistently gave numbers in excellent agreement with known values in our setup. Given the proven reliability and consistency of the system used here, it was felt that these dextrans may not be well characterized by the supplier, Polymer Standards Services. It is possible that the larger samples experienced some shear degradation in our system, which may be consistent with the noticeably lower polydispersity values. As all runs were performed at a constant flow rate, dependence of measured values on flow rate were not determined. All subsequent data presented will be plotted using the values measured here and not the advertised values, unless such a change dramatically influences any parameters determined by fits, then both values will be used. For consistency, advertised values will be kept in any tables. The ficoll 400 yielded a M_w = 428,000 ± 13,000 and a polydispersity M_w/M_n = 4.3. The root of the z-average of the squared radius of gyration was found to be 20 ± 3 nm.

The dependence of ficoll viscosity on concentration is found in Figure 8. To determine viscosities for exact concentrations used in DLS experiments, the curve was fit to two

Table 1 Weight average molecular weight, polydispersity and root of the weight average and z-average of the squared radius of gyration of dextrans by GPCLS.

		Advertised		Measured			
Catalog#	Lot#	$M_w/10^4$	M_w/M_n	$M_w/10^4$	M_w/M_n	R_g (R_w)/nm	R_g (R_z)/nm
19412[a]	497100	4.00	1.5	4.16 ± 0.15	1.1	-	-
19413[a]	503606	7.50	1.5	7.70 ± 0.36	1.3	-	-
19414[a]	410586	17.0	2.0	16.1 ± 0.64	1.7	17 ± 4	17 ± 3
D-1037[b]	90K-1897	41.3	-	37.0 ± 1.7	3.8	20 ± 3	21 ± 2
19415[a]	451049	60.0	1.7	53.6 ± 2.1	1.7	21 ± 2	24 ± 1
dxt670k[c]	- [d]	67.6	1.94	64.7 ± 3.0	1.7	19 ± 4	22 ± 2
dxt2370k[c]	- [d]	237	1.61	177 ± 3.4	1.3	24 ± 2	26 ± 2
dxt2750k[c]	- [d]	275	1.67	155 ± 3.0	1.4	28 ± 2	30 ± 2

[a] Polysciences. [b] Sigma. [c] Polymer Standards Services. [d] Same as catalog#

polynomials, one for concentrations below 11wt% and another for higher concentrations. The viscosity starts to rise quickly around 25 wt%. The concentration dependence of viscosity for a dextran of MW ≅ 647k (PSS cat# dxt670k) appears in Figure 9. The dotted line represents a similar two-stage polynomial fit. Plots of η_{sp}/c versus c and of ln η_{rel}/c appear in Figure 10 for dextran and ficoll. The y-intercepts of each type of plot (theoretically identical as mentioned above) vary slightly and the average value was taken as the intrinsic viscosity, [η]. The variation is likely due to lack of point density at what ideally would be lower concentrations. The values were determined to be [η] ≅ 0.52 dL/g for the dextran and [η] ≅ 0.15 dL/g for the ficoll 400. The value for ficoll agrees reasonably well with the advertised value by Sigma Chemical Co. of [η] ≅ 0.17 dL/g (www.sigma.com). No published value for the exact dextran used here could be found but the value is reasonable when compared to that of dextrans of similar molecular weight or molecular weights that bracket the one used here. [112;115;116] Taking the inverse of the intrinsic viscosity yields an overlap concentration of $c^* = 1.9$ wt% for the dextran and $c^* = 6.7$ wt% for ficoll 400.

3.4 SUMMARY

Samples of ficoll and dextran were characterized by Gel Permeation Chromatography with Light Scattering Detection. Measured values of molecular weight, radius of gyration and polydispersity agreed well with advertised values for most of the dextrans. Advertised values determined by the supplier differed greatly from measured values here for two of the samples. The macroscopic viscosity of ficoll 400 and a 647k MW dextran (dxt670k from Polymer Standards Services) was measured by cone/plate viscometry for a wide range of polymer concentrations. Values for intrinsic viscosity were determined to be [η] ≅ 0.52 dL/g for the dextran and [η] ≅ 0.15 dL/g for ficoll 400, in reasonable agreement with published values.

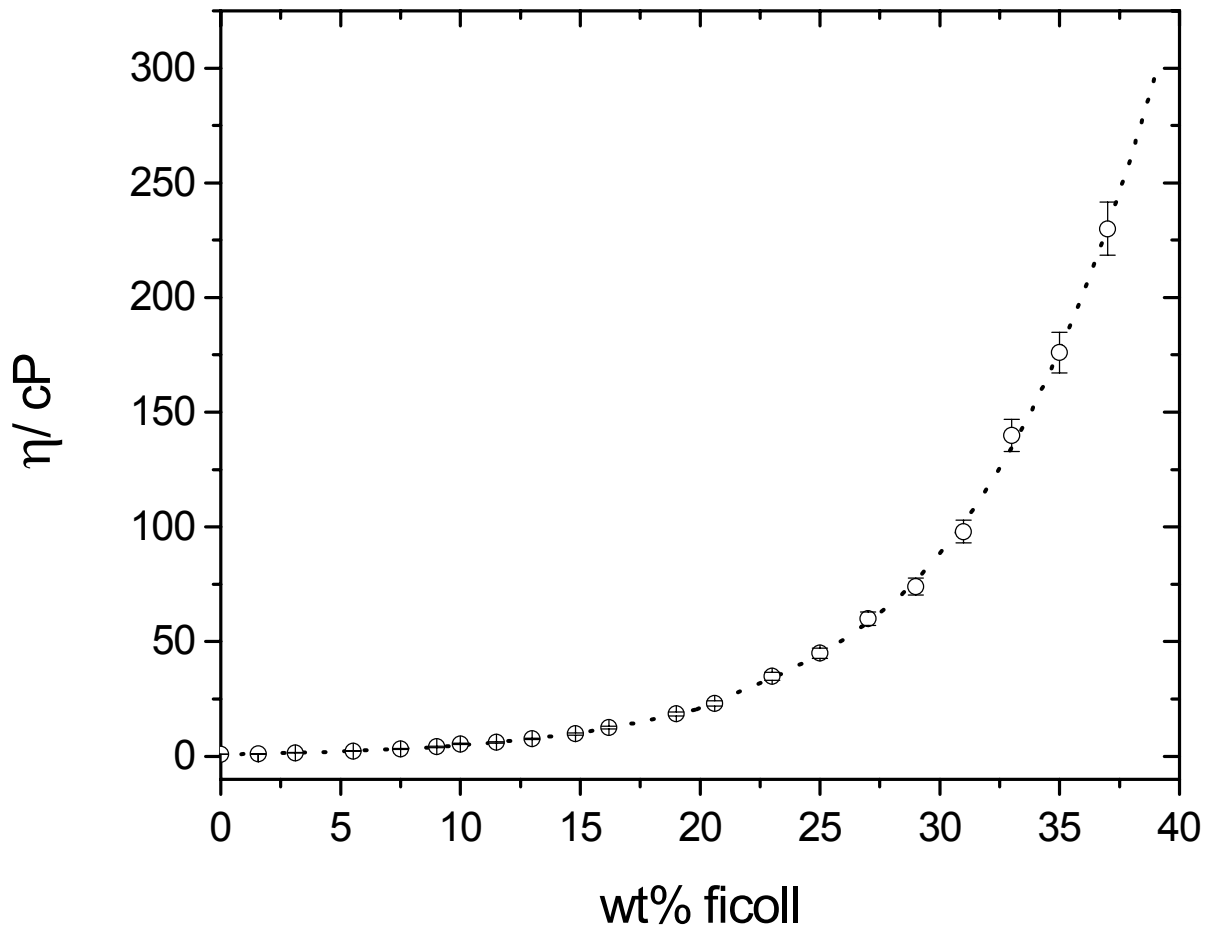

Figure 8. Concentration dependence of ficoll viscosity. Dashed line represents a polynomial fit performed in two stages (see text).

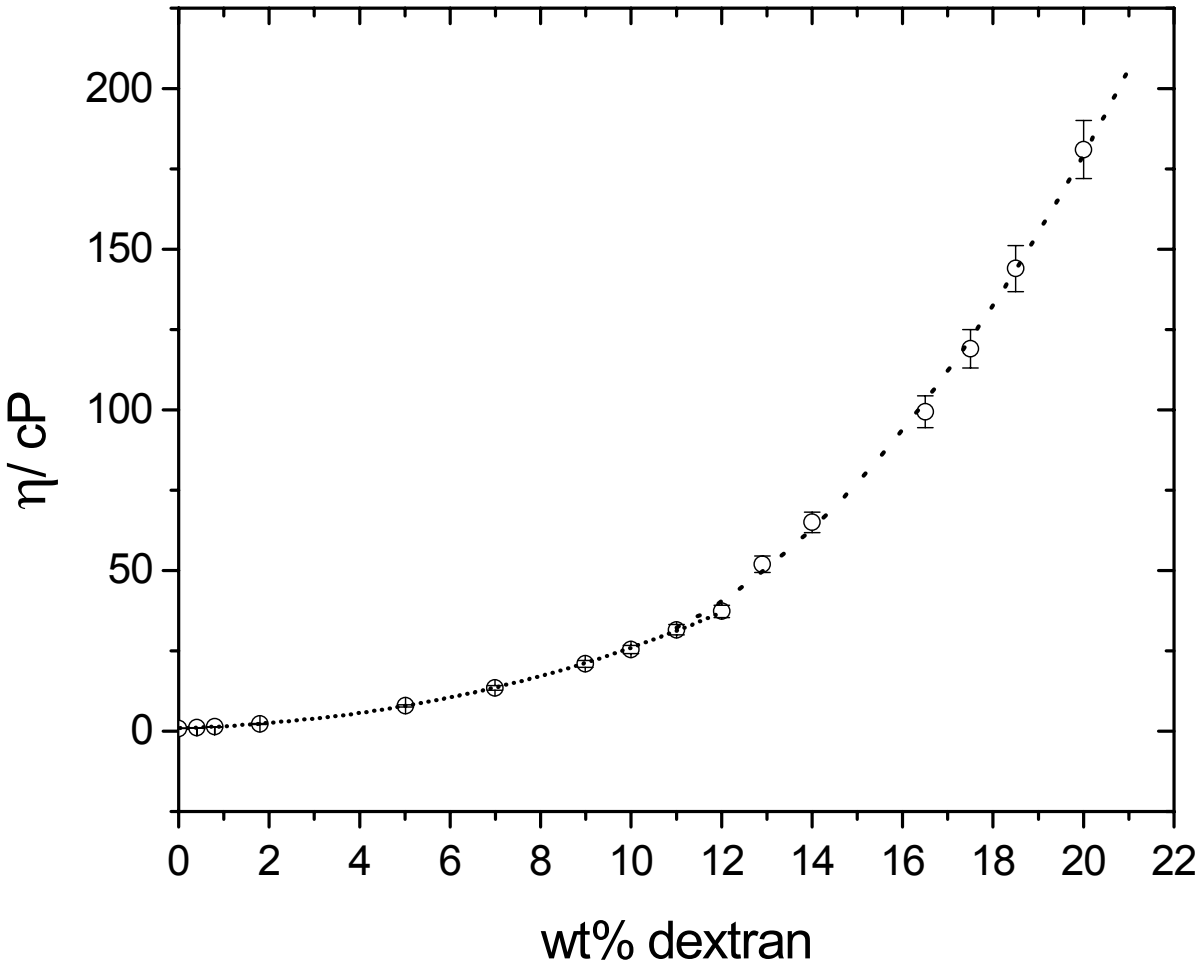

Figure 9. Concentration dependence of viscosity for a dextran of MW≈ 674k. Dashed line represents a polynomial fit performed in two stages (see text).

a)

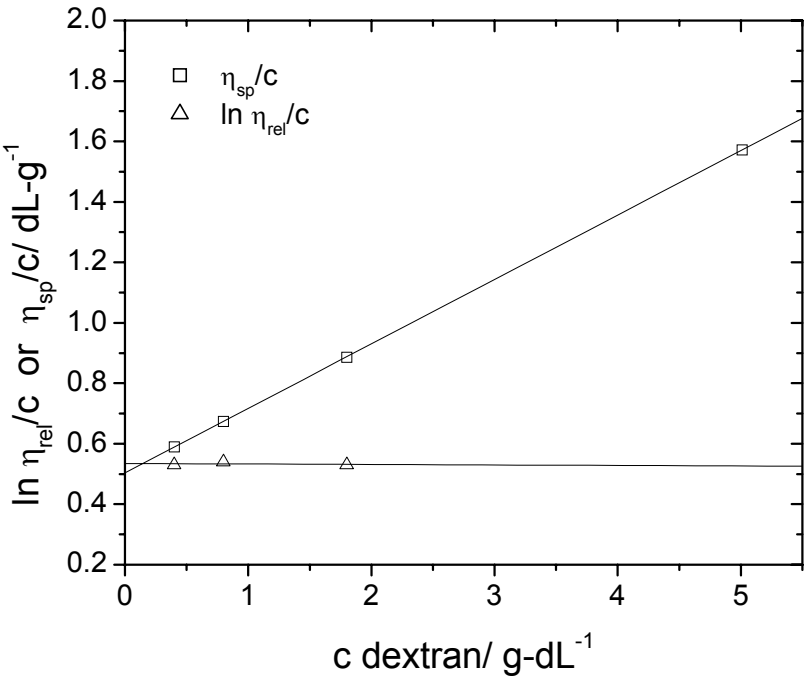

b)

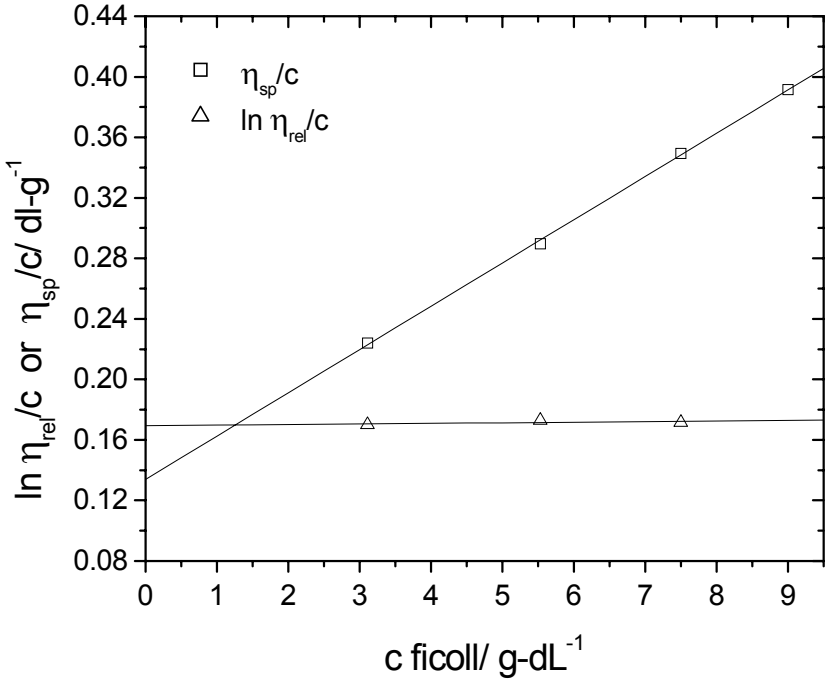

Figure 10. Dependence of the ratio of specific viscosity to concentration and of the natural log of relative viscosity to concentration on concentration for ficoll 400 (a) and for dextran of MW≈ 647k (b).

Overlap concentrations, taken as $1/[\eta]$, were found to be $c^* = 1.9$ wt% for the dextran and $c^* = 6.7$ wt% for ficoll 400.

CHAPTER 4

DIFFUSION OF TMV IN SOLUTIONS OF FICOLL AND DEXTRAN

4.1 INTRODUCTION

This study of TMV diffusion in ficoll and dextran solutions stems from earlier work in our lab on TMV diffusion in dextran.[56] In that study we observed a sharp decrease in the ratio of rotational to translational diffusion as the concentration of a 500,000 MW dextran was increased as seen in Figure 11. We attributed this sudden decrease to the onset of topological constraint to rotational motion relative to translational motion. This notion seemed reasonable given small angle x-ray scattering data and calculations for the dextran network mesh size yielding an average distance between strands of ξ=2.5 nm and an average distance between centers of mass of the chains of ξ_{cm} = 25 nm respectively where $\xi_{cm} = (c_{dextran} N_a / M_{dextran})^{-1/3}$. [56] Using the tube model, this corresponds to about 13 dextran chains surrounding each TMV particle (L/ξ_{cm} for rod of length L) supplying about 120 contacts (L/ξ). This suggests that the potential for topological constraints was present. Also, concentrations went well above $[\eta]^{-1}$ and η was rising rapidly. In addition, dramatic Stokes-Einstein failures were observed as seen in Figure 12 where diffusion coefficients are multiplied by viscosity; such deviations have been observed before as mentioned in section 1.1. If SE works, these plots should be flat. One area of concern in this work was values for the rotational diffusion coefficient that approached and eventually dipped below zero (within error). It was postulated that this was simply due to an inability to measure D_r reliably when rotation has slowed significantly. Given the uniqueness of the observed transition and potential uncertainties in D_r it was concluded that validity of depolarized DLS as a probe diffusion technique required testing in other systems. It was to this end that the present extension of this work was performed.

One goal of the current study was to see if such a transition would occur for polymers that should not form a transient network such as the internally cross-linked, compact

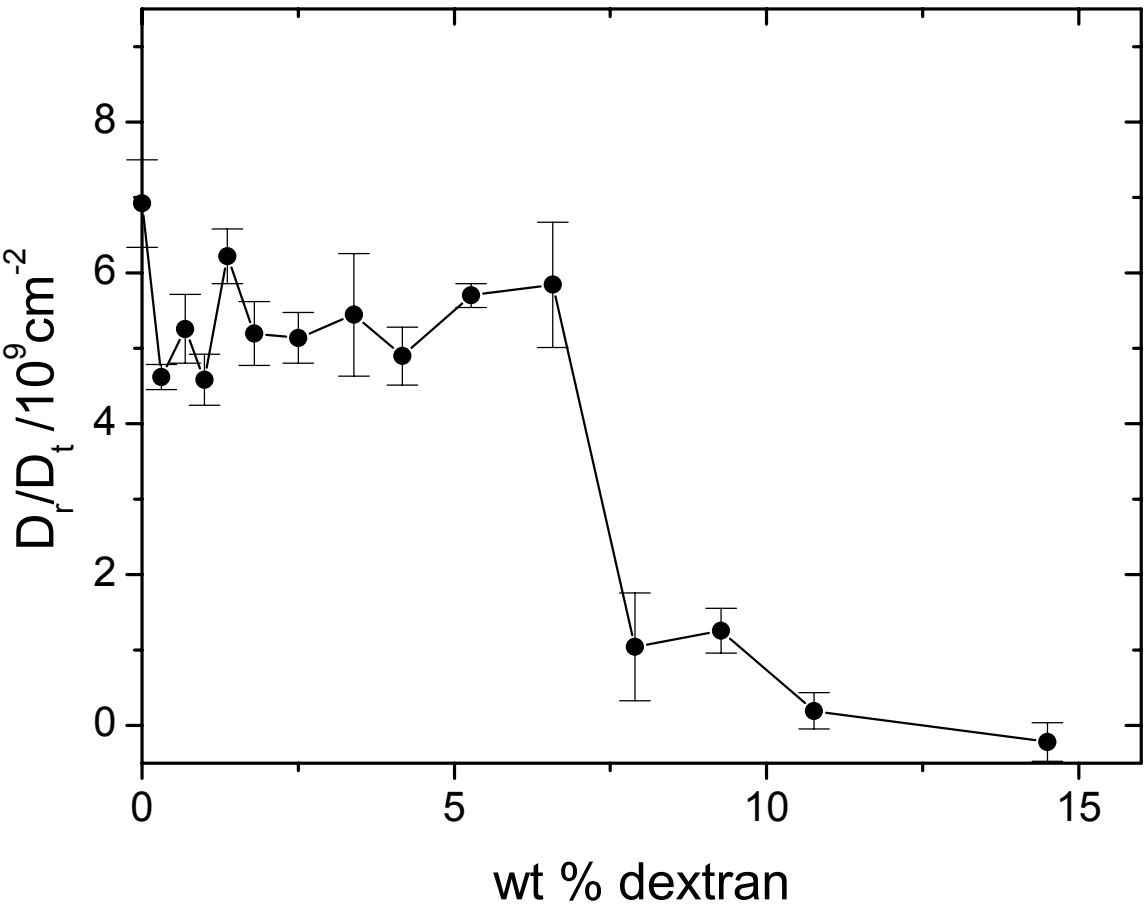

Figure 11. The ratio of rotational to translational diffusion of TMV in dextran vs concentration for a dextran MW≈ 500k.[56] Reproduced in part with permission from *Macromolecules* **1997**, *30*, 4920-4926. Copyright 1997 American Chemical Society.

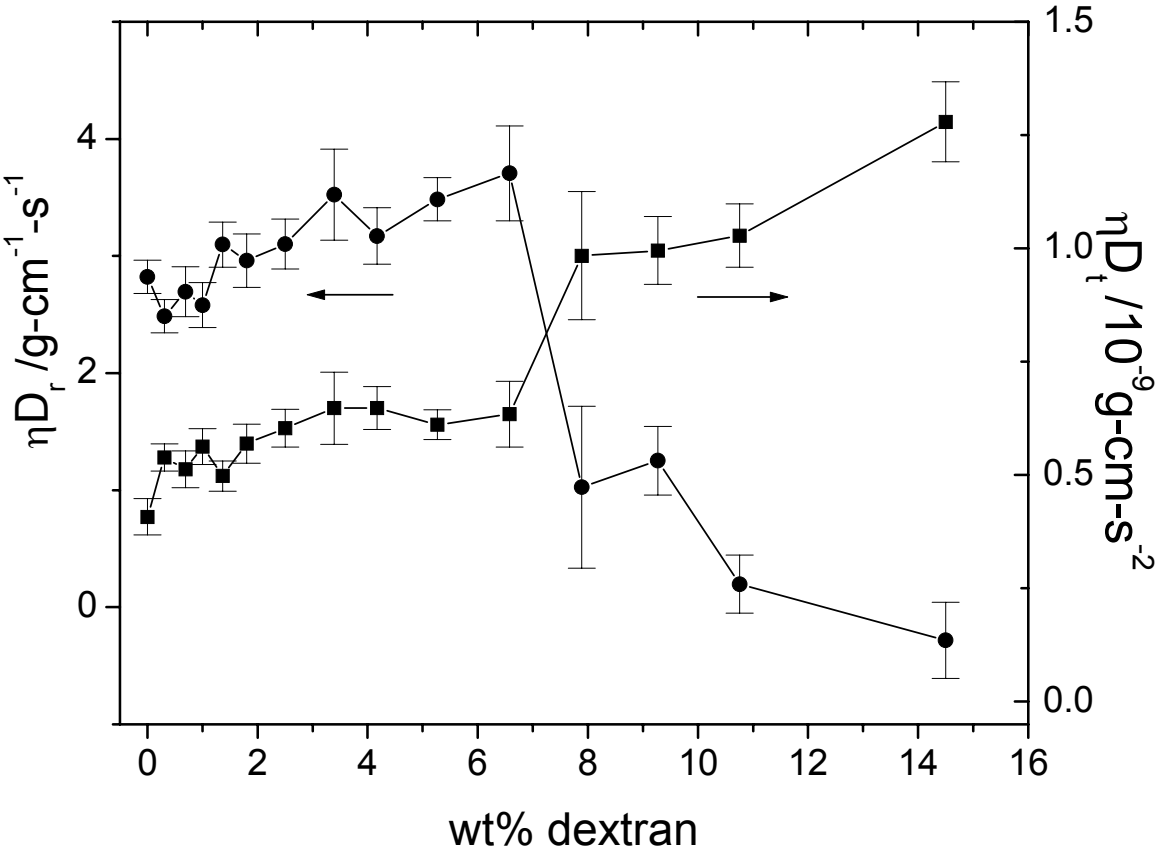

Figure 12. Product of solution viscosity and rotational diffusion coefficient (circles) and of solution viscosity and translational diffusion coefficient (squares) as a function of dextran concentration. [56] Reproduced in part with permission from *Macromolecules* **1997**, *30*, 4920-4926. Copyright 1997 American Chemical Society.

polysaccharide, ficoll. If hydrodynamic interactions dominate topological constraints then it may be expected that TMV cannot "sense" the difference between these polymers. Another goal was to see what effect dextran chain length had on TMV diffusion at a fixed concentration beyond the transition observed in the previous study. [56] As mentioned earlier, the mesh size of an entangled solution or melt should be molecular weight independent.[5] If any sudden transitions appear in TMV diffusion as a function of molecular weight, it might suggest that a critical molecular weight for entanglements (M_c) has been reached. For highly flexible polymers, M_c corresponds to about 300-600 atoms in the polymer chain. This corresponds roughly to a dextran of MW ~ 54k-108k.

4.2 EXPERIMENTAL METHODS

Depolarized dynamic light scattering (Hv DLS) was used to follow the translational and rotational diffusion of the TMV in solutions of either ficoll or dextran. The technique is explained in detail in section 2.3.1.1. The advantage of the technique in this experiment is that the rod-like TMV probe depolarizes significantly and the optically isotropic probed polymers, ficoll and dextran, do not depolarize much. This simplifies the experiment as TMV translation and rotation can be followed without significant scattering contribution from the matrix, a problem that usually complicates DLS probe diffusion experiments, especially in aqueous environments where refractive index matching of the matrix and the solvent is not possible. In addition, the depolarized intensity can be converted to an apparent radius of gyration, which can be used to check for aggregation of TMV particles. [117]

The translational diffusion of TMV in dextran solutions was also followed by fluorescence photobleaching recovery. This was done to compliment values for translational

diffusion measured by dynamic light scattering. Details of TMV labeling and the experimental methods appear in sections 5.2 and 5.3.

In both experimental methods it is important to keep the TMV concentration in the dilute regime to reduce interactions between the probe particles. The semidilute regime for rods of length L theoretically [6 25;26] begins at a number density of $1/L^3$, which corresponds to a TMV concentration of about 2.45 mg/mL. For all ternary solutions the TMV was held at a constant concentration of 0.5 mg/mL, well below this value.

4.3 PREPARATION OF TERNARY SOLUTIONS

The ficoll and dextrans, used without further purification, were prepared by allowing the appropriate amount of polymer to sit (or "swell") overnight in 0.01 M sodium phosphate buffer, pH = 7.5, with 0.003 M sodium azide. The solution was then mixed gently using 7 mm × 2 mm magnetic stirbars. Once dissolved, the solution was slowly filtered through a 0.10 μm Millex VV syringe filter, directly into a dust-free, weighed DLS cell. Part of this solution was filtered into a dry, weighed vial for later gravimetric analysis to check for polymer loss during filtration. One problem with this method is the difficulty in filtering highly viscous solutions through syringe filters. The filtering process was slow which increases the likelihood that dust from the air will enter the cell. An easier method of cleaning the samples was later found by preparing more dilute solutions (about 2 wt%) and filtering into a clean DLS cell and concentrating the solution using a Savant Speedvac concentrator. This device gently centrifuges samples under a vacuum generated by a vacuum pump using a refrigerated condenser to trap the vapors. Solutions were first dissolved in buffer at high concentration, (35% for ficoll and 18% for dextrans) and then diluted with pure water so that concentration in the Speedvac back to the original high concentration would not alter the salt concentration. To insure dust did not enter

the cell when the vacuum was released, a 0.1 μM Whatman Vacu-guard filter was inserted at the air inlet tube. Once the desired concentration was reached (determined gravimetrically), an appropriate amount of stock TMV solution was then added to give a final TMV concentration of 0.5 mg/mL. This method consistently produced highly concentrated polymer solutions with almost insignificant amounts of dust.

Once the TMV probe was added, the solution required mixing. Due to the delicate nature of the non-covalently assembled virus and the rather high viscosity of many of the solutions, it was felt that mixing needed to be slow. In addition, mixing a highly viscous sample at a high shear rates doesn't give the solution enough time to flow enough for efficient mixing. Samples were mixed using the slow rotating device described in section 2.4.1. The sample was usually rotated at 15 rpm for several hours per day for 1-3 days, depending on the solution viscosity. The sample was deemed mixed when no striations appeared in the solution and DLS experiments revealed no obvious large-scale intensity waves. Dilutions to lower ficoll concentrations were made using 0.5 mg/mL TMV solutions to keep the TMV concentration constant. All subsequent additions of this TMV diluent were done using a Pipetman with pipette tips rinsed well with dust free water.

4.4 RESULTS AND DISCUSSION

4.4.1 DIFFUSION OF TMV IN FICOLL SOLUTIONS

4.4.1.1 EFFECT OF FICOLL CONCENTRATION

As stated earlier (section 4.2) the advantage of this probe diffusion technique is that the probed polymer solution does not depolarize much light relative to TMV. To verify this, DDLS correlation functions were collected on ficoll alone. Seen in Figure 13 is a correlation function collected for 30 wt% ficoll with and without added 0.5 mg/mL TMV. There is little signal for

ficoll alone, which was a run of over 6000 seconds duration, but significant signal when TMV is added, for a run of only 300 seconds duration. The ficoll signal would be very noisy if run for the shorter duration used for the TMV measurement. After 6000 seconds, absence of low-frequency humps at long times testifies to the adequacy of the dust removal procedure.

Figure 14 shows a plot of Γ vs. q^2 for TMV alone and in some ficoll solutions. The slope (D_t) and intercept ($6D_r$) decrease with increasing ficoll concentration, while linearity between Γ and q^2 is maintained. The coefficients are plotted separately in Figure 15 for all concentrations used and as expected, diffusion coefficients decrease with increasing ficoll concentration (increasing viscosity). It should be noted that Error bars for this and all subsequent plots involving diffusion coefficents were derived from linear fits of Γ vs. q^2 and not from repeat measurements. The ratio of D_r/D_t appears in Figure 16, along with ficoll viscosity data. The quotient remains fairly level up to about 10 wt% ficoll (as expected by SE behavior if both coefficients are inversely proportional to viscosity), then begins to gradually decrease. This is similar to the behavior seen in Figure 7 (though less dramatic) for dextran [56] and suggests some constraint to rotational motion in ficoll solutions.

The product of diffusion and viscosity is plotted against ficoll concentration in Figure 17. A constant value would indicate Stokes-Einstein behavior. Notice that ηD_t increases slightly and ηD_r decreases significantly beyond about 12 wt% ficoll. This deviation from SE behavior means that rotation is more constrained than expected from viscosity and translation is slightly freer. Similar behavior was found in the previous study but the effect on translation was somewhat less significant here. In the previous TMV/dextran study, it was suggested that the observed decrease in the ratio of rotation to translation could be explained by the onset of an entangled transient network of dextran chains which hinders rotation but not, to a great extent, motion

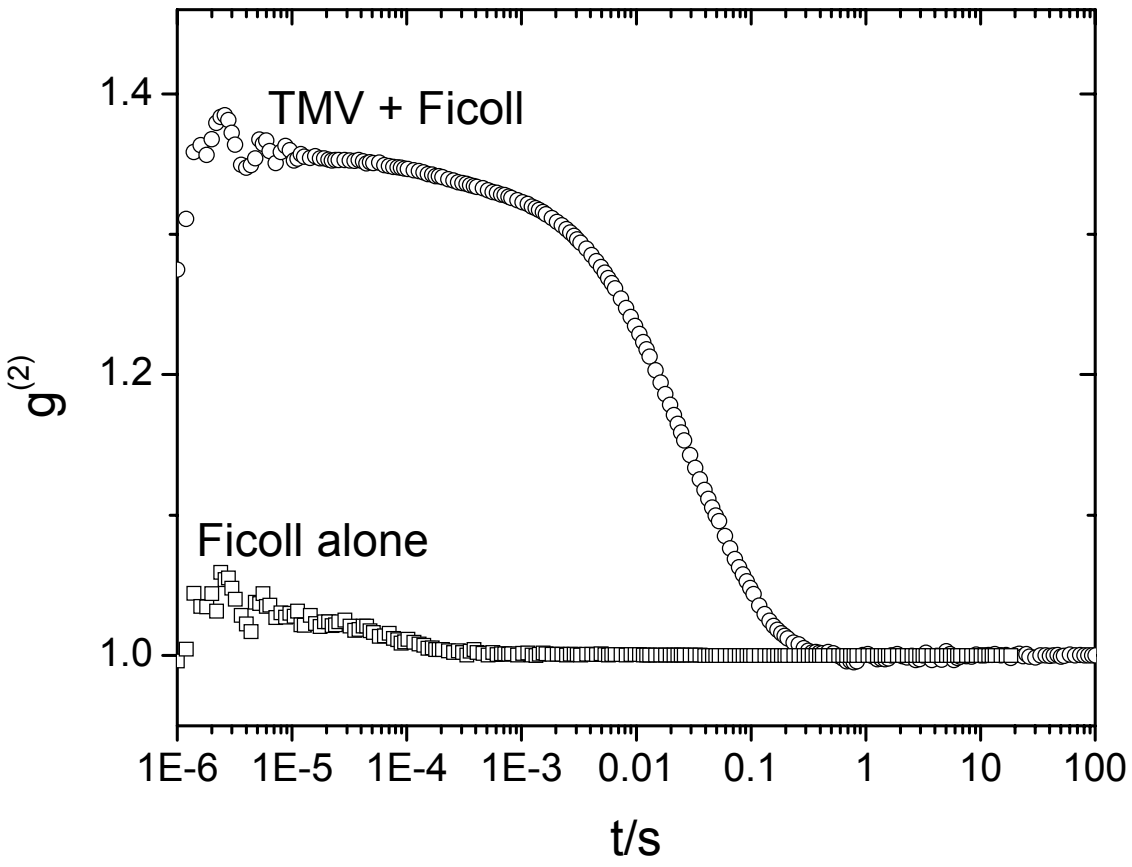

Figure 13. Hv correlation functions for samples of 30 wt% ficoll with and without added 0.5 mg/mL TMV. The collection duration for ficoll with 0.5mg/mL TMV added was about 300 seconds while that for ficoll alone was over 6000 seconds.

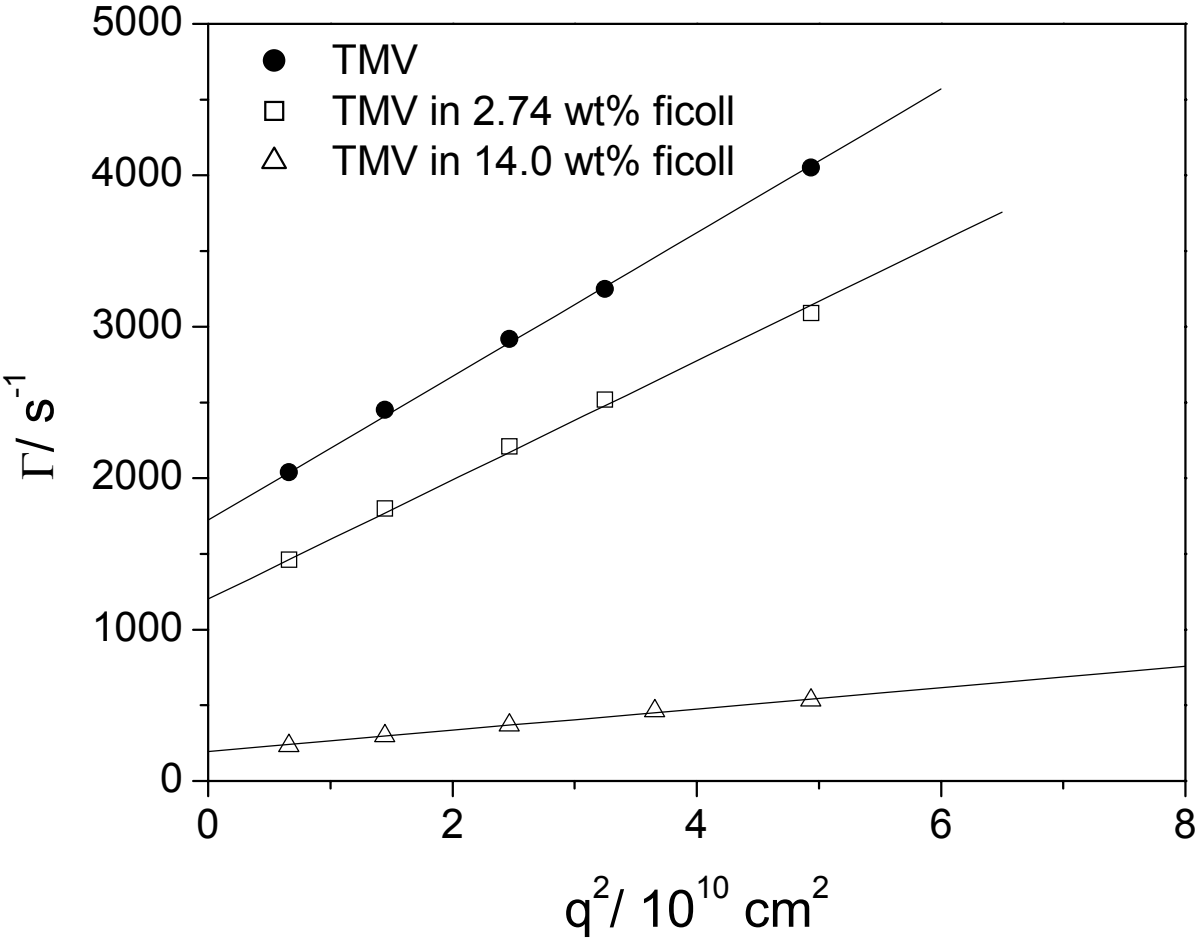

Figure 14. The dependence of Γ_{Hv} on squared scattering vector magnitude for 0.5 mg/mL TMV alone and in ficoll at two different concentrations.

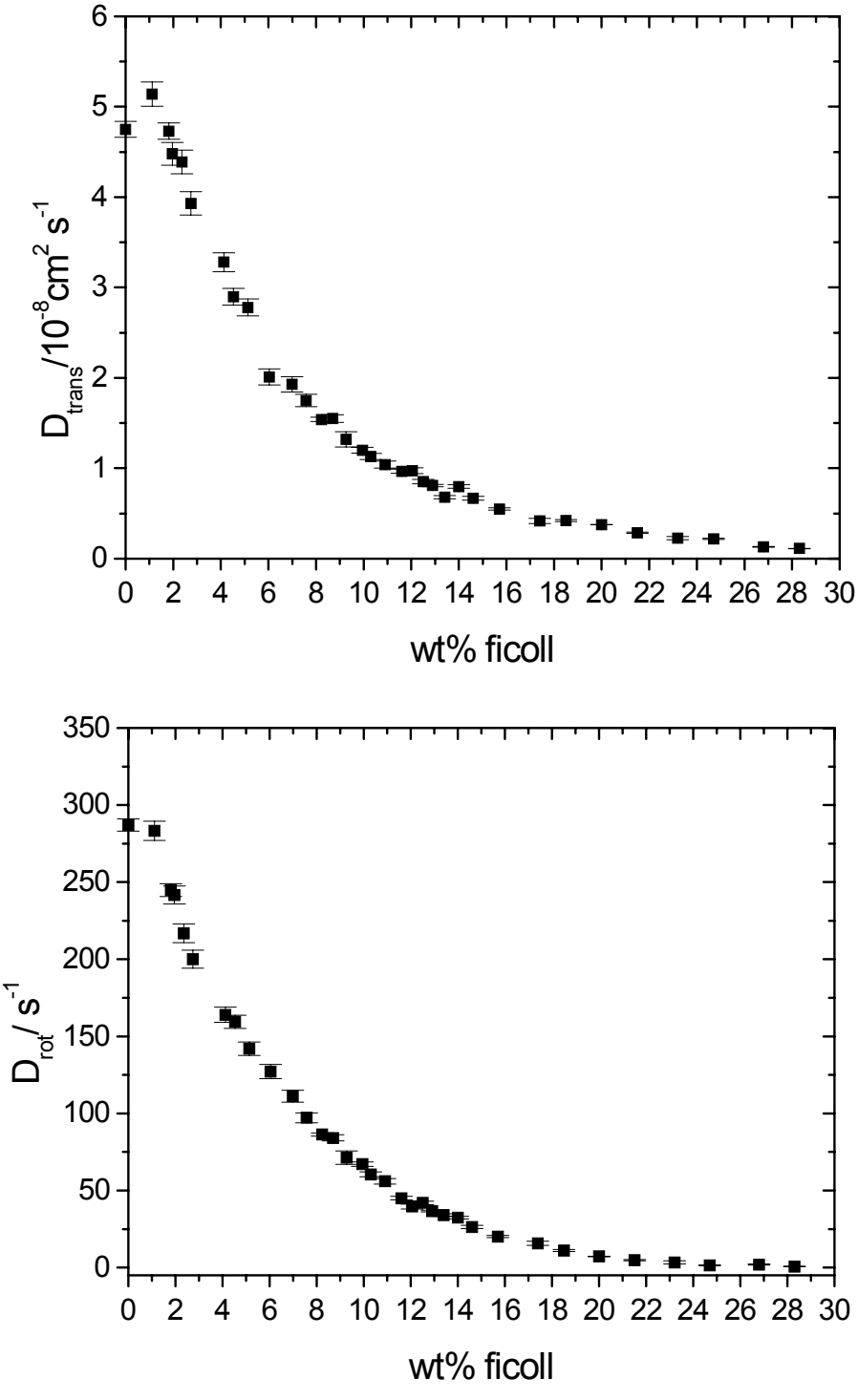

Figure 15. Dependence of translational diffusion (top) and rotational diffusion (bottom) of TMV upon ficoll concentration.

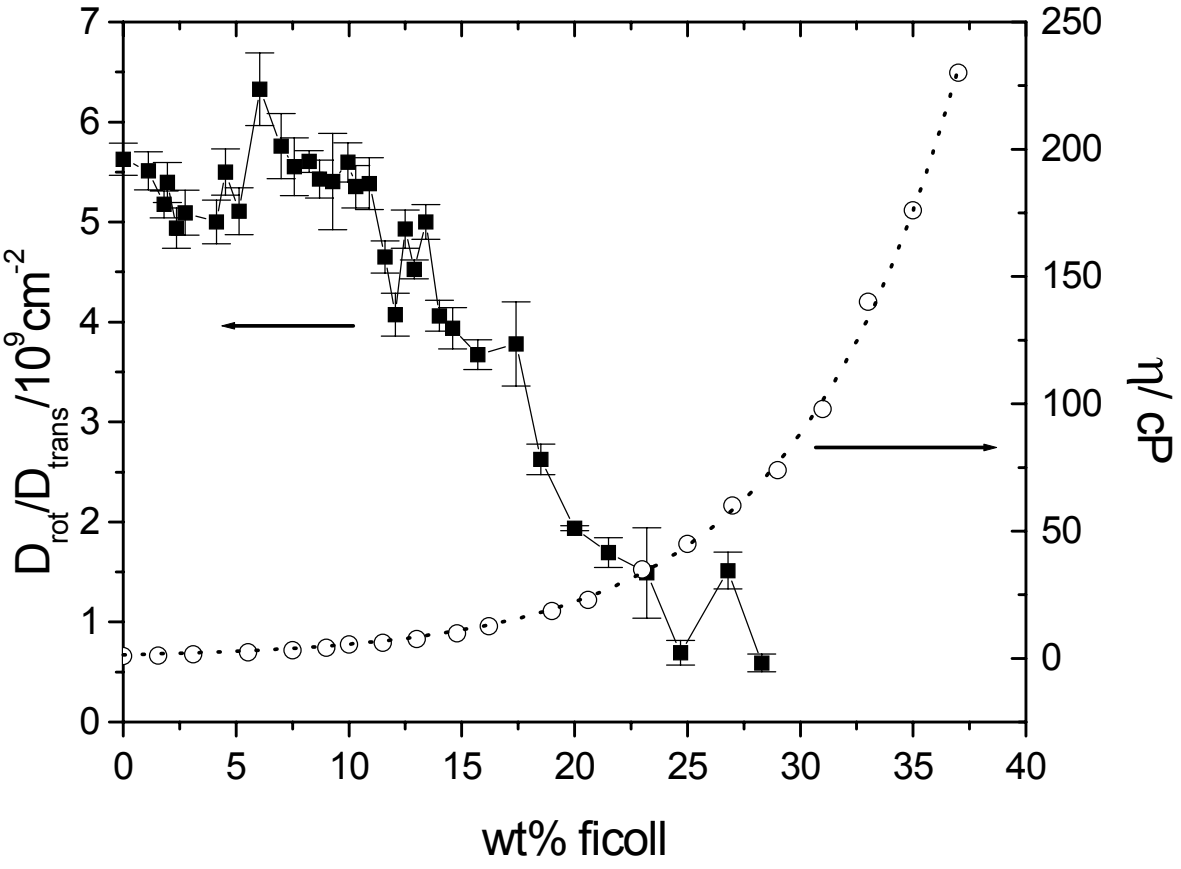

Figure 16. Dependence of the quotient of TMV rotational and translational diffusion coefficients (left axis) upon ficoll concentration. Also shown is the concentration dependence of ficoll viscosity (right axis) as seen in Figure 5.

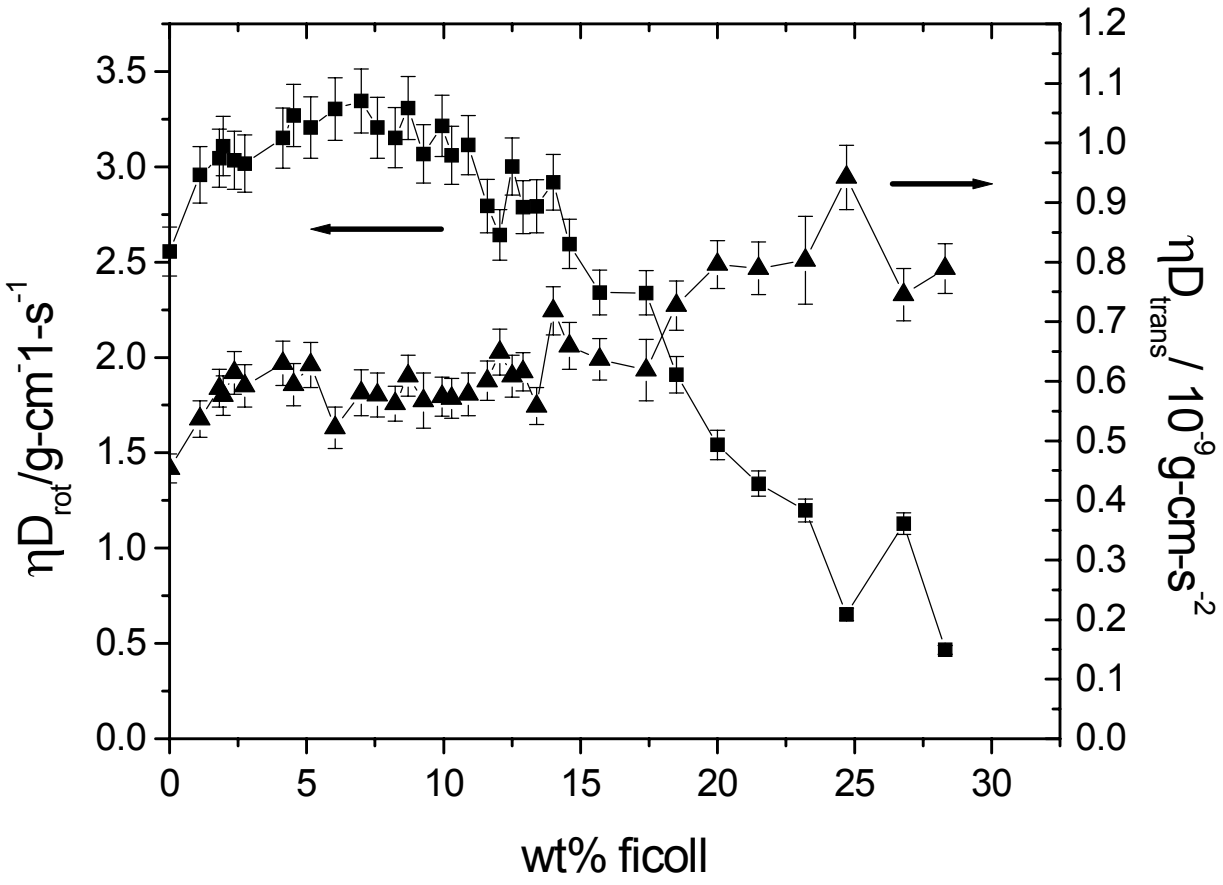

Figure 17. Product of solution viscosity and rotational diffusion coefficient (squares) and of solution viscosity and translational diffusion coefficient (triangles) as a function of ficoll concentration.

parallel to the virus. On this assumption, it is unclear why the ratio should decrease in ficoll, a system that should *not entangle.* A thought was that ficoll, which is often envisioned as a non-entangling, compact molecule, has dangling chain ends which can entangle somewhat at high enough concentration. Interpenetration of free chain ends in highly-branched polysaccharides has been suggested by other studies.[105;106]

Another possibility was that the effect was not physical in nature, but some optical aberrance. This unexpected decreasing ratio, combined with the negative (within error) values for D_r found in the previous study[56] suggested that leaked light could be dragging the intercept of the Γ vs. q^2 plots ($6D_r$) down relative to the slope, as the system strays towards the Uv geometry. We realized that in the minimization procedure used, we never took into account subtle effects due to *optical activity* of the matrix polymers which are composed of sugar units. The details about optical activity and significance of errors appear in the next sections.

4.4.1.2 EFFECT OF FICOLL OPTICAL ACTIVITY

To determine the extent of optical activity for alignment corrections, the optical rotation of light through ternary ficoll solutions was measured. This was done by crossing the two polarizers at zero angle and rotating one to minimize the light intensity after passing through the entire path length of solution in the glass DLS cells (internal diameter about 11mm). The polarizers used have a micrometer scale with a precision of five arc minutes. The amount of polarizer rotation needed to minimize the signal was recorded. This was done for a series of concentrations as seen in Figure 18. The dotted line represents a linear fit. The ficoll solutions are optically active, behaving linearly as expected with a total (dextrarotary) rotation at the highest concentration of about 3 degrees in the clockwise direction, viewed towards the laser source. The optical activity comes from the sucrose units from which ficoll is constructed.

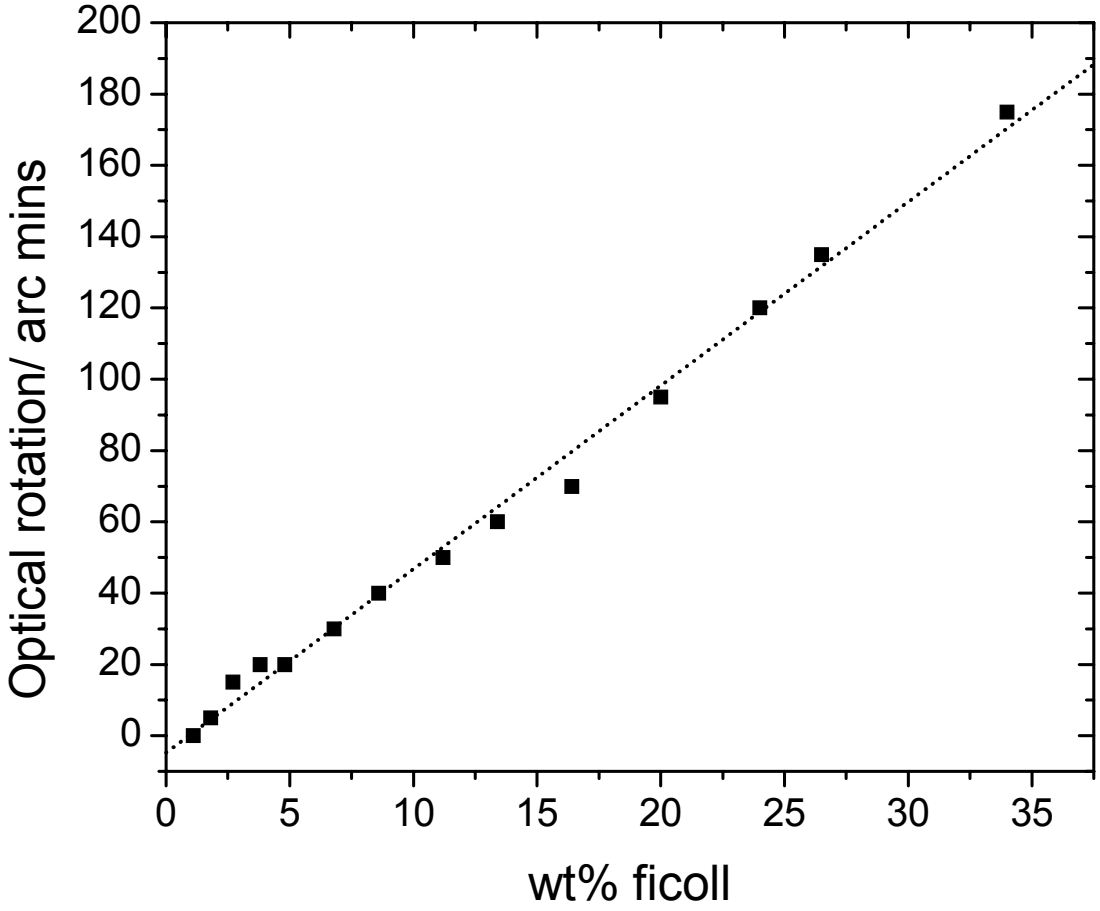

Figure 18. Optical rotation of ficoll as a function of concentration using a cell path length of about 11 mm.

Shown in Figure 19 is an illustration depicting the effect matrix optical activity has on the position of the incident and scattered beams, relative to the scattering geometry. All rotation directions described here are relative to a light of sight directed toward the laser source. The incident beam is rotated clockwise as it enters the optically active solution and is no longer vertical at the cell center. The scattered light then is rotated further as it exits the sample cell. The correct method for setting up the Hv geometry for an optically active matrix is as follows. Initially, the polarizers are aligned normally as described in section 2.3.1.2. By taking one half of the rotation through the entire cell path length and offsetting the vertical polarizer by this amount (counterclockwise), the incident beam will be rotated by the matrix to the vertical position at the cell center. The analyzer is then rotated by this same amount (clockwise) to compensate for clockwise rotation of the scattered (depolarized) light. The effect this has on angle dependence of scattered light intensity and measured diffusion coefficients depends on the method used to align the system for the Hv geometry as seen in Figure 20 for four different alignment schemes. This plot is for TMV in 14.7 wt% dextran (Sigma cat # D-1037, Lot# 90K1897). Method 1 is the correct alignment procedure as described above and a plot of Γ vs. q^2 yields a ratio of $D_r/D_t \sim 6.5 \times 10^9$, similar to the "pre-transition" level found in the previous study. Method 2 is the alignment procedure used in the previous study, which is identical to that described in section 2.3.1.2 except that the horizontal analyzer was tweaked at each angle to minimize the signal to account for possible irregularities in the plane of the rotating arm. Though this method is perfectly logical for a normal depolarized scattering situation (i.e. no optically active matrix), it results in a significantly different value for the ratio, $D_r/D_t \sim 1 \times 10^9$, which is similar to "post-transition" values found in the previous study. Perhaps more importantly is the overall trend and magnitude of the intensity, which differs only *slightly*

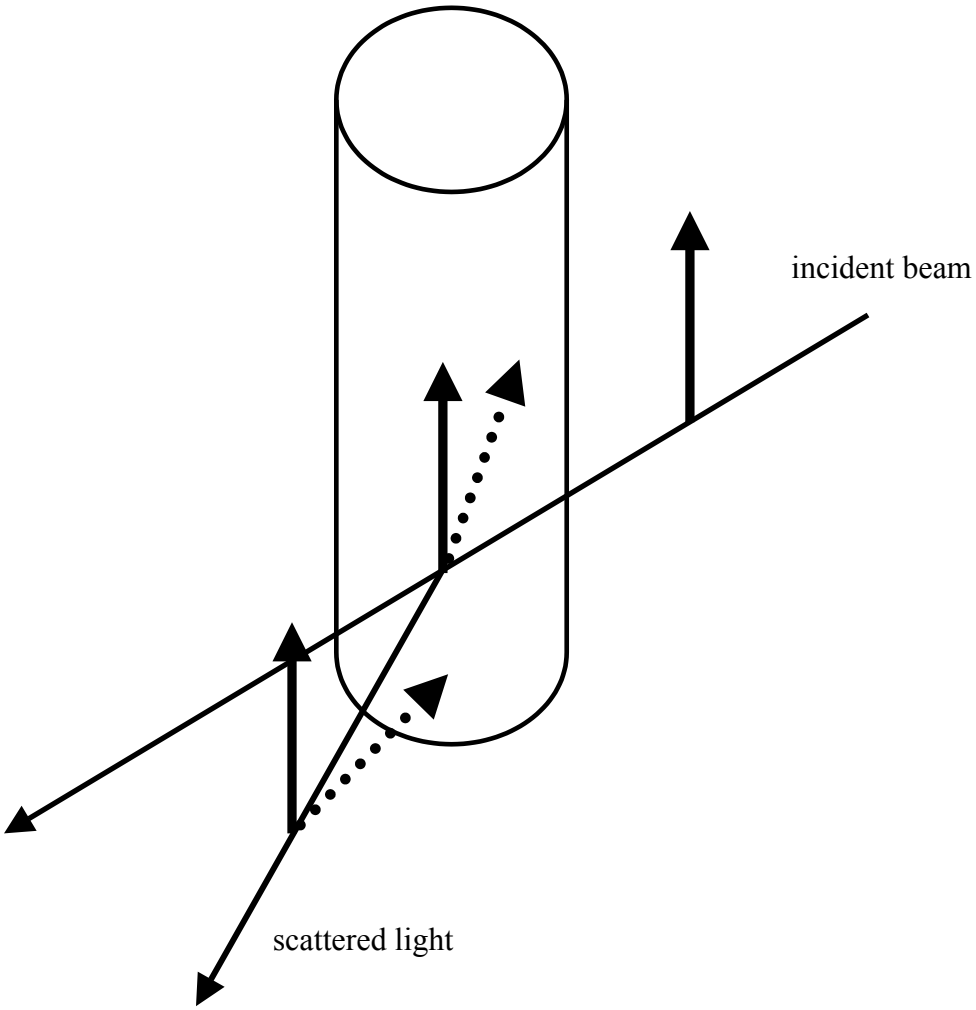

Figure 19. Illustration showing the effect of matrix optical activity on polarization of incident and scattered light (see text). The rotations are greatly exaggerated for clarity.

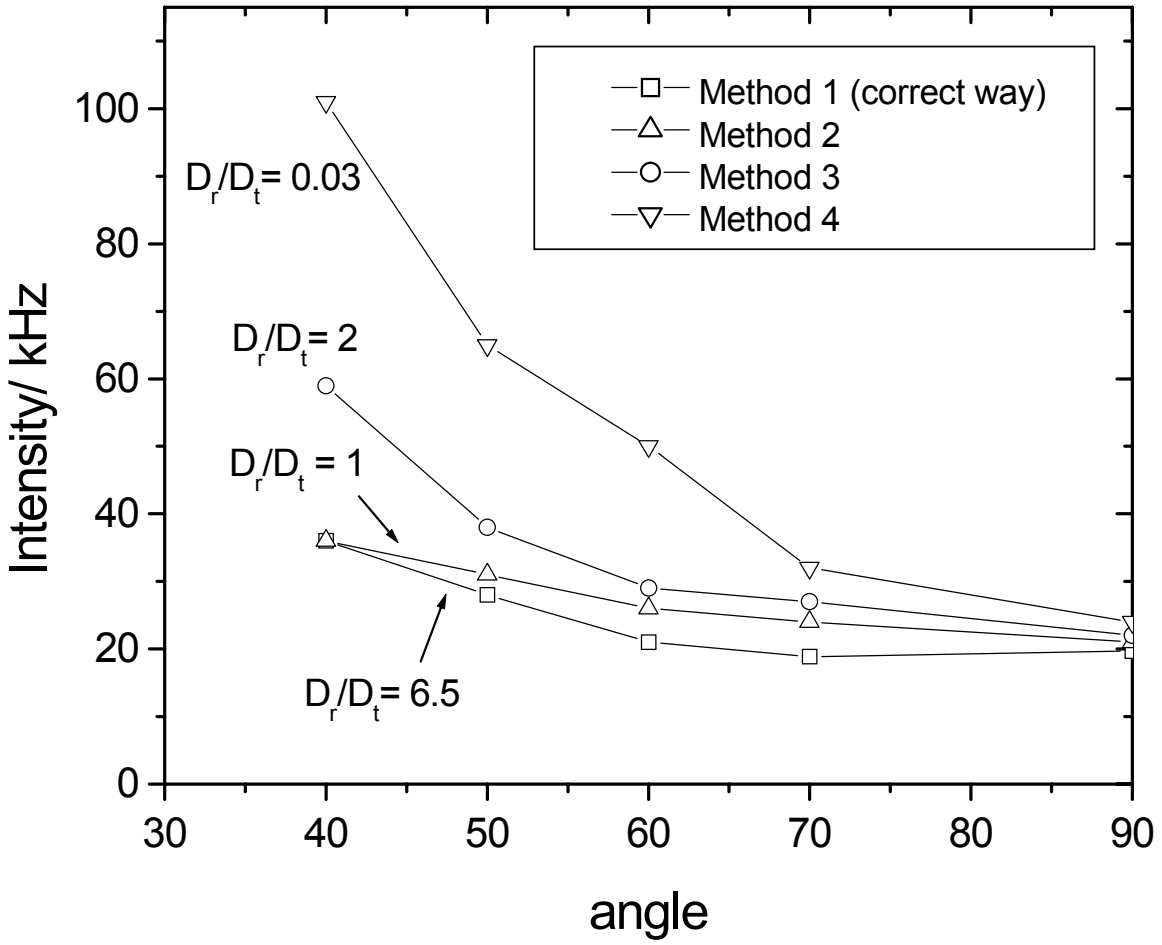

Figure 20. The angular dependence of measured intensity and corresponding values for the ratio of TMV rotational to translation in 14.7 wt% dextran (sigma cat #D-1037) using four different alignment procedures (see text).

(certainly not easily discerned by the naked eye) from that using the correct method, yet with such a dramatic change in the measured ratio, D_r/D_t. Method 3 differs from the above method in that the horizontal analyzer was rotated counterclockwise to increase the depolarized scattering intensity of dilute TMV alone by about 10% at 90 degrees. The analyzer was left in this position for subsequent angles. Again, the value for the ratio $D_r/D_t \sim 2 \times 109$ is quite low. Finally, in method 4, the polarizers were aligned using TMV as described in section 2.3.1.2 and left alone. This has the most dramatic effect on the angle dependence of the scatter light intensity and the ratio, yielding $D_r/D_t \sim 0.03 \times 10^9$. This procedure too would be perfectly acceptable for a normal Hv scattering experiment, yet the effects for an optically active matrix are quite severe. A more detailed analysis of the effects of solution optical activity on scattering is found in the appendix.

Given the dramatic effects that mis-aligning the polarizers can have, the DDLS experiments described in Section 4.4.1.1 were repeated using new ficoll samples and the correct Hv alignment procedure as described above. The ratio of D_r/D_t appears in Figure 21. The gradually decreasing function of concentration seen in Figure 16 is now a nearly level function, even up to the slightly higher concentrations used and well beyond the overlap concentration of $c^* = 6.7\%$. Again, we see that the correct Hv alignment has a dramatic effect on this plot. The coefficients are plotted separately in Figure 22 including fits to a simple stretched exponential in the form $D = D^\circ \exp(-\alpha c^\nu)$ where c is the ficoll concentration, D° is the zero concentration value, and ν is the stretching parameter. As described in section 1.2, probe diffusion has been observed to follow such a stretched exponential form and is consistent with theories for hydrodynamic interactions between polymers. [18;20;42;118] With the exception of a few points, the equation $\nu = 0.88 \pm 0.03$ for D_r and $\nu = 1.25 \pm 0.08$ for D_t. Given that the values are not quite unity as expected for simple exponential behavior, a stretched exponential description seems most

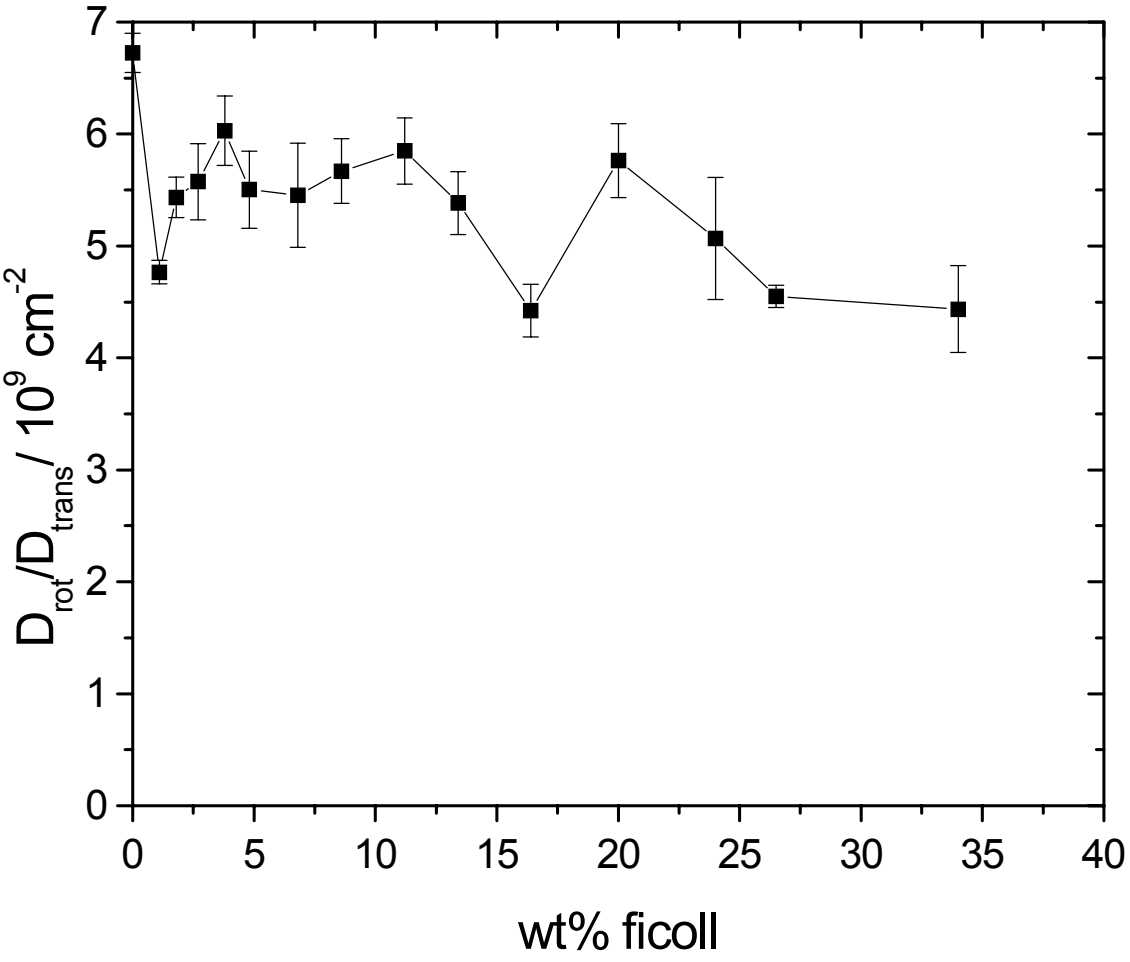

Figure 21. Dependence of the quotient of TMV rotational and translational diffusion coefficients upon ficoll concentration using an Hv optimization procedure for optically active matrices (see text).

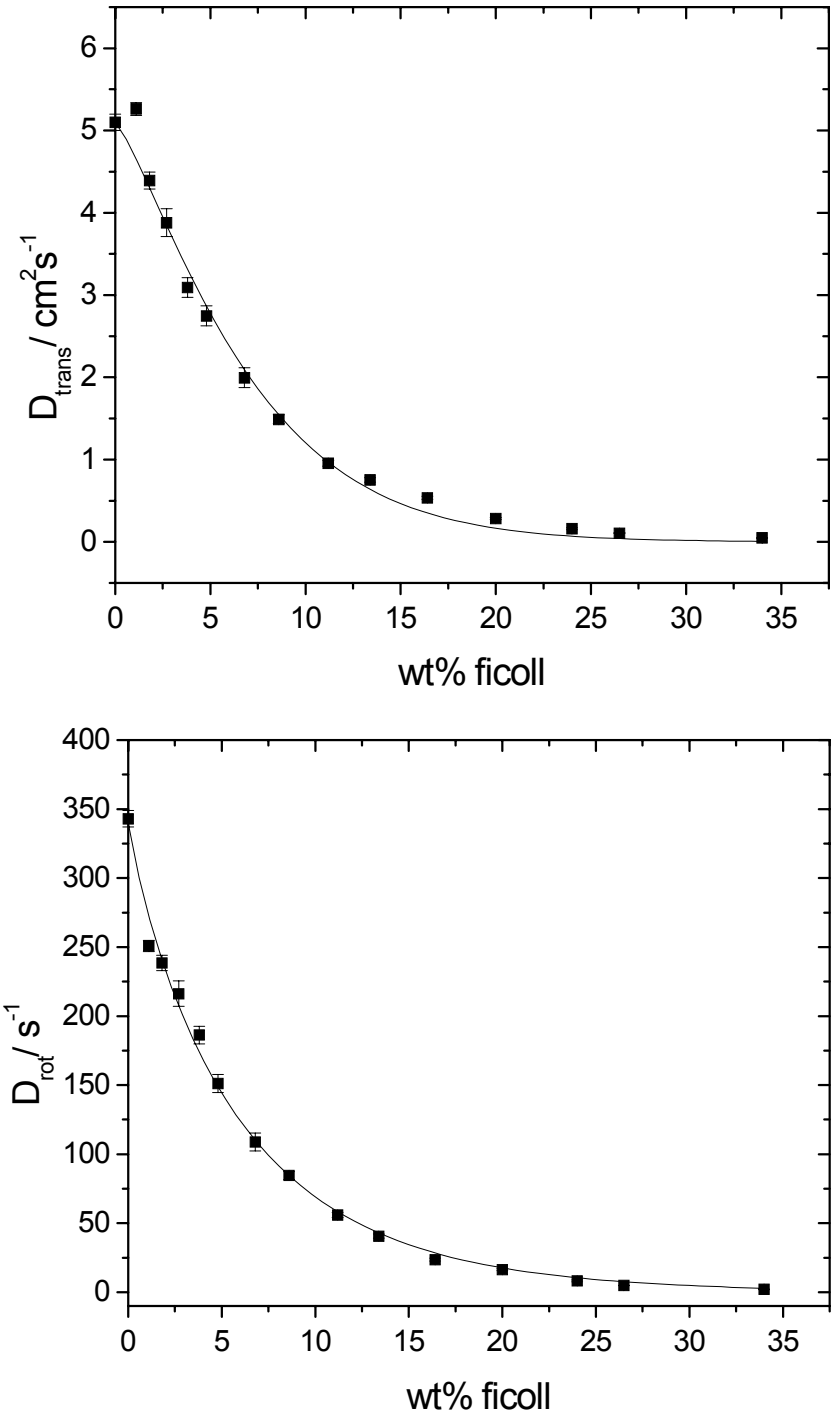

Figure 22. Dependence of translational diffusion (top) and rotational diffusion (bottom) of TMV upon ficoll concentration including fit to stretched exponential.

appropriate. The theory of Deutch and Pecora predicts $D_r \sim c_{matrix}^{-2/3}$ for rods immersed in a concentrated solution of spheres, seemingly applicable for the globular ficoll particles. Such power law fits do not describe the data well, even at higher ficoll concentrations, but the data are consistent with a much more negative exponent approaching –1.6. The product of diffusion and viscosity is plotted against ficoll concentration in Figure 23. With the exception of a short lived positive deviation for rotation, the products for both coefficients are almost level, as expected for Stokes-Einstein behavior, over a large concentration range.

4.4.2 DIFFUSION OF TMV IN DEXTRAN SOLUTIONS

4.4.2.2 EFFECT OF DEXTRAN CONCENTRATION

In a previous TMV/dextran study, the Hv correlation function for 14.5 wt% dextran of MW = 505,000 revealed weak depolarized scattering relative to TMV. [56] This was repeated here for a dextran from Sigma that had the same catalog number as that in the previous study, though at a slightly lower advertised MW = 413,000 (cat# D1037, lot #90K1897), as seen in Figure 24 for a dextran concentration of 17.6 wt% (without TMV) and 15 wt% (with TMV). This and all subsequent DDLS data are for the *correct* Hv alignment procedure for optically active matrices as described in section 4.4.1.2. The correlation function for dextran alone (hollow squares) was collected over a 600 second duration and shows almost no correlation while that for added dilute TMV was collected for only 90 seconds and has significant signal. Correlation functions taken on this dextran alone using the incorrect alignment procedure produced an almost identical level of signal as compared to using the correct procedure. It is apparent that a low scattering signal was not sufficient to describe the matrices as "invisible"; it required also that the matrix was "inert" in the sense that it did not alter the scattering geometry.

Given the dramatic effects of mis-aligning the polarizers seen in ficoll and a dextran, a

1

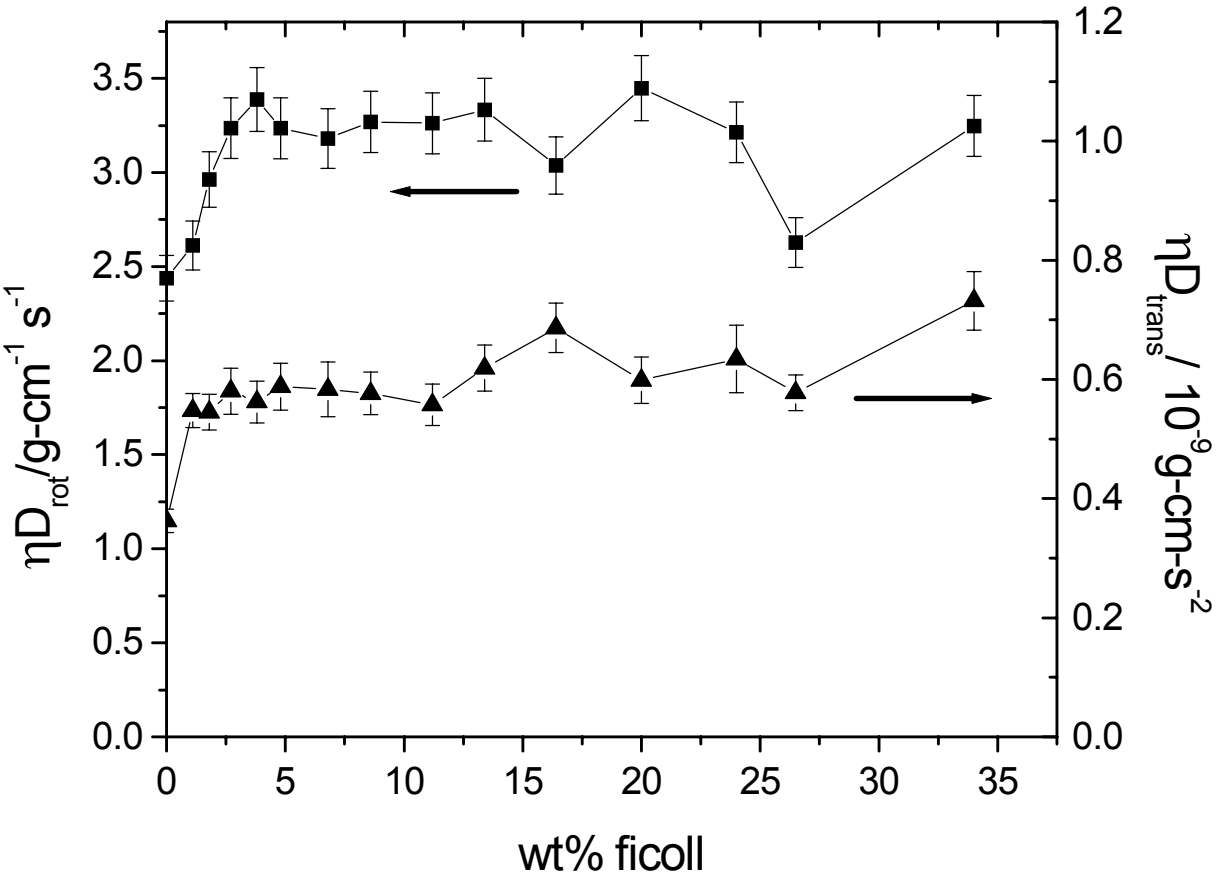

Figure 23. Product of solution viscosity and rotational diffusion coefficient (squares) and of solution viscosity and translational diffusion coefficient (triangles) as a function of ficoll concentration using an Hv optimization procedure for optically active matrices (see text).

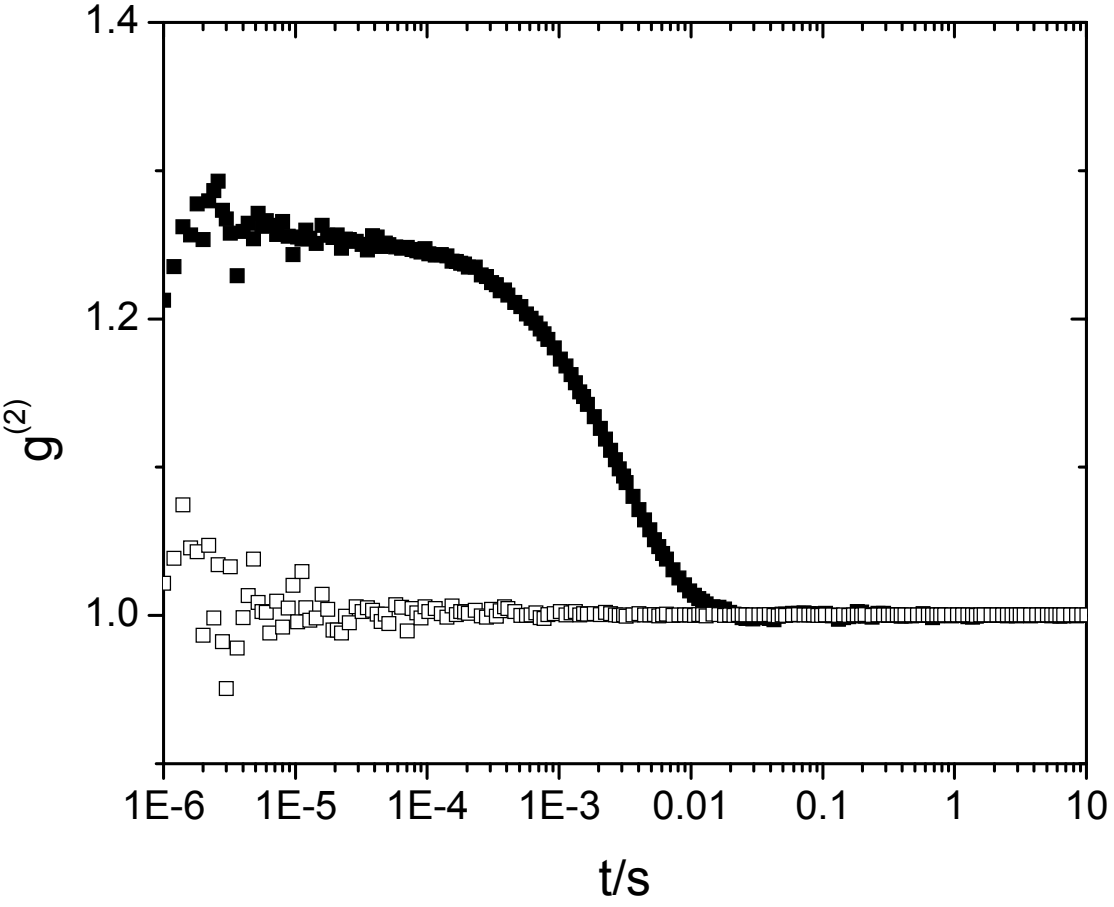

Figure 24. Hv correlation functions for samples of dextran with (solid squares) and without (hollow squares) added 0.5 mg/mL TMV. The collection duration for dextran with TMV added was 90 seconds while that for ficoll alone was 600 seconds.

concentration study of dextran was repeated using a dextran of $M_w \cong 647{,}000$ (dxt670k, Polymer Standards Services) and the correct Hv alignment procedure. The exact dextran product used in the previous study[56] could not be located. As described in section 4.4.1.2. for ficoll, the optical rotation as a function of dextran concentration was measured and is found in Figure 25, measured as described in Section 4.4.1.2 in a cell with ~ 11 mm path length. Linear behavior is found as expected with a total rotation at the highest concentration of about 4 degrees.

The concentration dependence of the rotational and translational diffusion coefficients appears in Figure 26 including fits to a stretched exponential equation as described in section 4.4.1.2. Again, simple stretched exponentials seem to describe the data well yielding values for the stretching parameter of $\nu = 0.95 \pm 0.03$ for D_t and $\nu = 0.72 \pm 0.01$ for D_r. Given that this parameter is near unity for D_t, a simple exponential would be appropriate. Stretched exponential behavior is more appropriate for D_r as the parameter is far from unity. This is particularly significant for dextran as this behavior was not found in the previous study, [56] as stretched or simple exponentials were ineffective beyond the transition at 6.5 wt% dextran. The predicted scaling $D_r \sim c_{matrix}^{-2/3}$ by Deutch and Pecora for rods immersed in a concentrated solution of spheres yields a stronger exponent for TMV in concentrated dextran at around –1.3. This value is less than the predicted $D_r \sim c_{matrix}^{-2}$ scaling by Soane *et. al.* for rods immersed in concentrated solutions of amorphous (coil-like) polymers. [60;61] The ratio of rotation to translation appears in Figure 27. The quotient does not exhibit the downturn observed in the previous study (Figure 11) and is a level function of dextran over a large range. This suggests that comments in the previous study about evidence for onset of topological constraints for rotation relative to translation may be inaccurate. [56] Further support of this notion comes from lack of a plateau modulus as described in section 3.2.1.2. The product of viscosity and diffusion coefficients is

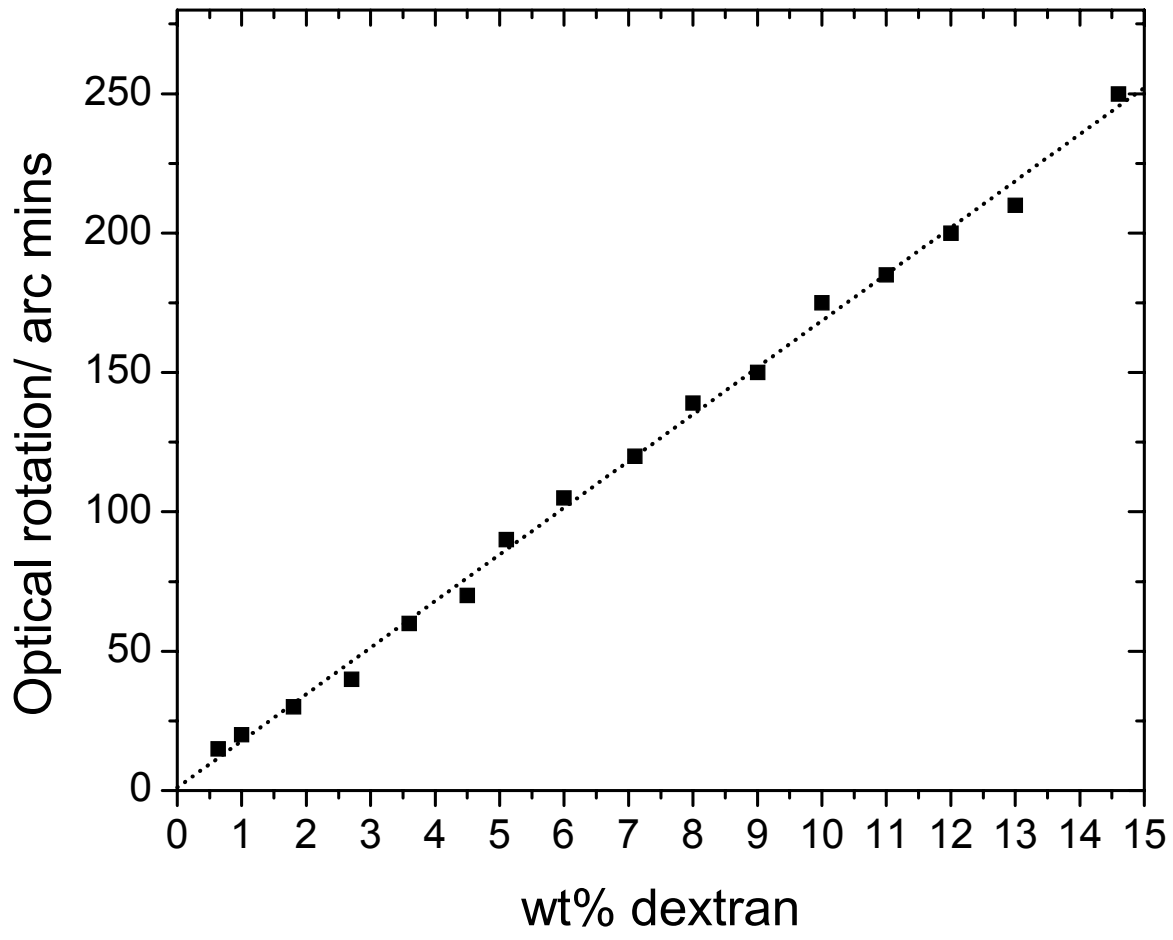

Figure 25. Optical rotation of dextran as a function of concentration using a cell with a path length of about 11 mm.

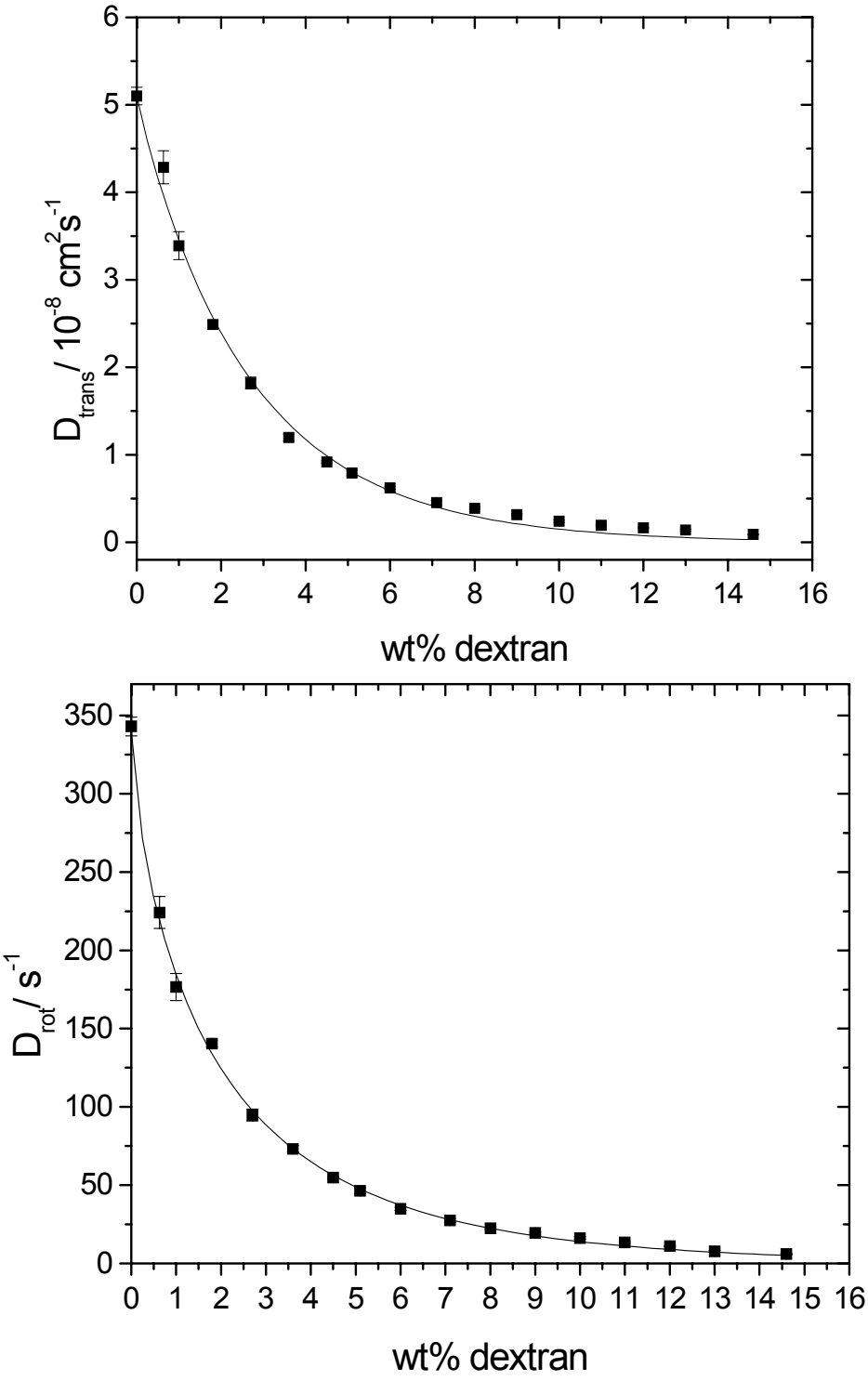

Figure 26. Dependence of translational diffusion (top) and rotational diffusion (bottom) of TMV upon dextran concentration including a stretched exponential fit.

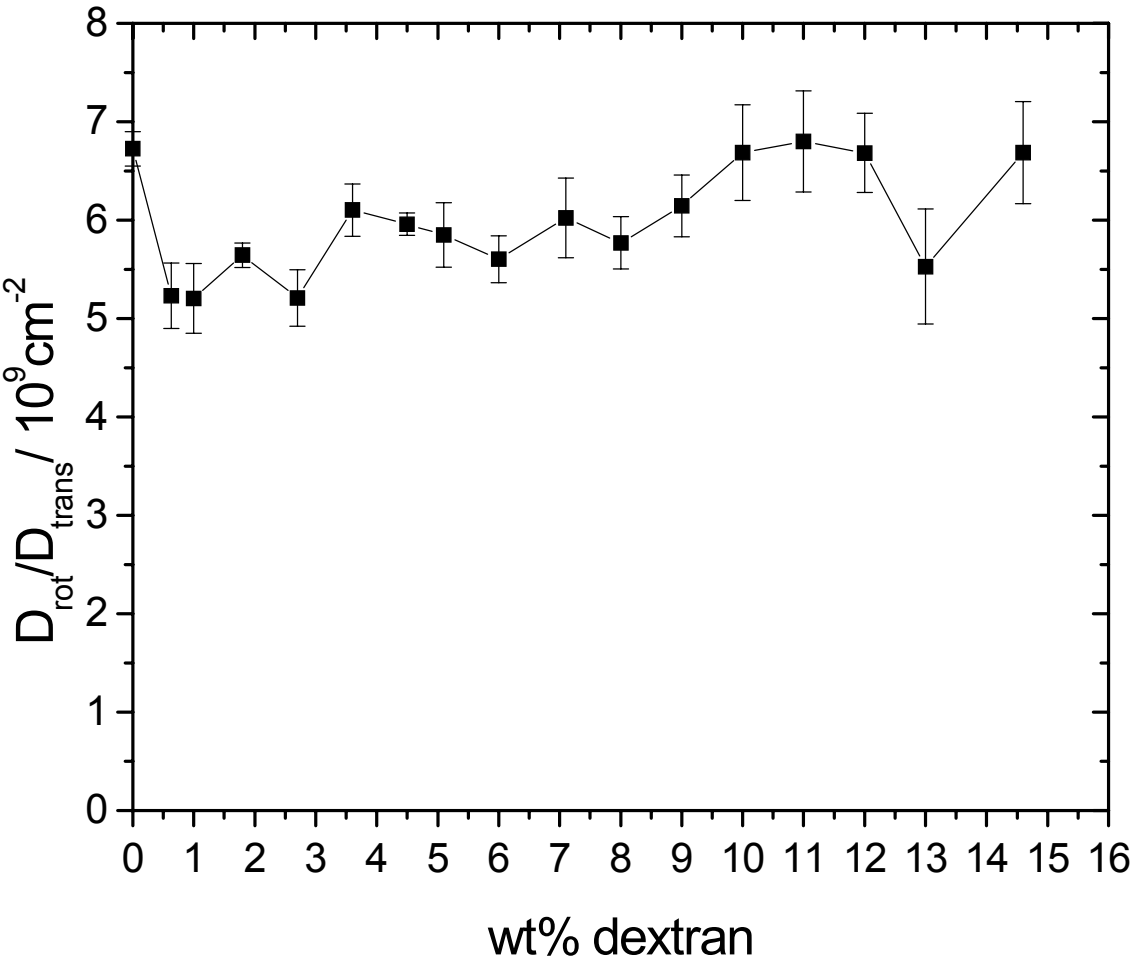

Figure 27. Dependence of the quotient of TMV rotational and translational diffusion coefficients upon dextran concentration.

found in Figure 28. It appears there is possibly a slight positive deviation from Stokes-Einstein behavior for both rotation and translation, but both products are nearly level within error. Large and sudden failures, as seen in the previous study (see Figure 12), can certainly be excluded. It appears that TMV follows SE behavior in both dextran and ficoll over very wide concentration ranges. To compliment the depolarized scattering experiments, translational diffusion of TMV in dextran was measured by fluorescence photobleaching recovery. Details about the technique are found later in Chapter 5. As seen in figure 29, $D_{t,}$ as measured by this very different technique seems to decrease with increasing dextran concentration similarly to DDLS results.

4.4.2.3 EFFECT OF DEXTRAN MOLECULAR WEIGHT

Diffusion of TMV was measured in dextrans of varying molecular weight at a concentration beyond the transition (now known to be an artifact) in the previous study where the ratio of D_r and D_t decreased sharply. The correct Hv alignment procedure for optically active matrices described above was again used. The dependence of rotational and translational diffusion of TMV on dextran molecular weight at 14.6 wt% is shown in Figure 30. The quotient of D_r and D_t is plotted against dextran molecular weight in Figure 31. Within experimental error, the quotient remains somewhat level as a function of matrix molecular weight, but a slight increase may be present. Any large transitions can be excluded. Also, note that the ratio is comparable to the *pre-transition* level found in the previous study (see figure 11.) and the norm for ficoll or dextran when the correct alignment procedure is used. Fits to discern scaling parameters yield similar molecular weight scaling exponents of $D_t \sim M^{-0.72 \pm 0.05}$ and $D_r \sim M^{-0.63 \pm 0.04}$. If TMV is truly sensing the macroscopic viscosity, it might be expected that diffusion should scale similarly since diffusion ~ 1/η by SE. The observed coefficients are much lower than the

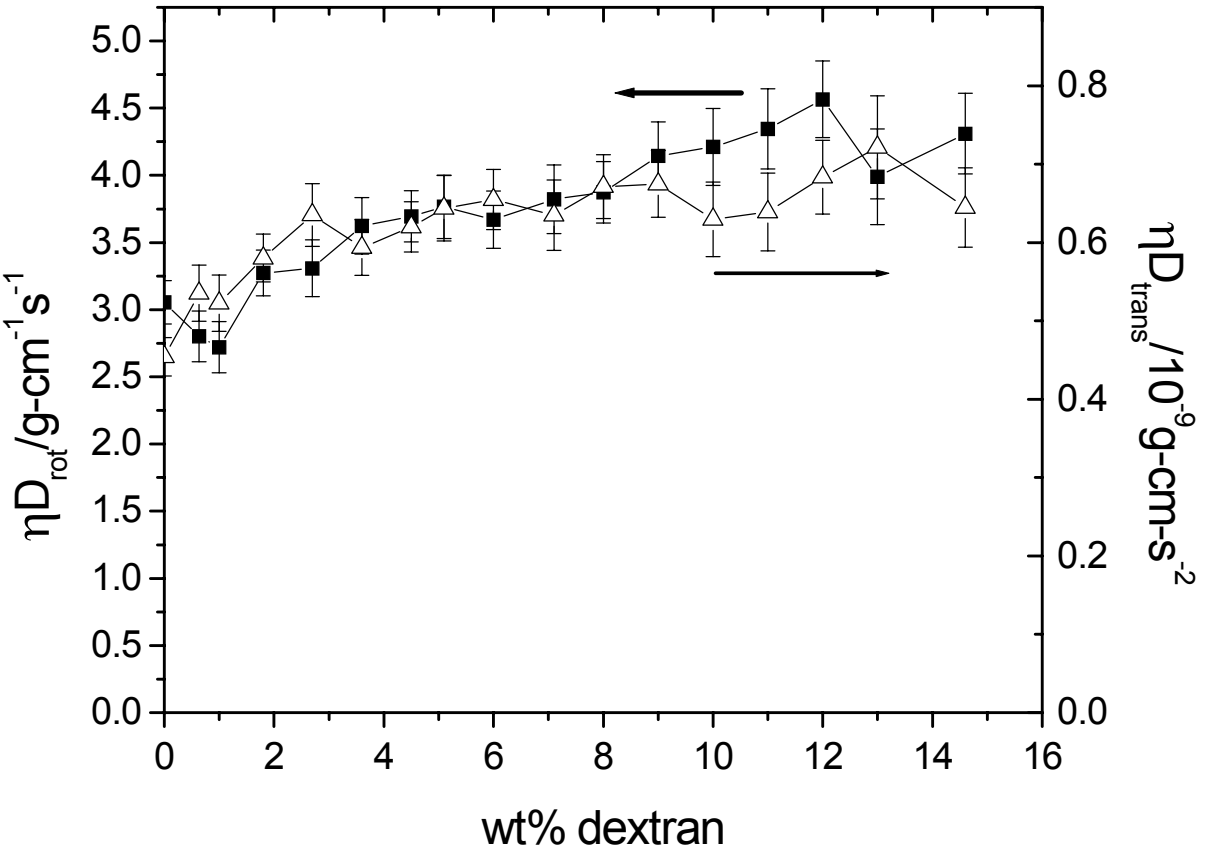

Figure 28. Product of solution viscosity and rotational diffusion (squares) and of solution viscosity and translational diffusion (triangles) as a function of dextran concentration using an Hv optimization procedure for optically active matrices.

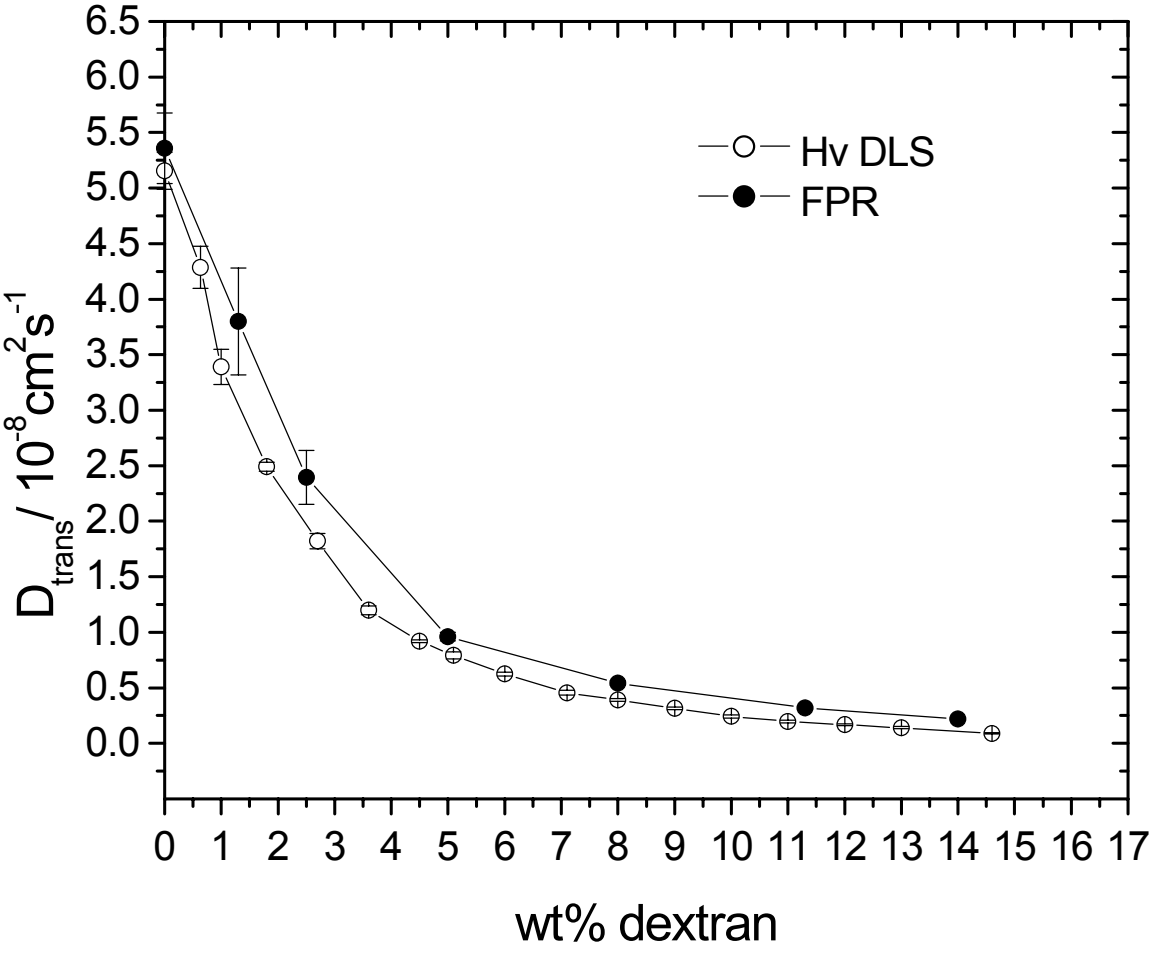

Figure 29. Dependence of TMV translational diffusion on dextran concentration, measured by DLS (open circles) and FPR (filled circles).

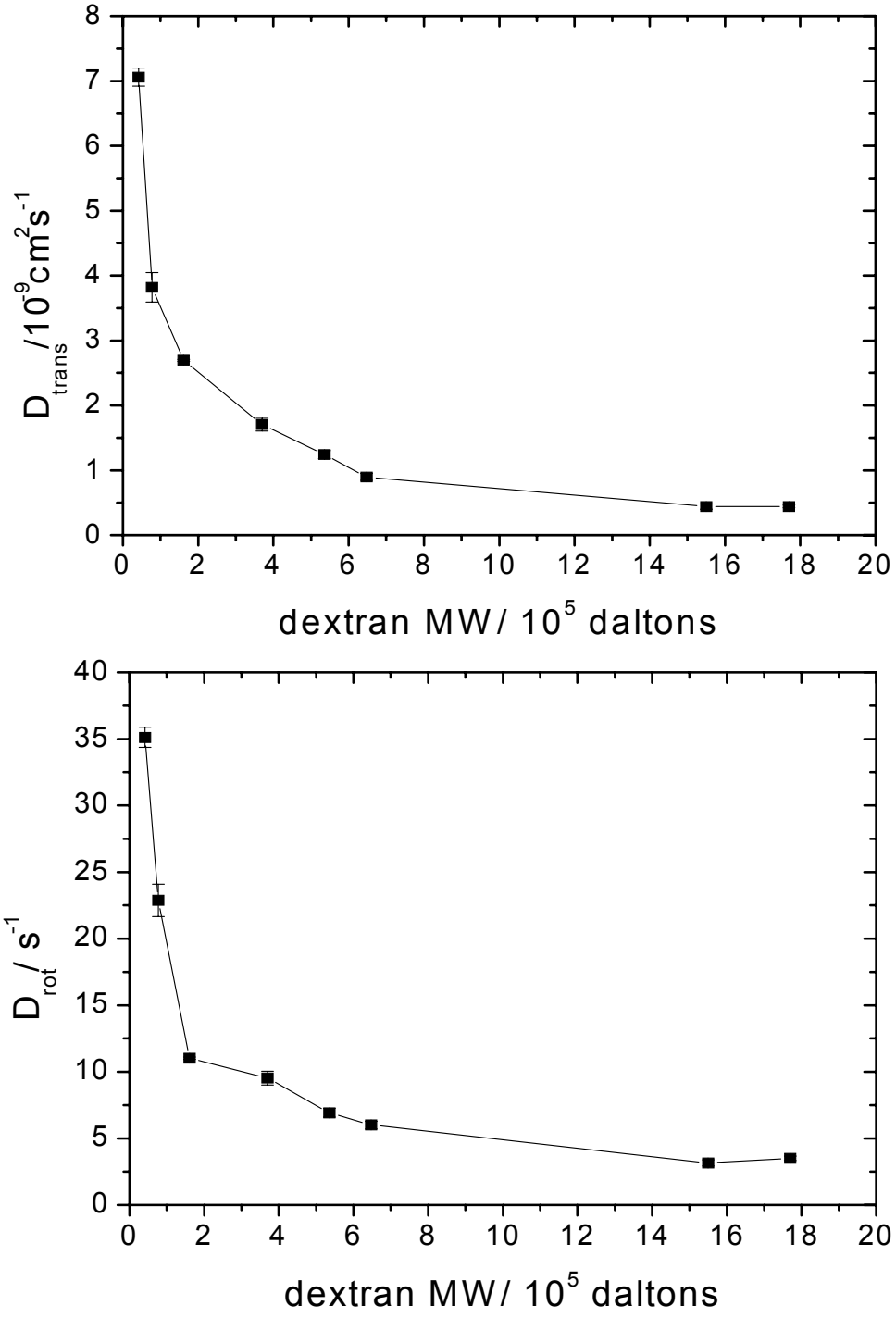

Figure 30. Dependence of TMV translation (top) and rotation (bottom) on dextran molecular weight at 14.6wt% dextran.

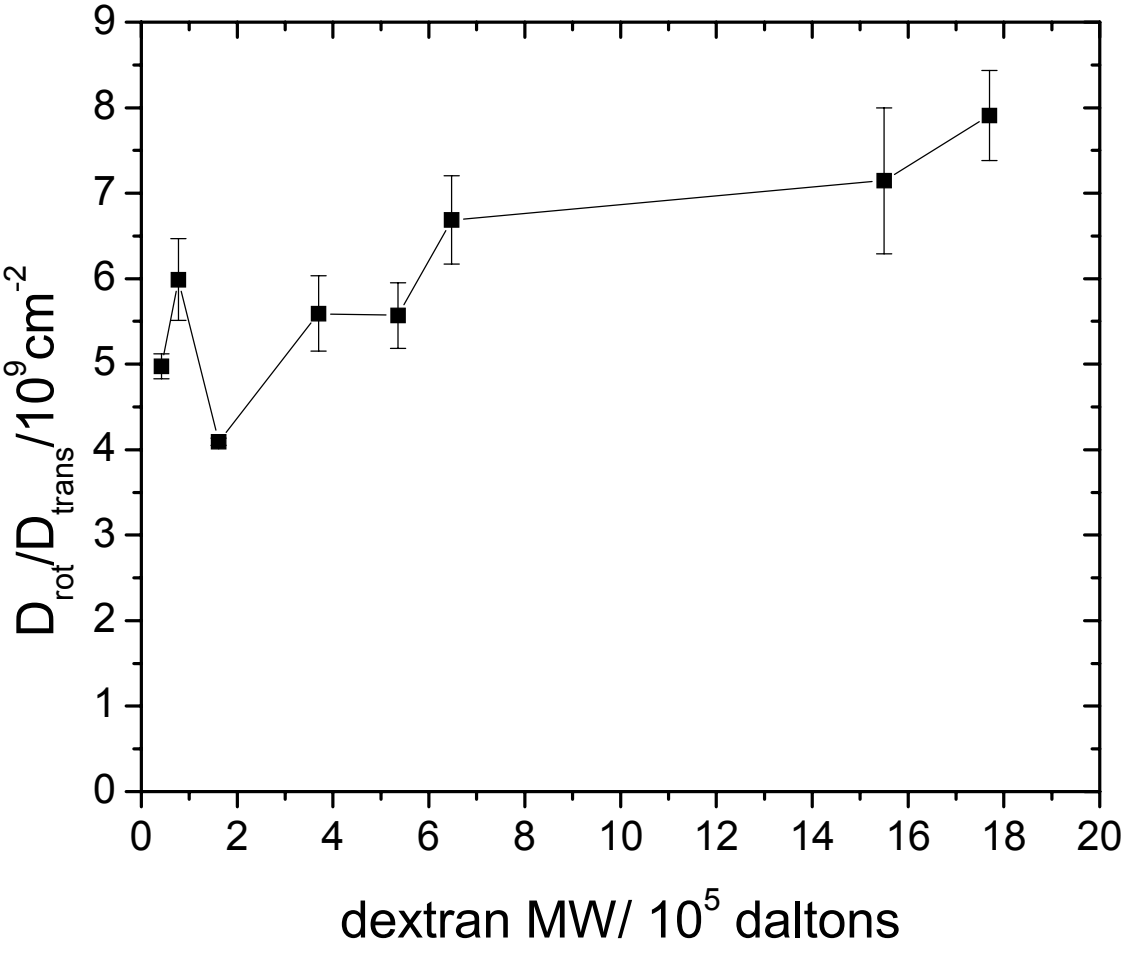

Figure 31. Dependence of the quotient of TMV rotational and translational diffusion coefficients on dextran molecular weight at 14.6wt%.

exponent for viscosity in melts of 3.4 but are close to the $\eta \sim M^{0.8}$ relationship observed previously for dextran.[112]

4.5 SUMMARY

Rotational and translational diffusion of tobacco mosaic virus in solutions of ficoll and dextran was followed by depolarized dynamic light scattering. The virus diffuses approximately as expected from the macroscopic solution viscosity for both polymers when the apparatus is correctly aligned for optically active matrices. Using the incorrect alignment procedure optical activity results in apparent Stokes-Einstein failures for rotation in ficoll. Failures observed in a previous study of dextran may also be attributed to this effect as they are not observed when this correction is made using a different but similarly sized dextran. This technique was also applied to follow diffusion of TMV in solutions of dextran of varying molecular weight at a concentration that should have presented some constraint to TMV rotation. The data reveal that at the concentration selected, no constraint to rotation relative to translation occurs. The ratio of rotational to translational diffusion is a level function of dextran molecular weight.

CHAPTER 5*

SELF DIFFUSION OF TMV IN ISOTROPIC SOLUTIONS

*Reproduced in part from *Macromolecules*. **2002**, *35*, 8659-8662.

5.1 INTRODUCTION

As described in section 1.1, the phenomenon associated with polymer coil entanglement is still unclear. If one turns to a simpler polymeric architecture, that of the rigid rod, the situation is not much better. The term entanglement or more appropriately, enmeshment, has been applied to systems of rodlike polymers where rods must escape from a cage of surrounding rods. As true for random coil polymers, hydrodynamic interactions may blur topological constraints. The challenge to understand rodlike dynamics in concentrated solution has been met by several theories [25-33] but experimental data is rather limited, [1;2;24;34-38] especially for rods in the very rigid limit [1;2].

Theoretical work on the translational diffusion of rods in concentrated solution began with the work of Doi and Edwards (DE). [25;26] In this early theory, DE assumed that thin rods will begin to interact (entangle) at a number density $\nu = 1/L^3$, where L is the rod length. When concentrations approach $\nu = 1/dL^2$, where d is the rod diameter, it was assumed that diffusion perpendicular to the rod, $D_\perp$, will fall to zero due to collisions with other rods and diffusion parallel to the rod, $D_\parallel$, will maintain its dilute solution value. In the dilute solution limit, a rod will diffuse twice as fast parallel to its access than it will perpendicular to it:[38;87;98]

$$D_\parallel^\circ = 2D_\perp^\circ \tag{4.1}$$

where the subscript zero indicates dilute solution limit. The average diffusion coefficient, D^0, is:

$$D^\circ = \frac{1}{3}\left(D_\parallel^\circ + 2D_\perp^\circ\right) \tag{4.2}$$

Setting $D_\perp=0$ and $D_\parallel = D_\parallel^\circ$ and using equation 4.2 we see that the diffusion of a rod will fall to one half its dilute solution value by DE assumptions:

$$D = \frac{1}{2}D^\circ \tag{4.3}$$

Eventually the rods will become aligned at a critical concentration, ν*, which Onsager predicted to be:

$$\nu^* = \frac{16}{\pi d L^2} \approx \frac{5}{d L^2} \qquad 4.4$$

The DE approach seems too simple, as noted later by its original developers.[6] More advanced theories exist. Edwards and Evan imagined a rod of finite thickness that escapes caging by other rods by a process of diffusion through a series of gates.[119] They predict that diffusion parallel to the rod should obey:

$$D_{\|} = \frac{3}{2} D^{\circ} \left(1 - C\left(\nu d L^2\right)^{3/2} \right) \qquad 4.5$$

where C is a unitless constant of order unity. Teraoka and Hayakawa[28] adopted a similar approach for diffusion perpendicular to the rod axis and find:

$$D = D_{\perp}^{\circ} \left(1 + \varepsilon \nu L^3\right)^{-2} \qquad 4.6$$

where ε is a unitless constant. The Edwards-Evans prediction for parallel diffusion was further refined to cover a wider concentration range by Sato and Teramoto [27]with the result:

$$D_{\|} = D_{\|}^{\circ} \left(1 - \alpha \nu d L^2\right)^2 \qquad 4.7$$

where α is a unitless constant. These expressions have been combined to obtain the average diffusion coefficient [24] yielding:

$$D \Big/ D^{\circ} = \frac{1}{2} \left[\left(1 - \delta \left(\nu / \nu^* \right)^{3/2} \right) + \left(1 + \psi \nu / \nu^* \right)^{-2} \right] \qquad 4.8$$

and

$$D \Big/ D^{\circ} = \frac{1}{2} \left[\left(1 - \kappa \nu / \nu^*\right)^2 + \left(1 + \psi \nu / \nu^*\right)^{-2} \right] \qquad 4.9$$

where κ= 16α/π and $\psi = \varepsilon \nu^* L^3$. The equations differ by the equation for parallel diffusion used,

where equation 4.8 uses equation 4.5 and equation 4.9 uses equation 4.7.

5.2 EXPERIMENTAL METHOD

The technique used to follow the self diffusion of TMV is known as Fluorescence Photobleaching Recovery (FPR). It is a powerful method for monitoring the diffusion of specific components in what may be a complex mixture. One of the main advantages of FPR is the elegant simplicity of the experimental concept. Usually the species of interest is labeled by covalent attachment of a fluorescent dye. A small region is exposed to a high intensity pulse of laser light, which irreversibly photobleaches some of the dye molecules. The region is then monitored by low intensity illumination. As bleached and unbleached molecules exchange positions due to diffusion, the fluorescence signal recovers. The technique has evolved to overcome challenges presented by some samples such as weak signals, extremely fast or slow dynamics, and photochemical damage to proteins. [24;120-130]

The instrument used here[24;130] is based on the modulation detection method developed by Lanni and Ware.[129] A schematic appears in Figure 32. The device is built around an Olympus BH2 epifluorescence microscope. A square piece of glass with a regular pattern of black stripes, known as a Ronchi ruling, is placed in the rear image plane of the microscope. By illuminating the ruling, an argon ion laser casts a striped pattern into the sample, which is contained in thin, glass microslides (Vitrodynamics). The Lexel Model 95 laser producing up to about 2 W at 488nm, was used for the bleach and observation beam which differ in brightness by a factor of 2000 (optionally 10,000). This difference is effected by passing the beam through an acousto-optic modulator (AOM, Newport EOS-N35085-3) which switches between the intense bleach beam and less intense observe beam. A bleach pulse of duration 0.5 to 2 seconds (much smaller than the recovery time) was used to photobleach about 10% of the dye molecules as determined

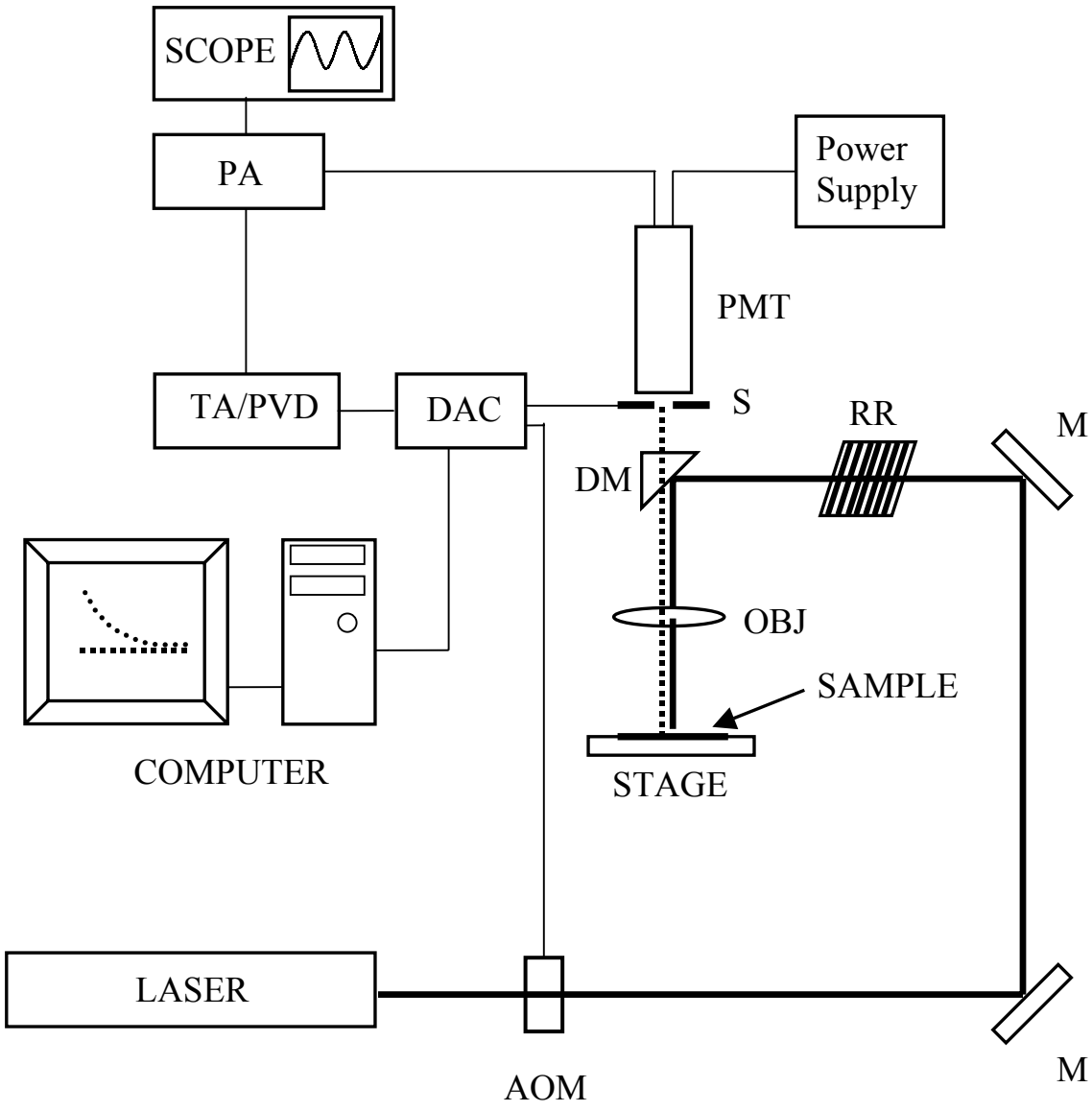

Figure 32. Schematic of the FPR apparatus. AOM = acousto-optic modulator, DAC = data acquisition card, DM = dichroic mirror, M = mirror, OBJ = objective, PA = preamplifier, PMT = photomultiplier tube, RR = Ronchi ruling, S = shutter, TA/PVD = tuned amplifier/peak voltage detection circuitry.

from the difference in the pre and post-bleach signals. The Ronchi ruling is then wiggled a distance equal to the width of one stripe by two opposing 4-inch loudspeakers (Radio Shack #40-1022b) driven by a 5-W audio amplifier, fed by a triangle wave. As the illuminated ruling pattern wiggles in and out of phase with the pattern written in the sample, a triangle ripple is produced on top of a steady dc signal detected by a photomultiplier tube. The ripple comes from the pattern bleached into the sample while the dc signal comes from the total fluorescence in the illuminated region. The peak to peak amplitude of the signal, representing contrast, is measured by a triggered peak voltage detector circuit. Due to diffusion, the contrast decays with time, t, according to:

$$C(t) = C(0)e^{-K^2Dt} \qquad 4.10$$

for a single diffuser where $K = 2\pi/l$ is the spatial frequency and D is the tracer diffusion coefficient of the labeled species. The period l in the sample is determined by the line spacing on the Ronchi ruling and the objective used and was measured by photomicroscopy using a standard graticule scale (Graticules LTD). Typically, a constant ruling of 100 lines/inch and objectives of varying power from 4× - 18× were used to vary the spatial frequency. The control software was written in Lab View (National Instruments) and the analysis software created using Visual Basic (Microsoft). The analysis software has the capability to perform multiexponential non-linear least squares fitting, polynomial fitting, cumulants analysis[131] and CONTIN.[90;91]

One of the main advantages of using modulation detection is that the post-bleach signal emerges from a quiet background. This allows for high sensitivity to shallow bleaches, which are desired to prevent photochemical damage to the species of interest and reduce local heating from the intense bleach pulse. Simpler instruments must measure a small change in fluorescence after the bleach pulse against a large fluorescent signal. Another advantage is the ability to ratio

the ac signal coming from the contrast decay to the steady dc signal from total fluorescence. This eliminates effects due to parasitic photobleaching that can occur during the measurement phase and to drifts in laser intensity or photomultiplier gain.

5.3 LABELING OF TMV WITH DTAF

With the exception of a few intrinsically fluorescent proteins, tracers are labeled with a fluorescent dye. The difficulty in accomplishing this varies from molecule to molecule, but is usually straightforward. Fluorescence techniques have become so popular that labeling kits are now available with all necessary components and detailed recipes (Molecular Probes). There are a few requirements for labeling samples for FPR. The dye must be firmly attached to the tracer, preferably through a covalent bond. Unreacted dye should be removed from the sample as much as possible; it can usually be accounted for during FPR data analysis for large tracers. The fluorescent tag should not perturb the structure of the tracer significantly.

As described earlier, TMV is composed of some 2130 protein subunits. One of most popular dyes for labeling proteins is fluorescein isothiocyanate (FITC) which couples to amine functionalities. It was found by several failed attempts that FITC does not label TMV well if at all. This may be due to lack of accessibility of free amine termini to dye molecules in solution. One alternative to FITC is the 5-isomer of fluorescein dichlorotriazine (5-DTAF) which can also label hydroxyl groups such as those in serine and threonine residues. [132] Each subunit of TMV contains 13 serine and 14 threonine residues. This dye proved to be successful and the labeling procedure will be described below. It should be noted that a scan of the literature revealed no published reports to date of labeling TMV covalently with a fluorescent dye. The labeling protocol used was based on a labeling procedure contained in the FluoReporter FITC labeling kit from Molecular Probes. To begin, 20 μL of 1 M sodium bicarbonate buffer at pH= 9.0 was

added to 200 μL of a stirred TMV solution at 20 mg/mL in 0.01 M sodium phosphate buffer at pH= 7.4 with 0.003 M sodium azide. To this 5-DTAF (Molecular Probes cat # D-16) in DMSO at 10mg/mL was immediately added and the reaction allowed to run for about one hour. A molar excess of 800 (relative to the number of TMV particles) of DTAF was used. Labeled TMV (L-TMV) was separated from free dye by gel permeation chromatography using Sephadex G-25 (Sigma). The labeled TMV and free dye bands were easily discernible during the separation. It is estimated from spectrophotometric measurements that the labeling ratio was 130 dyes per TMV particle, using a molar extinction coefficient of 82,000 $M^{-1}cm^{-1}$ at 492nm for DTAF. [132] Sample FPR runs on the labeled TMV revealed little if any free dye that appears as a very fast mode in the initial recovery profile as will be described in more detail later.

5.4 PREPARATION OF TMV SAMPLES FOR FPR

The DTAF used to label TMV is quite hydrophobic. To reduce the possibility of TMV aggregation due to the presence of the dye moieties, L-TMV was mixed with unlabelled TMV, holding the L-TMV concentration steady at a dilute 0.5 mg/mL. High concentrations of TMV were produced using Amicon Microcon YM-3 microconcentrators with a molecular weight cutoff of 3000 for globular proteins. The concentrators were spun in the SS-34 rotor of a Sorvall RC-2 centrifuge using custom made adapters to accommodate microfuge tubes. Concentrations were determined spectrophotometrically as mentioned previously.

Each FPR sample was prepared separately in Eppendorf tubes at total TMV concentrations ranging from 73 mg/mL down to 0.125 mg/mL with L-TMV concentration fixed at 0.5 mg/mL as stated earlier. Samples were loaded into rectangular capillary tubes with a pathlength of 100 μm (Vitrodynamics) by capillary action and quickly flamed sealed. The tubes were pretreated with a 10mg/mL TMV solution that was gently blown out with 0.1μm filtered

house nitrogen after one hour. The tubes were rinsed with two volumes of Nanopure water and dried using house nitrogen. The pretreatment was performed to reduce adsorption of L-TMV to the glass walls of the capillaries. All samples containing L-TMV were stored at 4°C in light-proof containers when not in use. At concentrations above about 40mg/mL, samples were examined through cross polarizers in an optical microscope to check for liquid crystal formation, revealed by the presence of birefringent regions in the sample. The lowest concentration sample to show evidence of this behavior set the upper concentration limit for the FPR experiments at 57 mg/mL.

5.5 RESULTS AND DISCUSSION

5.5.1 CHARACTERIZATION OF LABELED TMV

When labeling a macromolecule with a fluorescent dye it is advisable to characterize the labeled product to ensure no significant structural perturbation has taken place. The L-TMV was characterized by DLS in the Uv geometry as described in section 2.3.1, which measures the translational diffusion coefficient. The DLS apparatus was the same as described previously with the exception of the laser source. A He-Ne laser producing up to 100 mW at 632.8 nm, far from the absorption peak for DTAF, was used to avoid effects due to absorbance. The intensity of the laser precluded use of depolarized DLS experiments due to low signal. A plot of Γ vs. q^2 reveals a value for $D_t = (5.2 \pm 0.1) \times 10^{-8} cm^2 s^{-1}$ at 24.9°C or $D_{t,20w} = (4.6 \pm 0.1) \times 10^{-8} cm^2 s^{-1}$, in agreement with values for unlabeled TMV. Analytical ultracentrifugation of a sample of L-TMV at 0.25 mg/mL yielded a value for the sedimentation coefficient of $s_{20,w} = 193S$, again in agreement with values for unlabeled TMV. Without having the additional information from DDLS, it appears labeling did not damage the virus.

5.5.2 SELF DIFFUSION OF TMV

The labeled TMV behaved well in FPR experiments. There was sufficient signal despite the relatively light labeling, and the samples were bleachable with pulses over 100 times shorter than the recovery time. Bleaching during the measurement phase, or parasitic photobleaching, was minimal. As mentioned earlier one can account for this effect by analyzing the ratio of modulated (ac) signal to the steady (dc) signal, but no such corrections were necessary. Most recovery profiles exhibited two well-separated decay components as determined by two-exponential, nonlinear least squares fitting and by the inverse Laplace transform program, CONTIN. [90;91] The larger, primary mode is clearly diffusive, as it scaled with K^2 as seen in Figure 33. The much weaker and slower decay mode did not scale with K^2 and was not present in all runs. Due to a combination of low amplitude and large uncertainties in the decay rate, it is difficult to identify sources of this component. Possible causes include nonspecific binding of TMV to the cell walls or nascent liquid crystalline droplets at the higher concentrations. A weak, fast-decaying component was sometimes evident, probably due to free dye or protein subunits not attached to the virus particle; the corresponding channels at short times were not included in the CONTIN fits. The analysis below relies on the primary decay mode, using the chosen solution found by CONTIN.

The dependence of D_{self} on TMV concentration appears in Figure 34. Lower concentrations were limited by the signal strength while the upper bounds were set by the onset of liquid crystal formation, revealed as birefringent areas when observed through crossed polarizers in a light microscope. The value of D_{self} at the lowest concentrations agrees with the DLS result when corrected for temperature and viscosity. With concentration plotted logarithmically, the diffusion coefficient appears to be a nearly level function of concentration

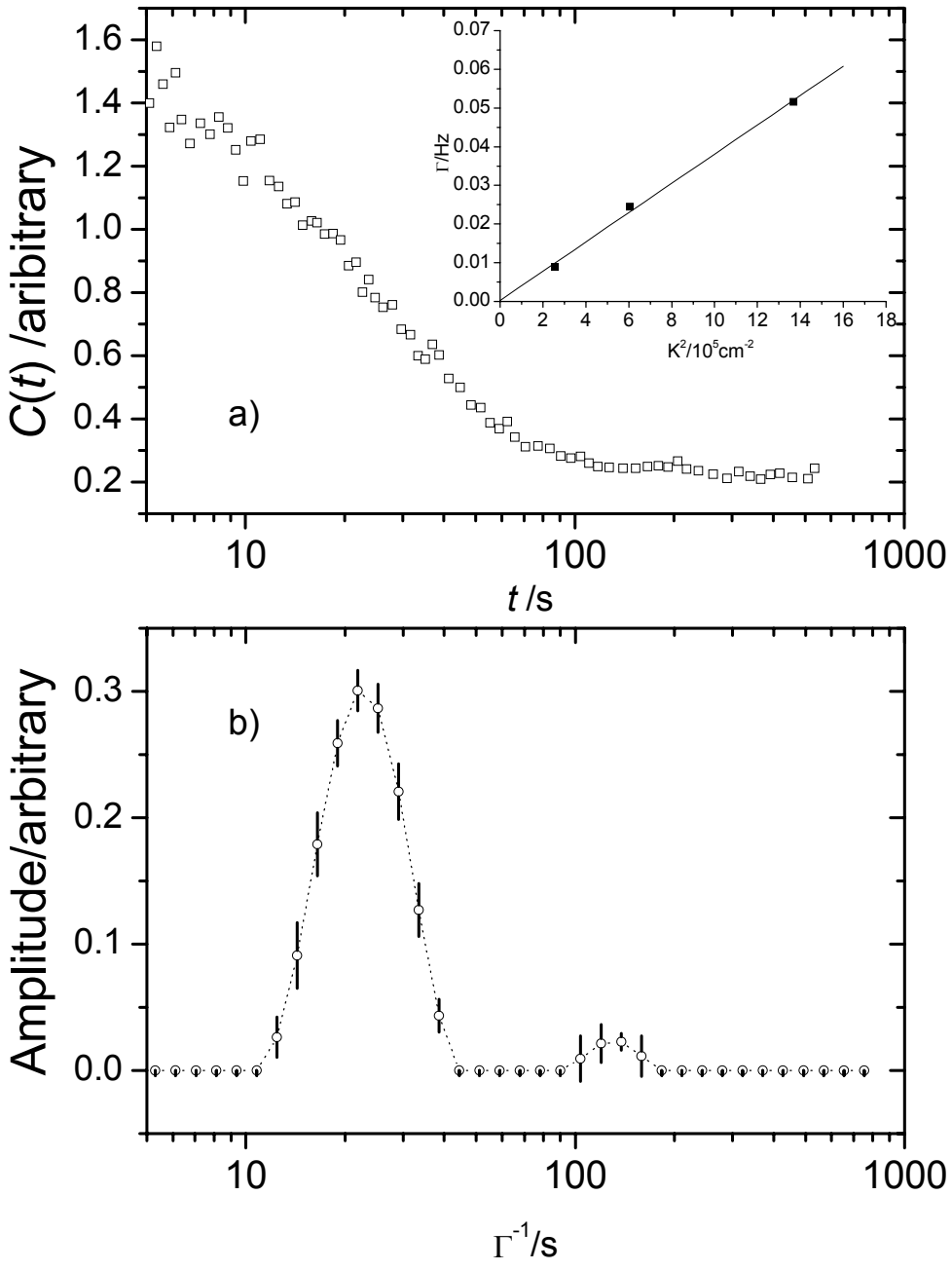

Figure 33. Sample FPR recovery for 1.0 mg/mL TMV (top). Inset: sample plot of the decay rate against the square of the spatial frequency (top). CONTIN analysis results for the same recovery profile (bottom).

below $\nu \cong 1/L^3$, which corresponds to 2.45 mg/mL for the 300nm long TMV. At $\nu \cong 2.5/L^3$, a downturn in D_{self} seems apparent. Eventually, D_{self} falls to a little less than half its value in dilute solution, as expected by Doi and Edwards. [25;26;26]

The diffusion behavior of TMV differs from that of PBLG. Sudden downturns were reported[24] for PBLG over a wide range of molecular weights, beginning at much higher number densities, approximately $1/dL^2$. PBLG diffusion exhibited a low-*c* plateau even in a linear plot; this is not true of TMV, as the inset shows. The curves in Figure 34, representing a simple exponential fit, do not make a compelling case for any sudden transition. Only two points lie (slightly) off the curve. While the decrease in PBLG diffusion was delayed until concentrations much higher than $1/L^3$, it ultimately exceeded that found for TMV. At the highest concentrations supporting an isotropic phase, PBLG diffusion loses about 90% of its dilute solution mobility. TMV more closely approximates the expected behavior for rods:[25;26] loss of translational mobility is limited to a little more than 50%.

The most obvious explanation for the delayed onset of mobility-restricting interactions in PBLG is flexibility. A recent attempt[133] by this laboratory to estimate the persistence length of PBLG met with limited success because the polymer is not available at molecular weights high enough to display much flexure. Even with chromatographic separation and on-line light scattering detection, we could only determine that values on the high side of the very wide published range were probably correct—i.e., the persistence length of PBLG probably exceeds 2000Å. Some of the PBLG samples were much shorter than any reasonable estimate of the persistence length and might have been expected to behave like rigid rods. Perhaps the slightest flexure is sufficient to help rods evade constraints to their motion. An alternative and very speculative explanation for PBLG's behavior concerns helix stability, especially near the ends.

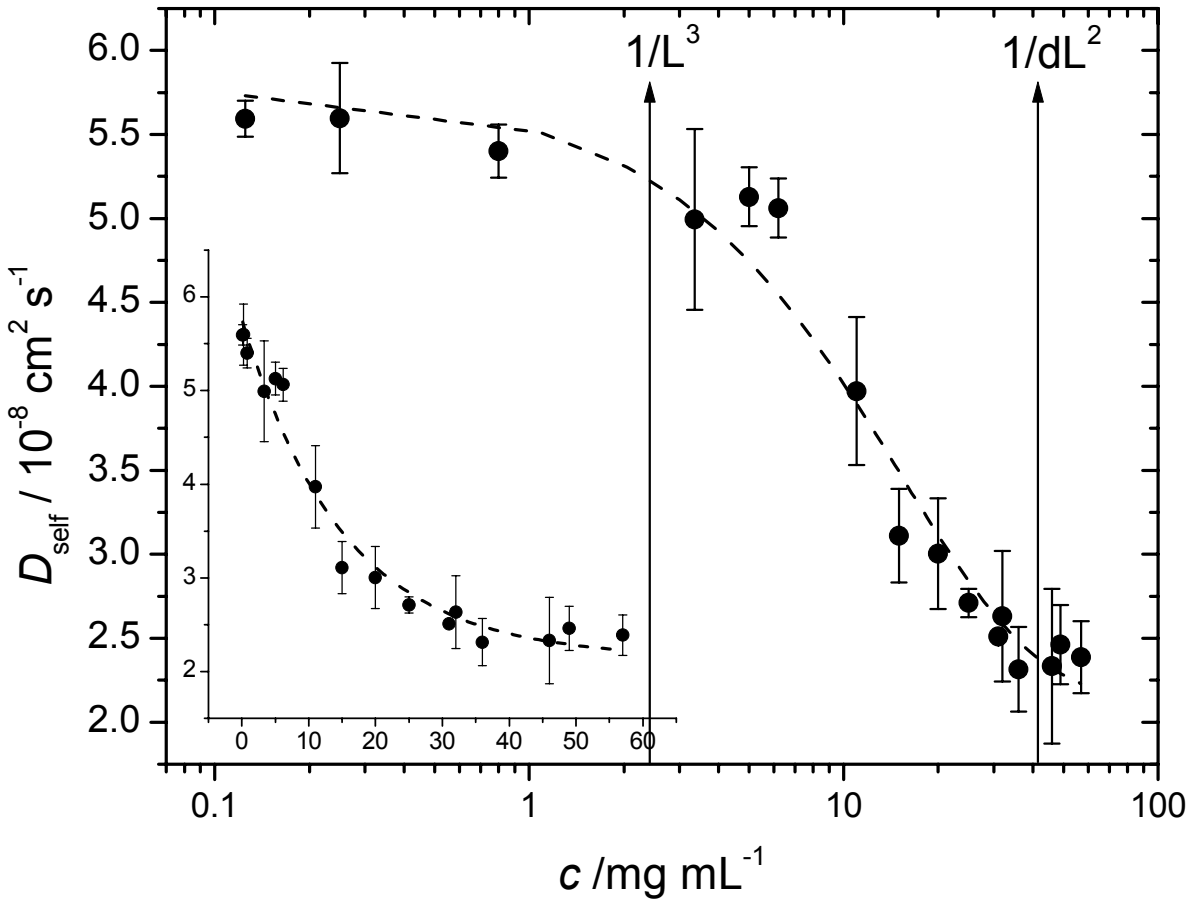

Figure 34. Measured self-diffusion coefficient plotted against concentration. The arrows define the semi-dilute regime for TMV of length, L = 3000 Å, and diameter, d = 180 Å. The error in measured diffusion coefficients comes from linear fits of Γ vs. K^2. The inset shows the same data using a linear scale for the concentration.

Floppy ends might help an otherwise rigid polymer avoid entanglements at low concentrations, even as they raise the effective cross-section for longitudinal motion, causing extra hindrance at high concentrations.

Several theories have considered mechanistic details. Comparisons to these revealed little. The scaling approach of Tinland, Maret and Rinaudo,[37] intended for wormlike chains, does predict the observed level then falling behavior of D_{self} on a log-log scale, though with a much stronger concentration dependence in the strongly decreasing regime. A fit of equation 4.9 to the data (Figure 35) yielded values of $\delta = 0.75 \pm 0.28$ and $\psi = 8.5 \pm 1.7$ which are fairly close to some values for PBLG.[24] Lack of variable length TMV particles precludes examination of the expected scaling of ψ with length. Equation 4.8 never approximated the data well. The variational approach of Dhont, van Bruggen, and Briels[31] treats the first order concentration dependence of the long-time self-diffusion coefficient for rods of finite aspect ratio, basically as $D_{self}/D_o = 1 - \alpha'\psi +$ higher terms. Using their equation 33 for α', a function of the aspect ratio, and the known dimensions of TMV predicts $\alpha' \approx 11.5$. A fit to the dilute regime TMV data yields a value about twice as large.

If the data fail to match any of the detailed mechanistic theories, they do at least exhibit a simple phenomenology. The available data can be fit to an exponential decay in any of several common concentration scales:

$$D_{self}/D_o = b + ae^{-k'x} \qquad 4.11$$

where $b = 0.38 \pm 0.03$, $a = 0.64 \pm 0.03$, and k' appears in Table 2 for the various concentration (x) scales commonly used. Exponential behavior is reasonably consistent with the PBLG study, but only after the onset concentration.[114] Exponential declines in diffusivity have been observed in many probe diffusion studies not involving rods as mentioned previously. [18;42;118]

Comparison to the available simulation [134-143] provides another frame of reference. Brownian dynamics simulations by Bitsanis, Davis and Tirrell[139] find that the center of mass diffusivity decreases to slightly less than half its value at zero concentration, as observed here. The Brownian dynamics simulations for infinitely thin rods by Doi, Yamamoto, and Kano[134] suggest a center of mass diffusion coefficient that smoothly decreases with concentration to a predetermined $0.5D_o$. In Figure 3 of this reference, the authors chose a logarithmic scale for their concentration axis, and the shape resembles Figure 36 here. Their simulation results appear on a linear scale alongside our TMV data in Figure 36. A very satisfying exponential fit to the simulation data gives $D/D_o \sim 0.5 + \exp(-\nu L^3/21)$. That is, $k' = 0.047$ (number densities scaled to L^3) for thin rods by the Brownian dynamics simulation of Ref. 130. TMV diffusion decreases with concentration about 3 times faster ($k' = 0.16$). Possible causes include the finite thickness of the TMV, or hydrodynamic interactions ignored by the simulations.

5.6 SUMMARY

With only two data points lying marginally above the exponentially decaying trend, it is not possible to make a compelling case that translational diffusion in TMV exhibits any sudden reduction to signal the onset of enmeshment. Interactions occur at lower concentrations than they did in PBLG, and are surely effective by $\nu \sim 2.5/L^3$. About 60% of the diffusion is lost before the liquid crystalline transition occurs, very close to the 50% expected by the Doi-Edwards theory for long, thin rods. The high axial ratio, stiffness and monodispersity of TMV make it a useful system for testing theories of rods. Drawbacks include thickness and inability to vary length. It remains to explain how PBLG evades enmeshment until the number density reaches about $1/dL^2$, independent of total length. Overall reductions are also larger for PBLG than for TMV, suggesting the importance of flexibility, helix instabilities near the ends, or both.

Table 2. Exponential decay parameters for various concentration scales. See Eq. 4.11

Concentration System	**Symbol**	**Concentration Units**	k’
Mass density	c	$g\text{-}mL^{-1}$	0.06 ± 0.01 $mL\text{-}g^{-1}$
Number density	ν	mL^{-1}	$(4.4 \pm 0.07) \times 10^{-14}$ mL
Number density reduced to Onsager critical density	ν/ν^*	None	14 ± 2
Number density reduced to dL^2	νdL^2	None	2.7 ± 0.4
Number density reduced to L^3	νL^3	None	0.16 ± 0.02

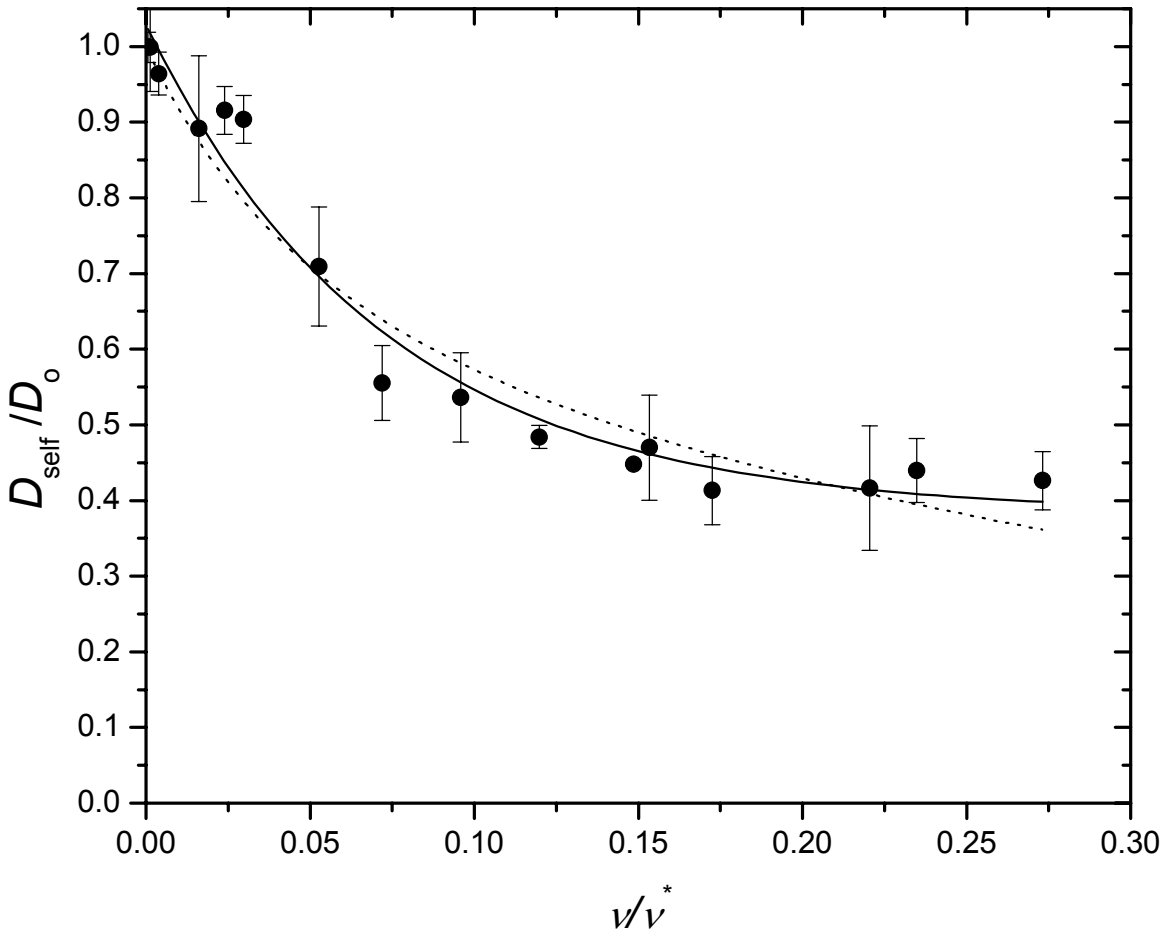

Figure 35. Sample fit to reduced diffusion data using equation 4.8 (dotted line) and using equation 4.11 (solid line).

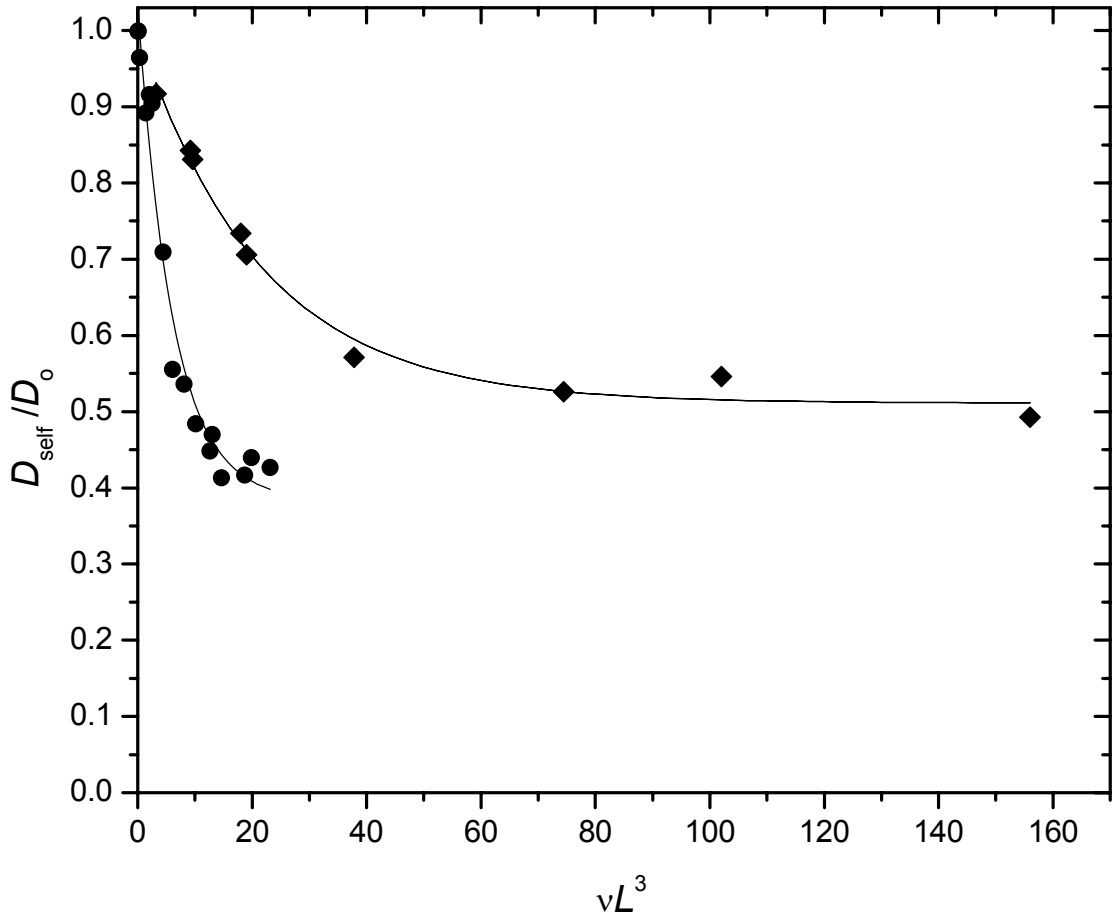

Figure 36. Simulations of Doi, Yamamoto and Kano (♦) compared to results for TMV (•). Exponential decay fits are drawn through both data sets.

CHAPTER 6
FINAL CONCLUSIONS AND FUTURE WORK

Previous experiments from this lab suggested that beyond a certain concentration, dextran solutions present considerable constraint to TMV rotation relative to translation. In addition, significant failures of the Stokes-Einstein equation were seen. It was concluded that the study presents insight into the onset of entanglement. It is now apparent that failure to consider the optical activity of the polysaccharide solutions when aligning the optical system raises serious doubts about the original conclusions. When this effect is properly taken into account, TMV appears to obey Stokes-Einstein diffusion over a wide range of polymer concentrations, even at high concentrations. The transitions seen in the previous work that suggest constraint to rotation relative to translation no longer appear. Optical activity of probed polymers must be taken into account when aligning polarizers in such experiments. Given that TMV senses the macroscopic viscosity of the solution, it seems that concepts of polymer depletion zones may not be significant for the TMV probe. Depolarized dynamic light scattering may be a valuable tool for probe diffusion experiments.

Experiments measuring the self diffusion of TMV are the first of their kind for truly rigid, monodisperse rods. While no theory matches the data trend exactly, diffusion falls very close to the value predicted by the early theoretical predictions of Doi and Edwards. Arguments for sudden onset of entanglement are hard to make as exponential equations seem to describe the data well. Onset of mobility-restricting interactions occur at higher number densities for semi-flexible rods, suggesting that flexibility allows rods to escape enmeshment more easily.

Though it appears that depolarized dynamic light scattering may be useful for probe diffusion experiments, other systems should be studied. Even optically active species can now be dealt with, albeit with a bit of effort. One potential candidate is poly(ethylene oxide) or PEO. This linear synthetic polymer should be a decent model random coil system and possesses no

optical activity. This well characterized system is available in a wide range of molecular weights and with low polydispersities. One caveat is that PEO tends to aggregate over time (several days), which is exacerbated by the presence of sodium azide, the preservative used in the studies presented here. Experiments will simply have to be performed quickly after sample preparation. One advantage over polysaccharides is that PEO can also be studied in the melt. Another possibility is the linear polysaccharide, pullulan, which is more similar to dextran and also available in a wide range of sizes and low polydispersity; though, optical activity must be dealt with.

REFERENCES

(1) van Bruggen, M. P. B.; Lekkerkerker, H. N. W.; Maret, G.; Dhont, J. K. G. *Physical Review E* **1998**, *58*, 7668-7677.

(2) van Bruggen, M. P. B.; Lekkerkerker, H. N. W.; Dhont, J. K. G. *Physical Review E* **1997**, *56*, 4394-4403.

(3) Lodge, T. P. *Physical Review Letters* **1999**, *83*, 3218.

(4) Tao, H.; Lodge, T. P.; von Meerwall, E. D. *Macromolecules* **2000**, *33*, 1747.

(5) de Gennes, P. *Scaling Concepts in Polymer Physics*; Cornell University Press: Ithaca, 1979.

(6) doi, M.; Edwards, S. F. *The Theory of Polymer Dynamics*; Clarendon Press: Oxford, 1986.

(7) Lodge, T. P.; Rotstein, N. A.; Prager, S. *Advances in Chemical Physics* **1990**, *79*, 1.

(8) de Gennes, P. G. *J Chem Phys* **1971**, *55*, 572.

(9) de Gennes, P. G. *Macromolecules* **1976**, *9*, 594.

(10) Ferry, J. *Viscoelastic Properies of Polymers*; Wiley: New York, 1980.

(11) Graessley, W. W. *Advances in Polymer Science* **1982**, *47*, 68.

(12) Milner, S. T.; McLeish, T. C. B. *Physical Review Letters* **1998**, *81*, 725.

(13) Nemoto, N.; Kojima, T.; Inoue, T.; Kishine, M.; Hirayama, T.; Kurata, M. *Macromolecules* **1989**, *22*, 3793.

(14) Nemoto, N.; Kishine, M.; Inoue, T.; Osaki, K. *Macromolecules* **1991**, *24*, 1648.

(15) Wheeler, L.; Lodge, T. P. *Macromolecules* **1989**, *22*, 3399.

(16) Kim, H.; Chang, T.; Yohanan, J. M.; Wang, L.; Yu, H. *Macromolecules* **1986**, *19*, 2737.

(17) Pearson, D. S. *Rubber Chem.Technol.* **1987**, *60*, 439.

(18) Phillies, G. D. J. *Macromolecules* **1986**, *19*, 2367-2376.

(19) Phillies, G. *Macromolecules* **1988**, *21*, 3101.

(20) Phillies, G.; Richardson, C.; Quinlan, C.; Ren, S. *Macromolecules* **1993**, *26*, 6849.

(21) Phillies, G. *Macromolecules* **1987**, *20*, 558.

(22) Phillies, G.; Gong, J.; Li, L.; Rau, A.; Zhang, K.; Yu, L.-P. *J Phys Chem* **1989**, *93*, 6219.

(23) Lodge, T.; Muthukumar, M. *J Phys Chem* **1996**, *100*, 13275-13292.

(24) Bu, Z.; Tipton, D. L.; Negulescu, I. I.; Russo, P. S. *Macromolecules* **1994**, *27*, 6871-6882.

(25) Doi, M.; Edwards, S. F. *Journal of the Chemical Society, Faraday Transactions II* **1977**, *74*, 918-932.

(26) Doi, M.; Edwards, S. F. *Journal of the Chemical Society, Faraday Transactions II* **1978**, *74*, 560-570.

(27) Sato, T.; Teramoto, A. *Macromolecules* **1991**, *24*, 193.

(28) Teraoka, I.; Hayakawa, R. *The Journal of Chemical Physics* **1988**, *89*, 6989.

(29) Szamel, G. *Physical Review Letters* **1993**, *70*, 3744.

(30) Semenov, A. N. *Journal of the Chemical Society, Faraday Transactions II* **1986**, *82*, 317-329.

(31) Dhont, J. K. G.; van Bruggen, M. P. B.; Briels, W. J. *Macromolecules* **1999**, *32*, 3809-3816.

(32) Kirchhoff, Th.; Lowen, H.; Klein, R. *Physical Review E* **1996**, *53*, 5011-5022.

(33) Odijk, T. *Macromolecules* **1986**, *19*, 2073-2074.

(34) Scalettar, B. A.; Hearst, J. E.; Klein, M. P. *Macromolecules* **1989**, *22*, 4550-4559.

(35) Wang, L.; Garner, M. M.; Yu, H. *Macromolecules* **1991**, *24*, 2368-2376.

(36) Seils, J.; Pecora, R. *Macromolecules* **1995**, *28*, 661-673.

(37) Tinland, B.; Maret, G.; Rinaudo, M. *Macromolecules* **1990**, *23*, 596-602.

(38) Zero, K. M.; Pecora, R. *Macromolecules* **1982**, *15*, 87-93.

(39) Gold, D.; Onyenemezu, C.; Miller, W. *Macromolecules* **1996**, *29*, 5700-5709.

(40) Gold, D.; Onyenemezu, C.; Miller, W. *Macromolecules* **1996**, *29*, 5710-5716.

(41) Turner, D.; Hallett, F. *Biochem.Biophys.Acta* **1976**, *451*, 305.

(42) Masaro, L.; Zhu, X. *Prog.Polym.Sci.* **1999**, *24*, 731.

(43) Langevin, D.; Rondelez, F. *Polymer* **1978**, *19*, 875.

(44) Onyenemezu, C.; Gold, D.; Roman, M.; Miller, W. *Macromolecules* **1993**, *26*, 3833.

(45) Russo, P.; Mustafa, M.; Cao, T.; Stephens, L. *J Colloid Interface Sci* **1988**, *122*, 120.

(46) Tracy, M.; Pecora, R. *Macromolecules* **1992**, *25*, 337.

(47) Zhou, P.; Brown, W. *Macromolecules* **1989**, *22*, 890.

(48) Gorti, S.; Ware, B. *J Chem Phys* **1985**, *83*, 6449.

(49) Lin, T.; Phillies, G. *J Phys Chem* **1982**, *86*, 4073.

(50) Lin, T.; Phillies, G. *J Colloid Interface Sci* **1984**, *100*, 82.

(51) Lin, T.; Phillies, G. *Macromolecules* **1984**, *17*, 1686.

(52) Mustafa, M.; Russo, P. *J Colloid Interface Sci* **1988**, *129*, 240.

(53) Tracy, M.; Garcia, J.; Pecora, R. *Macromolecules* **1993**, *26* , 1862.

(54) Ullman, G.; Ullman, K.; Linder, R.; Phillies, G. *J Phys Chem* **1985**, *89*, 692.

(55) Won, J.; Onyenemezu, C.; Miller, W.; Lodge, T. *Macromolecules* **1994**, *27*, 7389.

(56) Cush, R.; Russo, P. S.; Kucukyavuz, Z.; Bu, Z.; Neau, D.; Shih, D.; Kucukyavuz, S.; Ricks, H. *Macromolecules* **1997**, *30*, 4920.

(57) Pluen, A.; Netti, P.; Jain, R.; Berk, D. *Biophysical Journal* **1999**, *77*, 542.

(58) Lodge, T.; Markland, P. *Polymer* **1987**, *28*, 1377.

(59) Lodge, T.; Markland, P.; Wheeler, L. *Macromolecules* **1989**, *22*, 3409.

(60) Soane, D. S.; Hill, D. A. *J.Polym.Sci.Part B* **1989**, *27*, 2295.

(61) Hill, D.; Soane, D. *J.Polym.Sci.Part B* **1989**, *27*, 261.

(62) Camins, B. C.; Russo, P. S. *Langmuir* **1994**, *10*, 4053.

(63) Stanley, W. M. *Science* **1935**, *81*, 644.

(64) Caspar, D. *Advances in Protein Chemistry* **1963**, *18*, 37.

(65) Boedtker, H.; Simmons, N. *Journal of the American Chemical Society* **1958**, *80*, 2550.

(66) Steere, R. *Science* **1963**, *140*, 1089.

(67) *Commonwealth Mycological Institute, Association of Applied Biologists Descriptions of Plant Viruses*; Farnham Royal: Slough, England, 1975.

(68) Gooding; Hebert *Phytopathology* **1967**, *57*, 1285.

(69) Polson, A. *Preparative Biochemistry* **1977**, *7*, 207-215.

(70) Polson, A.; Kiefer, A. *Preparative Biochemistry* **1975**, *5*, 199-210.

(71) Johnson, P.; Brown, W. In *Laser Light Scattering in Biochemistry*; Harding, S., Sattelle, D., Bloomfield, V., eds. The Royal Society of Chemistry: Cambridge, 1992; p 161.

(72) Cummins, H.; Carlson, F.; Herbert, T.; Woods, G. *Biophysical Journal* **1969**, *9*, 518.

(73) Fujime, S. *Journal of the Physical Society of Japan* **1970**, *29*, 416.

(74) Hagenbuchle, M.; Graf, C.; Weber, R. *Progresss in Colloid and Polymer Science* **1991**, *89*, 49.

(75) King, T.; Knox, A.; McAdam, J. *Biopolymers* **1973**, *12*, 1917.

(76) Kubota, K.; Urabe, H.; Tominaga, Y.; Fujime, S. *Macromolecules* **1984**, *17*, 2096.

(77) Lehner, D.; Linder, H.; Glatter, O. *Langmuir* **2000**, *16*, 1689.

(78) Loh, E.; Ralston, E.; Schumaker, V. *Biopolymers* **1979**, *18*, 2549.

(79) Maeda, T.; Fujime, S. *Macromolecules* **1984**, *17*, 1157.

(80) Sano, Y. *Journal of General Virology* **1987**, *68*, 2439.

(81) SB, D.; Lunacek, J.; Benedek, G. *Proceedings of the National Academy of Science* **1967**, *57*, 1164.

(82) Santos, N.; Castanho, M. *Biophysical Journal* **1996**, *71*, 1641.

(83) Schaefer, W.; Benedek, G.; Schofield, P.; Bradford, E. *Journal of Chemical Physics* **1971**, *55*, 3884.

(84) Wada, A.; Suda, N.; Tsuda, T.; Soda, K. *Journal of Chemical Physics* **1969**, *50*, 31.

(85) Wada, A.; Ford, N. J.; Karasz, F. *Journal of Chemical Physics* **1971**, *55*, 1798.

(86) Wilcoxon, J.; Schurr, J. *Biopolymers* **1983**, *22*, 849.

(87) Berne, B.; Pecora, R. *Dynamic Light Scattering*; Wiley: New York, 1976.

(88) *Dynamic Light Scattering: the Method and Some Applications*; Oxford: New York, 1993.

(89) Chu, B. *Laser Light Scattering*; Academic Press: New York, 1991.

(90) Provencher, S. W. *Computational Physics* **1982**, *27*, 229.

(91) Provencher, S. W. *Computational Physics* **1982**, *27*, 213.

(92) Richards, E. *An Introduction to the Physical Properties of Large Molecules in Solution*; Cambridge University Press: Cambridge, 1980.

(93) Hansen, J.; Lebowitz, J.; Demeler, B. *Biochemistry* **1994**, *33*, 13155.

(94) Broersma, S. J. *Journal of Chemical Physics* **1960**, *32*, 1626.

(95) Broersma, S. J. *Journal of Chemical Physics* **1960**, *32*, 1632.

(96) Broersma, S. J. *Journal of Chemical Physics* **1981**, *74*, 6989.

(97) Tirado, M. M.; Martinez, C. L.; de la Torre, J. G. *Journal of Chemical Physics* **1984**, *81*.

(98) Russo, P. S. In *Dynamic Light Scattering: the Method and Some Applications*; Brown, W., ed. Oxford: New York, 1993.

(99) Stryer, L. *Biochemistry*; Stanford University: New York, 1995.

(100) Robyt, J. F. *Essentials of Carbohydrate Chemistry*; Springer-Verlag: New York, 1998.

(101) Jeanes, A.; Haynes, W. C.; Wilham, C. A.; Rankin, J. C.; Melvin, E. H.; Austin, M. J. *Journal of the American Chemical Society* **1954**, *76*, 5041.

(102) Larm, O.; Lindberg, B.; Svensson, S. *Computational Physics* **1971**, *20*, 39.

(103) Smit, J.; van Dijk, J. A. P. P.; Mennen, M. G.; Daoud, M. *Macromolecules* **1992**, *25*, 3585.

(104) Basedow, A. M.; Ebert, K. H. *Journal of Polymer Science: Polymer Symposium* **1979**, *66*, 101.

(105) Senti, J.; Hellman, N. N.; Ludwig, N. H.; Babcock, G. E.; Tobin, R. *Journal of Polymer Science* **1955**, *17*, 527.

(106) Deen, W.; Bohrer, M.; Epstein, N. *AlChEJ* **1981**, *27*, 952.

(107) Lavrenko, P.; Mikriukova, O.; Okatova, O. *Anal.Biochem* **1987**, *166*, 287.

(108) Wang, Y.; Dubin, P. *Journal of Chromatography A* **1998**, *800*, 181.

(109) Bohrer, M.; Patterson, G.; Carroll, P. *Macromolecules* **1984**, *17*, 1170.

(110) Larson, R. G. *The Structure and Rheology of Complex Fluids*; Oxford University Press: New York, 1999.

(111) Macosko, C. W. *Rheology: principles, measurements, and applications*; VCH: New York, 1994.

(112) Tirtaatmadja, V.; Dunstan, D. E.; Boger, D. V. *Journal of Non-Newtonian Fluid Mechanics* **2001**, *97*, 295.

(113) Doucet, G. 2003. Louisiana State University. Ref Type: Thesis/Dissertation in press.

(114) Russo, P. S.; Baylis, M.; Bu, Z.; Stryjewski, W.; Doucet, G.; Temyanko, E.; Tipton, D. *The Journal of Chemical Physics* **1999**, *111*, 1746-1752.

(115) Kuge, T.; Kobayashi, K.; Kitamura, S.; Tanahashi, H. *Carbohydrate Research* **1987**, *160*, 205.

(116) Ioan, C. E.; Aberle, T.; Burchard, W. *Macromolecules* **2001**, *34*, 3765.

(117) Cotts, P.; Berry, G. *Journal of Polymer Science Polymer Physics Edition* **1983**, *21*, 1255.

(118) Phillies, G. D. J. *Journal of Physical Chemistry* **1989**, *93*, 5029-5039.

(119) Edwards, S. F.; Evans, K. E. *Journal of the Chemical Society, Faraday Transactions II* **1982**, *78*, 113-121.

(120) Peters, R.; Peters, J.; Tews, K. H.; Bahr, W. *Biochem.Biophys.Acta* **1974**, *367*, 282.

(121) Jacobson, K.; Wu, E.; Poste, G. *Biochem.Biophys.Acta* **1976**, *433*, 215.

(122) Axelrod, D.; Koppel, D. E.; Schlessinger, J.; Elson, E.; Webb, W. *Biophysical Journal* **1976**, *16*, 1055.

(123) Koppel, D. E.; Axelrod, D.; Schlessinger, J.; Elson, E.; Webb, W. *Biophysical Journal* **1976**, *16*, 1315.

(124) Thompson, N. L.; Burghardt, T. P.; Axelrod, D. *Biophysical Journal* **1981**, *33*, 435.

(125) Smith, B. A.; McConnell, H. M. *Proceedings of the National Academy of Science* **1978** , *75*, 2759.

(126) Rigler, R.; Grasselli, P.; Ehrenberg, M. *Physica Scripta* **1979**, *19*, 486.

(127) Koppel, D. E. *Biophysical Journal* **1979**, *28*, 281.

(128) Webb, W. *Annals of the New York Academy of Sciences* **1981**, *366*, 300.

(129) Lanni, F.; Ware, B. R. *Review of Scientific Instrumentation* **1982**, *53*, 905.

(130) Fong, B.; Stryjewski, W.; Russo, P. S. *Journal of Colloid and Interface Science* **2001**, *239*, 374-379.

(131) Koppel, D. E. *Journal of Chemical Physics* **1972**, *57*, 4814.

(132) Haugland, R. P. *Handbook of Fluorescent Probes and Research Chemicals*; Molecular Probes: 1996.

(133) Temyanko, E.; Russo, P. S.; Ricks, H. *Macromolecules* **2001**, *34*, 582-586.

(134) doi, M.; Yamamoto, I.; Kano, F. *Journal of the Physical Society of Japan* **1984**, *53*, 3000-3003.

(135) Fixman, M. *Physical Review Letters* **1985**, *54*, 337-339.

(136) Frenkel, D.; Maguire, J. F. *Molecular Physics* **1983**, *49*, 503-541.

(137) Keep, G. T.; Pecora, R. *Macromolecules* **1985**, *18*, 1167-1173.

(138) Lowen, H. *Physical Review E* **1994**, *50*, 1232-1242.

(139) Bitsanis, I.; Davis, H. T.; Tirrell, M. *Macromolecules* **1990**, *23*, 1157-1165.

(140) Fixman, M. *Physical Review Letters* **1985**, *54*, 337-339.

(141) Frenkel, D.; Maguire, J. F. *Molecular Physics* **1983**, *49*, 503-541.

(142) Keep, G. T.; Pecora, R. *Macromolecules* **1985**, *18*, 1167-1173.

(143) Lowen, H. *Physical Review E* **1994**, *50*, 1232-1242.

(144) Doty, J. *Journal of Polymer Scienc*e **1948**, *3*, 750

APPENDIX: DETAILS OF SOLUTION OPTICAL ACTIVITY EFFECTS ON SCATTERING

This appendix will provide a detailed description of the effect solution optical activity has on the scattering geometry. Geometric arguments will be used to show how the optically active polymer solution rotates the plane of polarization of the incident beam and the scattered light, revealing the significance of these effects on measured scattering intensity.

The scattering geometry is depicted in Figure A1. The incident light emerges from the polarizer with vertical polarization and is denoted E_i. The beam passes through the optically active polymer solution and its polarization is rotated by angle ϕ_i^c by the time it reaches the cell center. This induces an oscillating dipole μ mostly in the zy_i plane. To treat the effect of optical rotation on the scattered light, a second coordinate system is used, with the subscript, s. This "scattering" coordinate system is rotated from the first by θ degrees. Light propagates along the x_s axis and contains contributions only in the y_s and z directions. A line is constructed at the origin parallel to y_s, onto which μ is projected to determine the y_s and z components. The scattered field near the cell center is:

$$E_s^c = 0\hat{x}_s + \mu \sin\phi_i^c \cos\theta \hat{y}_s + \mu \cos\phi_i^c \hat{z} \qquad \text{A.1}$$

The angle ϕ_s^c lies between E_s^c and the z axis and depends on the scattering angle, θ. At θ=0° the y_s axis is parallel to y_i and $\phi_i^c = \phi_s^c$. At θ=90° there is no projection of μ onto y_s and ϕ_s^c=0. The general expression for ϕ_s^c is:

$$\phi_s^c = \tan^{-1}\left(\frac{\sin\phi_i^c \cos\theta}{\cos\phi_i^c}\right) = \tan^{-1}\left(\cos\theta \tan\phi_i^c\right) \qquad \text{A.2}$$

As the scattered light passes away from the center and through the optically active solution, it

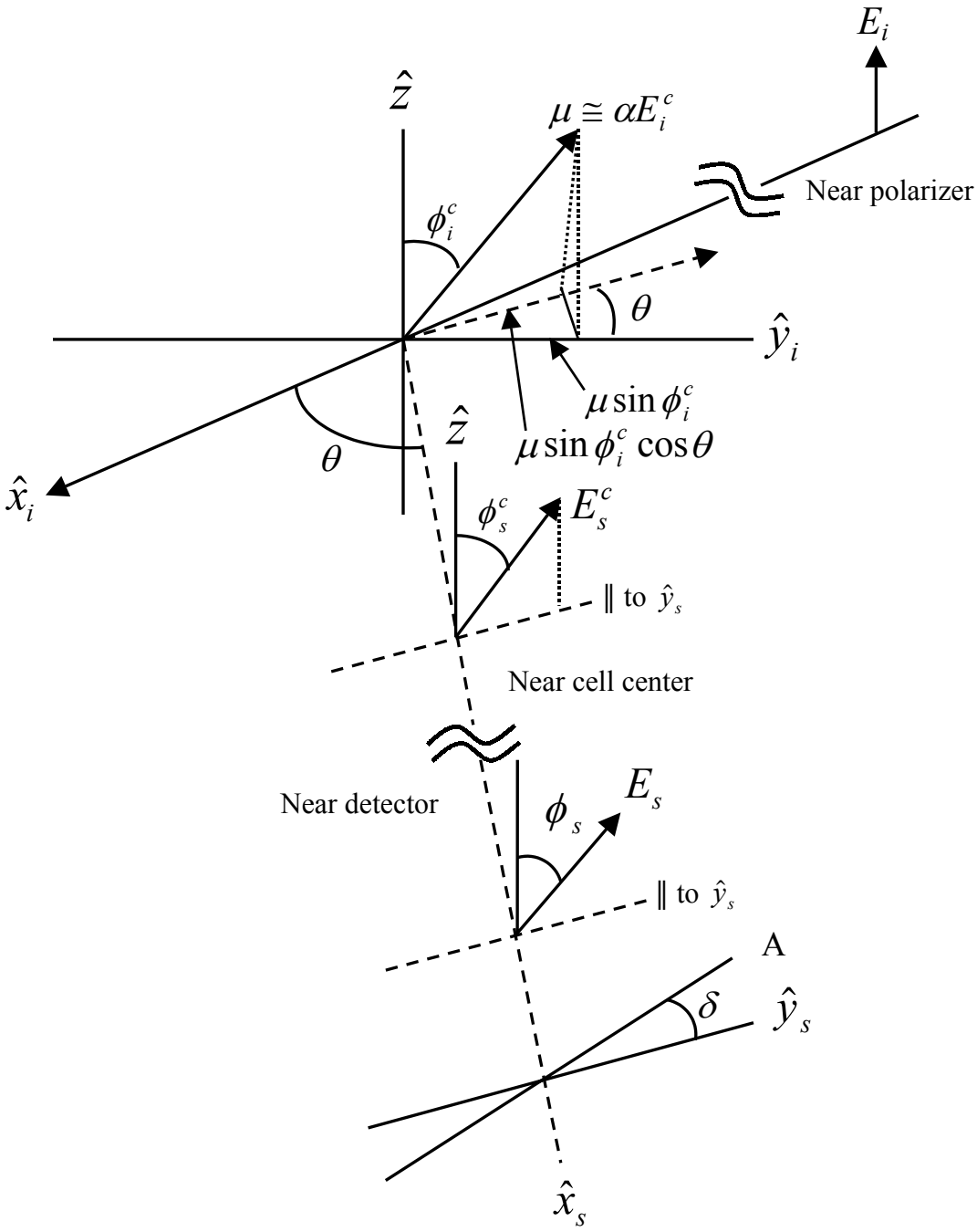

Figure A1. Diagram of the scattering geometry. Subscripts i = incident, s = scattered, and c = near the cell center. Angles θ = scattering angle, ϕ = angle of rotation of incident or scattered light, δ = angle between the analyzer and the y_s axis. E = electric field, μ = induced dipole moment, α = polarizability, A = analyzer.

will be rotated again. The total rotation of the scattered light, ϕ_s, depends on the scattering angle as:

$$\phi_s = \phi_i^c + \tan^{-1}\left(\cos\theta \tan\phi_i^c\right) \qquad \text{A.3}$$

with the limits :

$$\text{At } \theta = 0 \qquad \phi_s \to 2\phi_i^c$$

$$\text{At } \theta = 90 \qquad \phi_s \to \phi_i^c$$

$$\text{At } \theta = 180 \qquad \phi_s \to 0$$

The scattered field, E_s, can then be decomposed into z and y_s components as:

$$E_s^c = 0\hat{x}_s + \mu \sin\phi_i^c \cos\theta \hat{y}_s + \mu \cos\phi_i^c \hat{z} \qquad \text{A.4}$$

giving a magnitude of:

$$\left|E_s^c\right| = \mu\left(\sin^2\phi_i^c \cos^2\theta + \cos^2\phi_i^c\right)^{1/2} \qquad \text{A.5}$$

The scattered field that finally reaches the detector is then given by:

$$E_s = \left|E_s^c\right|\left(\sin\phi\hat{y}_s + \cos\phi_s\hat{z}\right) \qquad \text{A.6}$$

Substituting equation A.5 yields:

$$E_s = \mu\left(\sin^2\phi_i^c \cos^2\theta + \cos^2\phi_i^c\right)^{1/2}\left(\sin\phi_s\hat{y}_s + \cos\phi_s\hat{z}\right) \qquad \text{A.7}$$

The scattered field reaching the detector can now be projected onto the horizontally polarized analyzer which is represented by:

$$A = 0\hat{x}_s + \cos\delta\hat{y}_s + \sin\delta\hat{z} \qquad \text{A.8}$$

where δ is the angle between the analyzer and the y_s axis in the y_sz plane (ideally δ=0)..

The projection is:

$$E_s \bullet A = \mu\left(\sin^2\phi_i^c \cos^2\theta + \cos^2\phi_i^c\right)^{1/2}\left(\sin\phi_s \cos\delta + \cos\phi_s \sin\delta\right) \qquad \text{A.9}$$

which is squared to give the intensity. This value was plotted against the scattering angle in Figure A.2 for. ϕ_i^c=1 degree (approximately equivalent to values that would be observed at 7wt% dextran), and δ=0 degrees (standard vertical-horizontal alignment) The fraction of polarized scattered light leaking through the analyzer is about 0.001, or 1 part per thousand, at θ=30, decreasing as the scattering angle increases, approaching zero at θ=0. Figure A.3 shows a similar plot for ϕ_i^c=2 degrees (approaching values observed at about 14wt% dextran). This seemingly small amount of leakage has dramatic effects due to the very low TMV depolarization ratio, I_{Hv}/I_{Vv}, which has been reported to be only about 0.003.[144] Measurements in our lab suggest an even lower value, approaching 0.001. The amount of polarized scattered light leaking through the analyzer approaches the level of the weakly depolarized light. This significantly decreases the intercept in the Γ vs. q^2 plots giving a D_r value that is too low. The absence of significant effect at high angles, combined with the low intercept, results in a slope D_t that is too high. The ratio D_r/D_t decreases, becoming more significant as D_r approaches zero in the more highly concentrated solutions. An example of the effect on the Γ vs. q^2 plot is seen in Figure A.4 using ϕ_i^c values and diffusion coefficients that correspond to TMV in 7 wt% dextran.

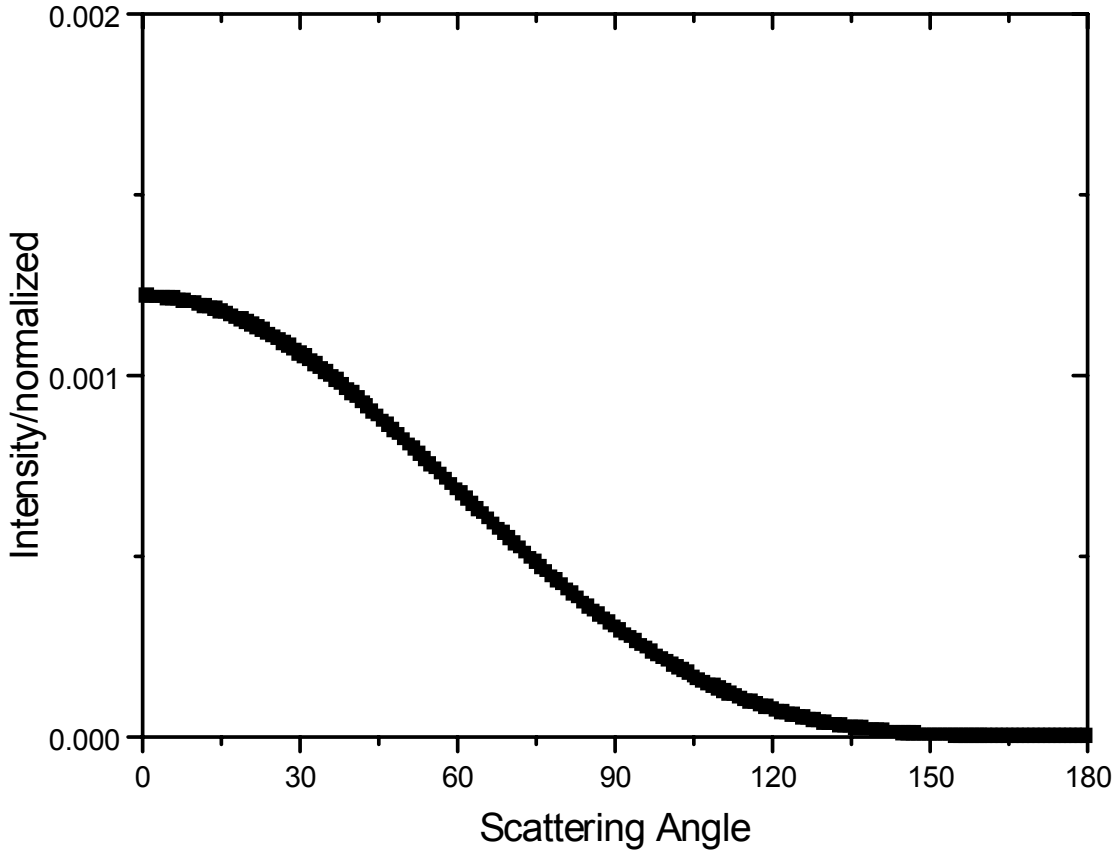

Figure A.2. Normalized intensity of polarized light projected onto the analyzer vs. scattering angle for ϕ_i^c=1 degree and δ=0, using the square of equation A.9.

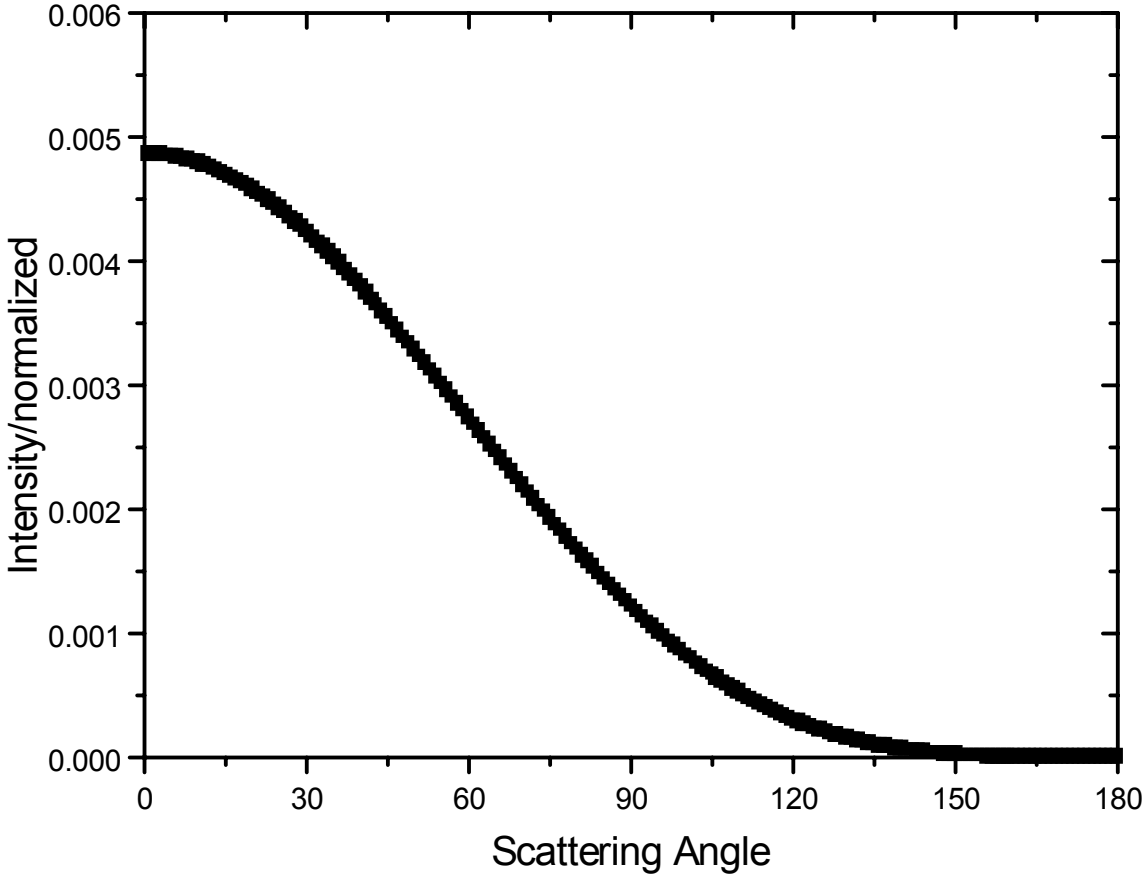

Figure A.3. Normalized intensity of polarized light projected onto the analyzer vs. scattering angle for ϕ_i^c=2 degrees and δ=0, using the square of equation A.9.

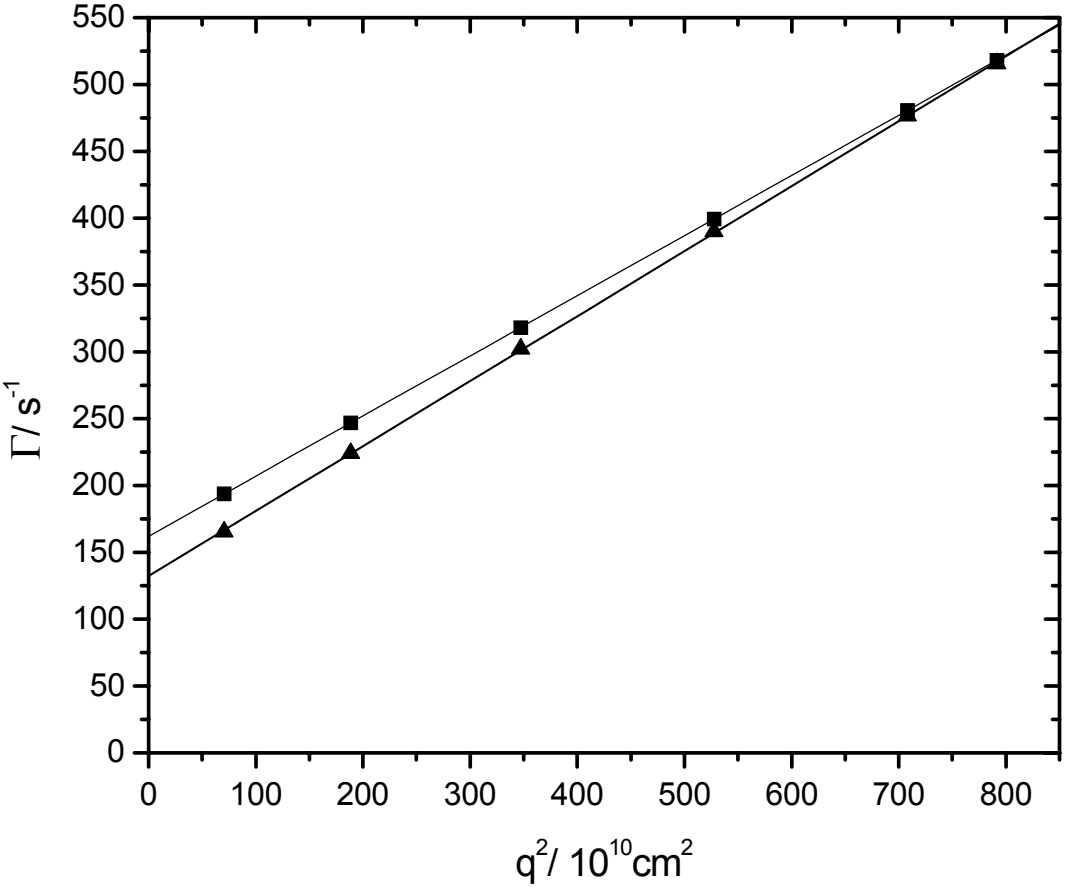

Figure A.4. Simulated plot of Γ vs. q^2 for TMV in 7wt% dextran with ϕ_i^c=1 degree, and diffusion coefficients values obtained from measurements performed using the correct alignment procedure, showing the difference between behavior with (triangles) and without (squares) an optically active matrix .

VITA

Randy Cush was born in Shreveport, Louisiana, where he graduated from C. E. Byrd high school. He began his undergraduate education at Centenary College of Louisiana and completed his Bachelor of Science degree in biochemistry at Louisiana State University in Baton Rouge, Louisiana, where he later transferred. He attended graduate school at Louisiana State University in Baton Rouge in the macromolecular division of the department of chemistry. Midway through his graduate career he and his wife Sarah moved to Mebane, North Carolina, and Randy completed his dissertation research at the University of North Carolina at Chapel Hill in the lab of Dr. Nancy Thompson. After receiving the degree of Doctor of Philosophy in chemistry he began work at Syngenta in Greensboro, North Carolina, as a senior formulation chemist.